AN ABSTRACT OF THE THESIS OF

<u>Lerssak Boonsongsup</u> for the degree of <u>Master of Science</u> in

<u>Chemical Engineering</u> presented on <u>September 3, 1993</u>

Title : <u>SO2 Capture and HCl Release at Kraft recovery boiler conditions</u>

Abstract approved : <u>Redacted for privacy</u>

Professor William James Frederick

The reactions of SO_2 with Na_2CO_3 and $NaCl$ are important in the capture of sulfur gases in black liquor combustion and in the purging of chlorides from the soda cycle in kraft pulp mills. The $NaCl$-SO_2 reaction, in the presence of water vapor and oxygen, also provides a way to eliminate chlorides form the kraft recovery cycle. There has been relatively little information available on the rate of sulfation of Na_2CO_3, and almost no information of relevance on SO_2-$NaCl$ reactions.

The previously published data on the sulfation of solid Na_2CO_3 and $NaCl$ were first evaluated. The reaction of Na_2CO_3 with SO_2 in the presence of oxygen when the products are Na_2SO_4 and CO_2 has been studied by several investigators but no data were found on the reactions of molten Na_2CO_3 with SO_2. The shrinking unreacted core model which included both chemical reaction kinetics and product layer diffusion was used to fit Backman et al. (2) data whereas Keener and Davis data were suitable for general model developed by Wen. The models gave an activation energy of chemical reaction about 60-65 KJ/mol, and an apparent activation energy of the product layer diffusion about 65-100 KJ/mol. The rate of sulfation of Na_2CO_3 is mainly controlled by intraparticle diffusion in the temperature range 120-700 ^oC. Based on the intraparticle diffusion rate, the residence time of solid fume particles in a recovery furnace is too short for any substantial sulfation to take

place. Thus any substantial sulfation of Na_2CO_3 have to take place in the molten phase.

HCl is released when NaCl reacts with SO_2 in the presence of O_2 and water vapor. This reaction is slow relative to that of Na_2CO_3 with SO_2 and O_2, which accounts for the observation that recovery boiler dust contains significant NaCl even when the residual Na_2CO_3 approaches zero. This reaction is controlled by chemical reaction in the temperature range 400-600 °C. It was not strongly temperature dependent, with an activation energy of 17.3 KJ/mol. The reaction rates were dependent on the SO_2 partial pressure but were independent of the water vapor and O_2 partial pressures. The mechanism of this reaction was suggested and the adsorption of SO_2 on the surface of NaCl should be the main step to control the overall rate of reaction. The mechanisms of this reaction when the presence and absence of SO_3 takes place are different.

SO_2 Capture and HCl Release

at Kraft Recovery Boiler Conditions

by

Lerssak Boonsongsup

A THESIS

submitted to

Oregon State University

in partial fullfillment of

the requirements for the

degree of

Master of Science

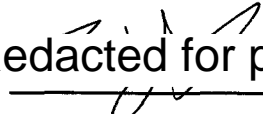Completed September 3, 1993

Commencement June, 1994

APPROVED :

Redacted for privacy

Professor of Chemical Engineering in charge of major

Redacted for privacy

Head of Chemical Engineering Department

Redacted for privacy

Dean of Graduate School

Date of thesis is presented _____September 3, 1993_____

Typed by researcher

TABLE OF CONTENTS

LIST OF FIGURES

LIST OF TABLES

LIST OF APPENDIX FIGURES

LIST OF APPENDIX FIGURES (continued)

LIST OF APPENDIX TABLES

CHAPTER 1

INTRODUCTION

1.1 Kraft recovery cycle

Pulping is the process by which wood is reduced to pulp which is the fibrous raw material for papermaking. This process can be accomplished mechanically, thermally, chemically or by combinations of these treatments. At present, chemical pulping is the most practical method of pulping process. The most widely practiced chemical method is the kraft process. The kraft pulping chemical recovery cycle is an integral part of the process. It consists of a series of processes to destroy toxic waste from pulping, to recycle pulping chemicals and to co-regenerate steam and power. A schematic of kraft recovery cycle is shown in Figure 1.1.

In cooking or digestion process, wood chips are cooked in digesters by white liquor containing the active pulping chemicals, NaOH and Na$_2$S. The lignin in wood is dissolved from the cellulose fiber in the wood by white liquor. The cellulose fibres, pulp, from pulping process are separated from the spent pulping liquor by washing. The pulp is often bleached before being used to make paper or other cellulose products.

The residual liquor from washing process, weak black liquor, contains the inorganic and dissolved organic material. Weak black liquor is then concentrated in an evaporation process to become strong black liquor. Steam

driven evaporators, concentrators are used in this process, and strippers are often used to recover methanol from the condensate.
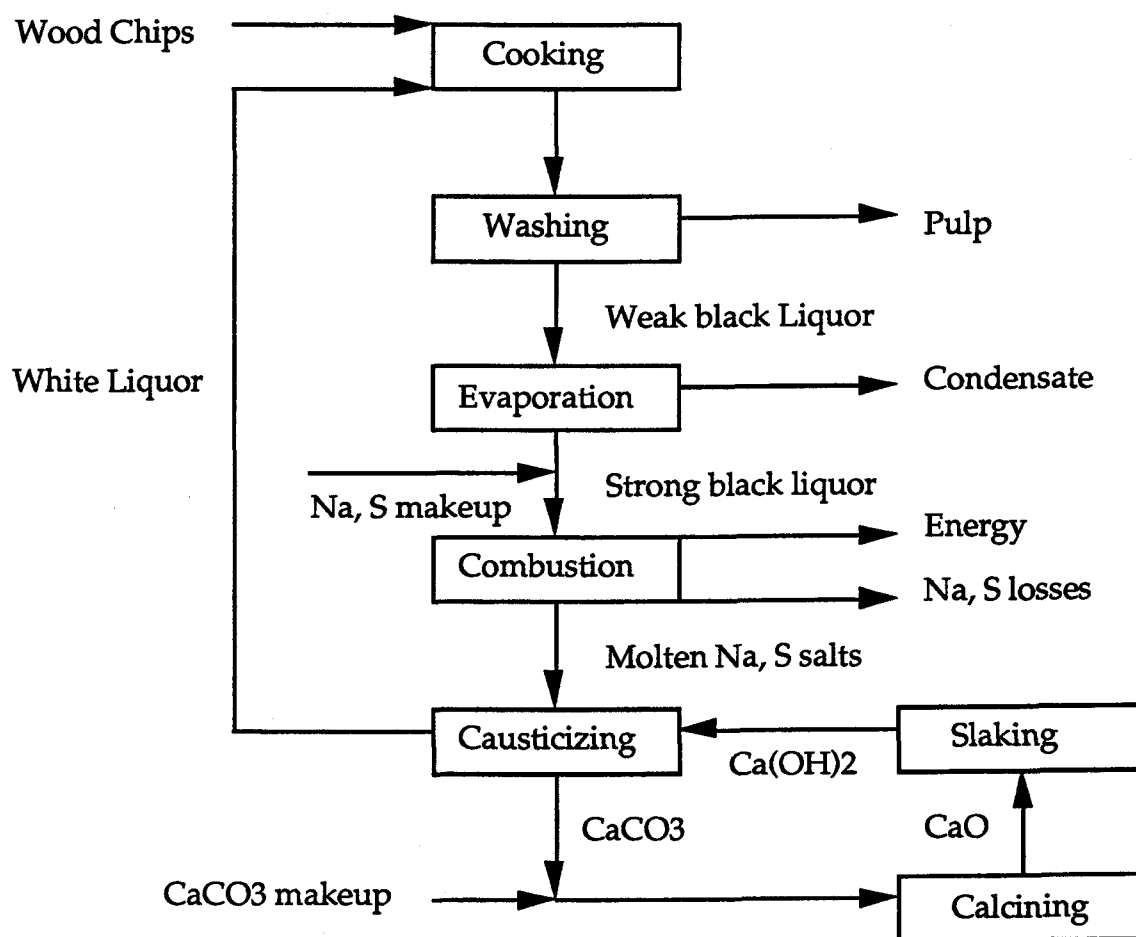
Figure 1.1 : Schematic of kraft recovery cycle

The strong black liquor is sprayed into the lower section of the chemical recovery furnace. The black liquor is converted to heat, flue gas and inorganic smelt. The heat is recovered as steam and may be used for electicity generation or other functions in the mill. Losses of chemicals in the kraft process are usually made up by the addition of sodium-sulfur salt which is often salt cake, Na_2SO_4.

The inorganic molten smelt of Na_2CO_3 and Na_2S from the bottom of furnace is dissolved to form green liquor to recover pulping chemicals.

The green liquor is reacted with reburned lime, CaO, to convert Na_2CO_3 to NaOH and regenerate the white liquor in recausticizing process. The white liquor is then clarified to remove precipitated "lime mud", $CaCO_3$, and is then ready for reuse in the pulping process. Lime mud, $CaCO_3$, is then reburned in calcining or reburning process to regenerate lime, CaO. The causticizing reaction occurs in two steps. The lime first reacts with water in slaking process to form slaked lime, $Ca(OH)_2$ which is then reacts with Na_2CO_3 to form NaOH. The causticizing reactions are shown below :

$$CaO + H_2O \longrightarrow Ca(OH)_2 + heat$$
$$Ca(OH)_2 + Na_2CO_3 \longrightarrow 2\,NaOH + CaCO_3$$
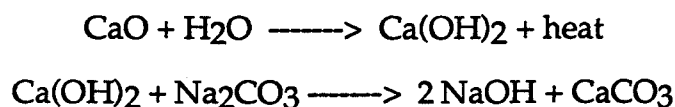
The kraft furnace is the most significant equipment in the kraft recovery process. A general schematic diagram of a kraft furnace is shown in Figure 1.2. Kraft furnace have two main sections which are a furnace section and a convective heat transfer section. All mixing and combustion of the fuel and air should be completed in the furnace section.

After being concentrated, the black liquor is first combined with makeup chemical which is a sodium-sulfur salt. The mixed fuel is then heated in order to reduce its viscosity to control its spray characteristics. The mixed black liquor fuel enters the furnace through spray nozzles to break black liquor into coarse droplets. The black liquor droplets are dried and partiallly devolatilized during the way down to the bed. The material on the bed consists of the inorganic material, a portion of the volatile organics and the solid residual carbon from devolatilization of the organic matter.
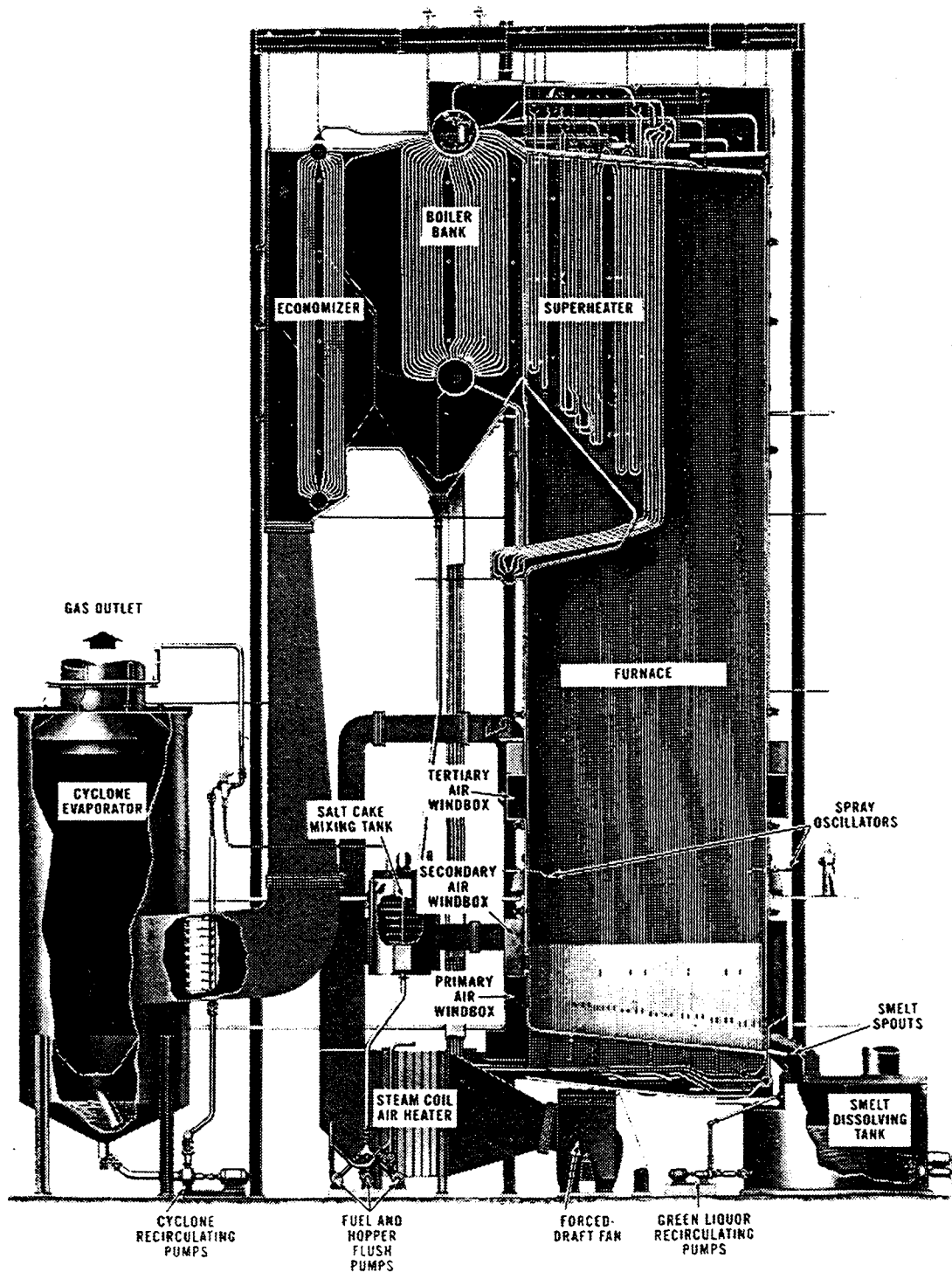
Figure 1.2 : Schematic diagram of a kraft recovery furnace

The combustion air is introduced at several locations around the furnace. Primary air is introduced into the lower furnace to provide a reducing zone in the lower furnace. It used to control the shape and position of the perimeter of the char bed and to provide a portion of the air for char combustion. Secondary and tertiary air are added in the combustion or oxidation zone for the completion of the combustion. Secondary air controls the position of the top of the bed and burns the pyrolysis gases and CO rising from the bed. Tertiary air controls the complete combusiton and the final mixing of the combustion gases.

The convective heat transfer section consists of the superheater, boiler bank, and economizer. The deposition of particles occurs on the heat transfer surface in the convective heat transfer section. The deposits formed result from two distinct types of particles. First is from the entrainment of black liquor droplets in the furnace gases. Second is fume generated by volatilization of the low melting point sodium compound and then condenses in the upper furnace to form solid paricles smaller than 0.5 μm in size. The deposits formed from entrained liquor droplets are mainly Na_2CO_3 and Na_2SO_4.

Sodium-based fume generated in kraft recovery furnace deposits on the convective section tubes. These deposits reduce the heat transfer rates and may plug gas passages in the superheater and boiler bank. The deposits also enchance the corrosion of fireside surfaces. However sodium-based fume formed behaves as a collector for sulfur dioxide in the furnace. This reduces the sulfur level emitted from the furnace. The capture of SO_2 in the furnace is from the sulfation of NaCl and Na_2CO_3. The reactions are shown below :

$$Na_2CO_3 \text{ (s,l)} + ^1/_2 O_2 + SO_2 \longrightarrow Na_2SO_4 \text{ (s,l)} + CO_2$$
$$NaCl \text{ (s,l)} + ^1/_2 SO_2 + ^1/_4 O_2 + ^1/_2 H_2O \longrightarrow HCl + ^1/_2 Na_2SO_4 \text{ (s,l)}$$
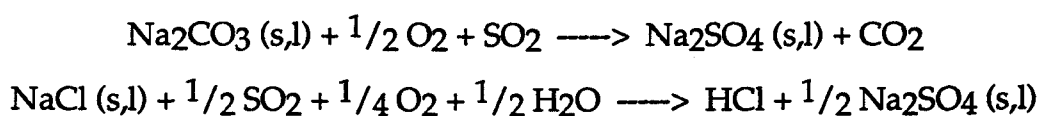
The NaCl-SO_2 reaction also provides a way to eliminate chlorides from the kraft recovery cycle but at the same time it produces HCl emissions which , in addition to detrimental effects on the environment, can cause corrosion in the boiler.

These two reactions are very significant to understand and control the SO_2 capture and HCl release from kraft recovery cycle. They also provide a way to control the deposits on the heat transfer surface in the convective heat transfer section.

These two reactions can occur in both solid and liquid form of NaCl and Na_2CO_3. The melting point of NaCl and Na_2CO_3 are about 800 and 855 ^oC respectively. The melting points will be changed in the presence of Na_2SO_4 as shown in phase diagram of the system NaCl-Na_2SO_4 and Na_2CO_3-Na_2SO_4 in Appendix E.

1.2 Other Applications

The sulfation of NaCl and Na_2CO_3 is important in other applications, hot corrosion of gas turbine engine, HCl manufacture and flue gas desulfurization system.

Hot corrosion degradation of components of gas turbine engines burning relatively clean fuels usually involves deposits of only Na_2SO_4. This deposit can be from the deposition by impaction of NaCl particles on the turbine surfaces and subsequent reaction of the condensed NaCl with SO_2. Another possible reason for deposition is the reaction in the hot combustion stream to form Na_2SO_4 with subsequent deposition. Understanding the sulfation of NaCl may be important in controlling corrosion in gas turbine engines.

The reaction of NaCl and SO_2 in the presence of O_2 and H_2O is the reaction used in HCl production which is called the Hargreaves process. This process is operated at temperature between 430-540 ^oC. This process is used by the Morton Chemical Company at Weeks, Louisiana.

The flue gas desulfurization (FGD) system is the injection of dry sodium bicarbonate additive to capture sulfur compounds in flue gas from coal-fired boilers. The decomposition of $NaHCO_3$ to Na_2CO_3 takes place at 270 ^oC but it is known to occur partially at temperature as low as 100 ^oF. In addition, Na_2CO_3 is also a candidate for FGD systems. Thus understanding the sulfation of Na_2CO_3 is important in the capture of SO_2 in FGD systems.

1.3 Research Objectives

The objectives of this thesis are to :
- obtain the kinetic data for the sulfation of NaCl and Na_2CO_3 at
  temperature below the melting point
- understand the mechanism of these reactions
- obtain rate equations for the sulfation of NaCl and Na_2CO_3 at
  temperature below the melting point
- apply the results to kraft recovery boilers

CHAPTER 2

LITERATURE REVIEW

2.1 Sulfation of Na_2CO_3

The reaction between Na_2CO_3 and SO_2 has been studied by several researchers. The objective and condition of each study were different. Keener and Davis [1], Backman et al. [2], Maule and Cameron [3] and Lloyd-George [4], studied this reaction in the presence of oxygen whereas Smith and Kimura [5] and Butler and Waites [6] studied in the absence of O_2. The products of this reaction were Na_2SO_3 in the absence of O_2 and Na_2SO_4 in the presence of O_2. These two reactions are shown below :

$$Na_2CO_3\ (s) + SO_2\ (g) \ \text{---------->} \ Na_2SO_3\ (s) + CO_2\ (g)$$
$$Na_2CO_3\ (s,l) + SO_2\ (g) + {}^1/_2\ O_2\ (g) \ \text{---------->} \ Na_2SO_4\ (s,l) + CO_2\ (g)$$
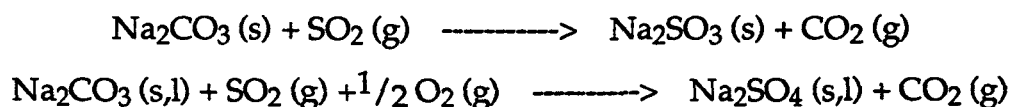
The conditions of interest for sulfation of solid Na_2CO_3 that is of interest for kraft recovery boilers is for temperatures less than 800 $^\circ C$ in the presence of oxygen.

Keener and Davis [1] studied this reaction in the presence of oxygen between 122 and 344 $^\circ C$. The materials used in this study were commercial grade Na_2CO_3 and were classified to 20, 90 and 200 μm diameter respectively. The preheated gas stream was passed through a stainless steel fixed bed reactor and sulfur content in solid product was analyzed. The reaction rate depended greatly on the particle size. The reaction rate was enhanced by increasing temperature up to 344 $^\circ C$ but the reaction rate at 400 $^\circ C$ was less

than the reaction rate at 344 °C. Based on visual observation, it was proposed that there was a sintering effect at temperatures above 344 °C. The rate limiting step of this reaction was determined to be diffusion through product layer.

Backman et al. (2) studied this reaction with presintered particles by heating at 600 °C for 12 hours to avoid sintering effects for Na_2CO_3 particles above 450 °C. Above this temperature the inner pores of Na_2CO_3 started to close and reduced the active surface area. The mean presintered particle diameter was about 55 μm and temperature range studied was 350 to 700 °C. A thermogravimetric method was used to study this reaction. All high temperature parts in the gas flow path were made of quartz glass in order to avoid uncontrolled catalytic oxidation of SO_2 to SO_3 on metal surfaces. The chemical kinetic rate versus temperature data showed no dramatic changes over any part of the temperature range when we compared to non-presintered particles data. The chemical kinetic rates were determined based on the initial rate of reaction based on the assumption that pore diffusion effects were eliminated for presintered particles. These data followed the Arhenius law quite well and the apparent activation energy was about 65 KJ/mol. The chemical kinetic rate was affected by only SO_2 whereas the diffusion controlled part of the reaction was influenced by both SO_2 and O_2. The presence of SO_3 in the gas phase gave a higher rate of reaction than with SO_2 and O_2. The different mechanisms of this reaction with and without SO_3 present were suggested.

Maule and Cameron (3) studied this reaction with sub-micron Na_2CO_3 (fume) particles from the oxidation of Na_2S in a Na_2CO_3 melt. The fume particles generated were between 0.25 and 1 μm in diameter. The 316 stainless steel fixed bed reactor was used to study this reaction between 120 and 246 °C.

They used shrinking unreacted core model (8) with chemical reaction control to fit the data to find chemical kinetic rates. They found that the activation energy for the reaction obtained from the Arhenius plot was about 23 KJ/mol. In the diffusion controlled part of this reaction, the shrinking unreacted core model with both chemical reaction and diffusion through product layer control was used to fit the data to find the effective diffusivity. They also reported that the reaction was first order with respect to SO_2 and zeroth order with respect to O_2 and this reaction was diffusion through product layer control. Significant sintering of the solid particles occurred during the reaction. Thus Na_2CO_3 deposited on a heat transfer surface in the kraft recovery furnace can react at relatively low temperature with SO_2 to form Na_2SO_4, a very hard, highly sintered deposit.

Lloyd-George (4) also studied this reaction in the presence of O_2. The purpose of this study was to consider the significance of pyrosulfate on the sulfation of Na_2CO_3. The platinum boat in a horizontal tubular furnace with temperature controller was used to study this reaction. The temperature range studied was 180 to 700 ^oC. The sudden decrease in overall rate of reaction between 350 and 550 ^oC reported by Lloyd-George (7) was the effect from liquid sodium pyrosulfate formed between these temperatures. The mechanism of this reaction was also proposed.

2.2 Sulfation of NaCl

The reaction between NaCl and SO_2 in the presence of O_2 and water vapor has been studied by few researchers. This reaction was previously studied by Henriksson and Warnqvist (13) and Fielder et al. (14).

Henriksson and Warnqvist (13) studied the sulfation of NaCl in the presence of O_2 and water vapor. Their experimental procedure involved placing Al_2O_3 boats which contained NaCl into a long Al_2O_3 tube within an electrically heated tube furnace. The temperature range studied was from 500 to 800 °C which included both the solid and molten regions of the phase diagram for NaCl and Na_2SO_4. The rate of conversion exhibited an unexpected flow dependence, i.e. rate of reactions decreased while increasing flow rate above 10 cm^3/sec., which may have resulted from mass transfer effects in the experimental apparatus. The reaction was 0.5 order with respect to SO_2 partial pressure and also 0.5 order with respect to O_2 partial pressure but it was independent of water vapor partial pressure. An unexpected temperature dependence, i.e. rate of reactions increased while decreasing temperature below 500 °C, was observed in this study. The chemical reaction was reported to be the rate limiting step of this reaction. The following mechanism of this reaction was also suggested. SO_2 and O_2 are adsorbed on the NaCl surface and then react together to form SO_3 (ads). The SO_3 (ads) reacts with adsorbed water and NaCl to form HCl and Na_2SO_4 with the intermediates H_2SO_4 (ads) or $NaHSO_4$ (ads).

Fielder et al. (14) followed this reaction by suspending a sample inside a quartz tube from a sensitive electrobalance. A Pt catalyst was used to produce the desired concentration of SO_3 in SO_2-O_2 mixture. High pressure mass spectrometric sampling techniques were used to analyze the gaseous reactant compositions and to identify the gaseous products. The temperature range studied was from 100 to above 650 °C. There were different films formed on the NaCl surface at different ranges of temperature in the anhydrous condition, water less than 20-40 ppm. The reaction, film formed and rate limiting step reported were shown below :

100 - 150 °C   solid $NaCl \cdot SO_3$

$$NaCl\,(s) + SO_3\,(g) \longrightarrow NaCl.SO_3\,(s)$$

mass transfer controlled process

400 - 450 °C   molten $Na_2S_2O_7$

$$2\,NaCl\,(s) + 2\,SO_3\,(g) + {}^1/_2\,O_2\,(g) \longrightarrow Na_2S_2O_7\,(s) + Cl_2\,(g)$$

mass transfer controlled process

450 - 625 °C   solid Na_2SO_4

$$2\,NaCl\,(s) + SO_3\,(g) + {}^1/_2\,O_2\,(g) \longrightarrow Na_2SO_4\,(s) + Cl_2\,(g)$$

chemical reaction controlled process

above 625 °C   molten $Na_2SO_4 \cdot NaCl$

$$2\,NaCl\,(l) + SO_3\,(g) + {}^1/_2\,O_2\,(g) \longrightarrow Na_2SO_4\,(l) + Cl_2\,(g)$$

mass transfer controlled process

Fielder et al. (14) also studied of this reaction in the presence of O_2 and water vapor between 400 - 450 °C. The products were Na_2SO_4 and HCl instead of Cl_2. This reaction were first order with respect to SO_3 and also first order with respect to water vapor. The reaction was reported to be controlled by the chemical reaction step.

From these two previously studies, almost all of the Fielder et al. (14) were for anhydrous condition. The data in this study were reported in total weight of sample gained versus time. These data could not be transformed to conversion versus time data based on the information available in the paper and the temperature dependence of reaction rate in each range of temperature was not reported in this study also. Thus no kinetics could be obtained from their data. For Henriksson and Warnqvist (13) study, the results were dependent on the gas flow rate and an unexpected

temperature dependence was observed below 500 $^{\circ}$C. It was concluded that more reliable kinetic data were needed for this reaction.

CHAPTER 3

ANALYSIS OF THE KINETIC DATA FOR SULFATION OF Na_2CO_3

The kinetic data of the sulfation of Na_2CO_3 in the presence of O_2 have been reported by Keener and Davis (1), Backman et al. (2) and Maule and Cameron (3). The reaction rates as reported in these three studies are considerably different. The comparison of the reaction rates is shown in Figure 3.1. They differ as much as a factor of more than 100 when compared at the same temperature.
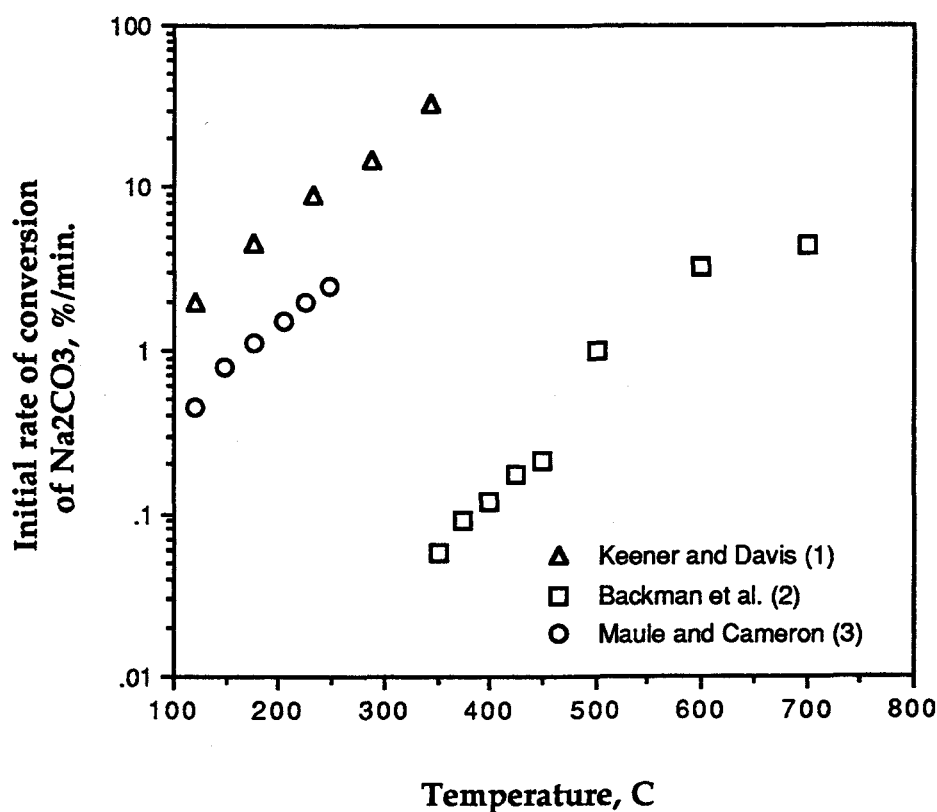
Figure 3.1 : Comparison of the initial rates of Na_2CO_3 sulfation as reported by Keener and Davis (1), Backman et al. (2) and Maule and Cameron (3)

3.1 Calculations

The material used in these three studies are varied considerably. Keener and Davis (1) used a relatively porous commercial grade Na_2CO_3. Backman et al. (2) used particles that had been presintered by heating at 600 °C for 12 hours to minimize the sintering effect during the reaction. Maule and Cameron (3) generated submicron Na_2CO_3 fume particles by the oxidation of Na_2S in a Na_2CO_3 melt. In addition to material, the experimental conditions such as gas concentration were varied also. The details of the experimental conditions employed from these studies are shown in Table 3.1.

Table 3.1 : Comparison of experimental conditions of previously reported studies of Na_2CO_3 sulfation

	Keener and Davis (1)	Backman et al. (2)	Maule and Cameron (3)
Paricle size, μm	20, 90, 200	55	0.25-1.0
Temperature, °C	121-344	350-700	120-246
Specific surface area, m²/g	1.72 (20 μm) 1.25 (90 μm) 0.91 (200 μm)	0.132	6.56
Ratio of total and external surface area	14.3 (20 μm) 46.9 (90 μm) 75.8 (200 μm)	3.03	1.71
SO_2, %	2.45	1-5	0.25-0.43
O_2, %	4.9	5-20	0.34-2.15

The Na_2CO_3 specific surface areas from different studies differ by a factor of 50 from smallest to largest. Chemical kinetic rates were estimated from initial rate data from these three studies by the assumption that the total surface area of the particles was available for the reaction, not only the external surface area of the particles. The calculations are as followed :

moles SO_2 reacted = k S C_{SO_2} (first order reaction with respect to SO_2)

molar rate of Na_2CO_3 conversion = $(dX/dt)V\rho/M$

where   k   = chemical kinetic rate constant

        S   = surface area per particle

        C_{SO_2} = SO_2 concentration = P_{SO_2}/RT

        V   = volume per particle

        X   = conversion

        t   = time

        ρ = density of Na_2CO_3 = $2.5\,g/cm^3$

        M   = molecular weight of Na_2CO_3 = 106

        dX/dt = slope of conversion versus time data

one mole of Na_2CO_3 reacted with one mole of SO_2, so that :

$$k\,S\,C_{SO_2} \; = \; (dX/dt)V\rho/M$$

specific surface area per gram of particles= S' = $S/\rho V$

so S = S'ρV, we will get :

$$kS'(P_{SO_2}/RT) = (dX/dt)/M$$

$$k = [\,(dx/dt)\,(RT/P_{SO_2})\,]\,/\,S'M$$

The initial rates based on total surface area of different studies are shown in Table 3.2.

Table 3.2 : The initial rates (cm/s) based on the total surface area of different studies

Keener and Davis (1)	Backman et al. (2)	Maule and Cameron (3)
0.01189 (343 °C)	0.00847 (700 °C)	0.00059 (246°C)
0.00487 (288 °C)	0.00546 (600 °C)	0.00046 (224 °C)
0.00242 (232 °C)	0.00151 (500 °C)	0.00033 (204 °C)
0.00118 (177 °C)	0.00030 (450 °C)	0.00023 (177 °C)
0.00021 (121 °C)	0.00024 (425 °C)	0.00015 (149 °C)
	0.00015 (400 °C)	0.00008 (121 °C)
	0.00012 (375 °C)	
	0.00007 (350 °C)	

Figure 3.2 shows the comparison of the chemical reaction rates at each temperature for the three different studies. The agreement of these studies is improved. The range of variation was reduced by an order of magnitude when compared with the data in Figure 3.1.

For the data of Backman et al. (2), the material used was presintered particle that pore diffusion effects should be eliminated. The relatively low internal surface area compared with the external surface area of the 55 mm
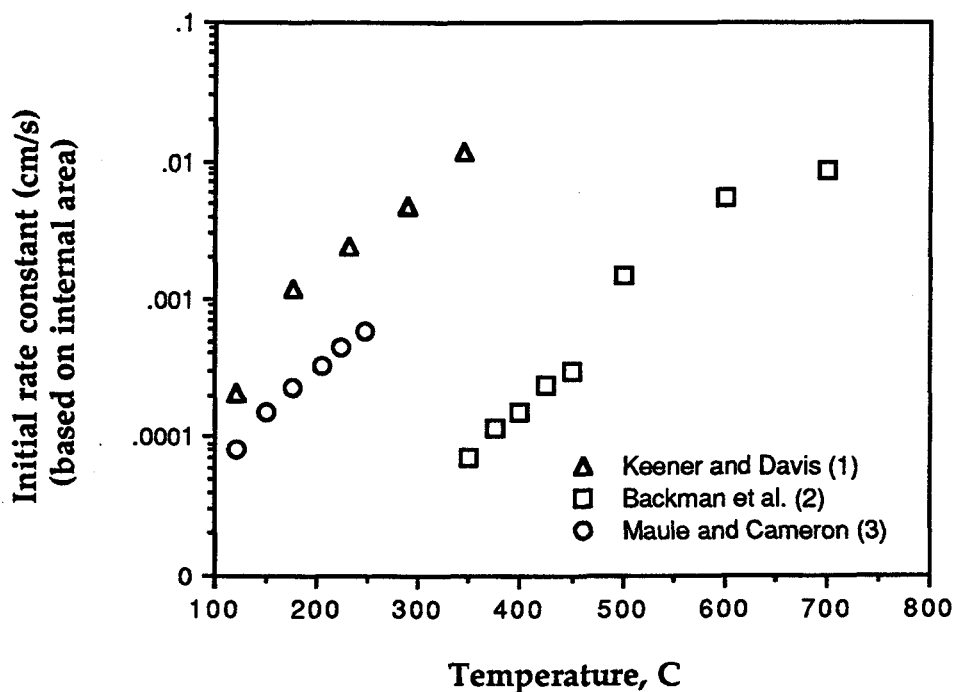
Figure 3.2 : The chemical reaction rates calculated from initial rate data for the sulfation of Na_2CO_3

particle used in this study indicated that the particle was indeed not very porous. The shrinking unreacted core model (8) was suitable for this study to describe this reaction. The shrinking unreacted core model (8) describes gas-solid reactions when the porosity of the unreacted solid is very small. In this model, the reaction is assumed to start at the surface of the solid and to proceed at the interphase between the unreacted core and the porous product layer which is formed on the outer surface of the particles.

The rate equation of the shrinking unreacted core model (8) when external mass transfer controlled the reaction is:

$$t = \frac{\rho R}{3k_g C_{SO_2}} [X] = \frac{\rho R}{3k_g C_{SO_2}} f_1(X)$$

The rate equation with diffusion through product layer control is :

$$t = \frac{\rho R^2}{6D_e C_{SO_2}} [1-3(1-X)^{2/3}+2(1-X)] = \frac{\rho R^2}{6D_e C_{SO_2}} f_2(X)$$

The rate equation with chemical reaction control is :

$$t = \frac{\rho R}{k_s C_{SO_2}} [1-(1-X)^{1/3}] = \frac{\rho R}{k_s C_{SO_2}} f_3(X)$$

where D_e = effective diffusivity of the reactant gases in the particle

b = reaction stoichiometry, mol Na_2CO_3 reacting/mol SO_2 reacting

k_s = chemical kinetic rate

k_g = gas film mass transfer coefficient

C_{SO_2} = concentration of diffusing species, SO_2

ρ = density of Na_2CO_3

R = radius of particle

X = fractional conversion of Na_2CO_3

For Backman et al. (2) data, the conversion versus time data can be seperated into two parts. The first part of the curve was nearly straight line which was influenced by chemical reaction with the negligible external mass transfer and porous effects. The slope decreased at higher conversion in

second part. This was from the effect of diffusion through the product layer. Thus the shrinking unreacted core model (8) with both chemical reaction and diffusion through product layer control was used to fit Backman et al. (2) data. The rate equation of the shrinking unreacted core model (8) when both the chemical reaction and diffusion through product layer are important is :

$$t = \frac{\rho R^2}{6 b D_e C_{SO_2}} [1-3(1-X)^{2/3}+2(1-X)] + \frac{\rho R}{k_s C_{SO_2}} [1-(1-X)^{1/3}]$$

$$t = A f_1(X) + B f_2(X)$$

where $\quad A = \rho R^2 / 6 b D_e C_{SO_2}$

$\qquad\quad B = \rho R / k_s C_{SO_2}$

The fit was done by using the method of least squares. For each of p data points, the error, ε_i, as the difference between the observation t_i, i = 1, 2, 3, ..., p, and the predicted model response $t_i(X)$ is :

$$\varepsilon_i = t_i - t_i(X) \qquad\qquad i = 1, 2, ..., p$$
$$\varepsilon_i = t_i - (A f_1(X)_i + B f_2(X)_i) \qquad i = 1,2, ..., p$$

Let f = error criterion

$$f = \sum_{i=0}^{p} \varepsilon_i{}^2 = \sum_{i=0}^{p} (t_i - (A f_1(x)_i + B f_2(x)_i))^2$$

The error criterion, f, have to be minimized with respect to A and B. This condition is :

$$(df/dA)_B = (df/dB)_A = 0$$

The fit of the shrinking unreacted core model with Backman et al. (2) data was shown in Figure 3.3. It showed that the shrinking unreacted core model described Backman et al. (2) very well.
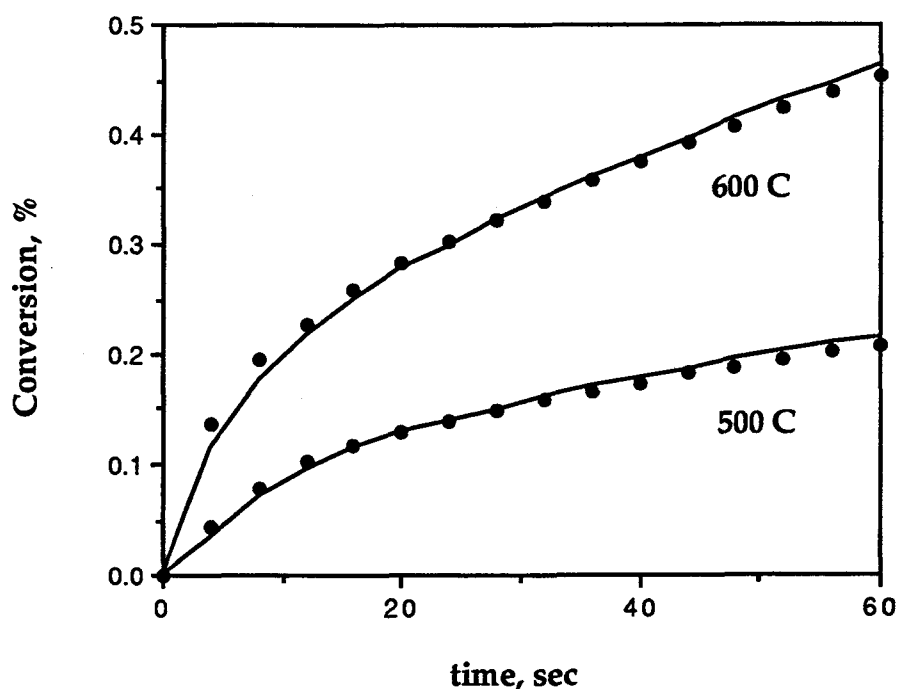
Figure 3.3 : The fit with shrinking unreacted core model with both chemical and diffusion control with Backman et al. (2) data at 500 and 600 °C.

When conversion versus time data at each temperature are fitted with the shrinking unreacted core model, the chemical kinetic rate constant (k_s) and effective diffusivity (D_e) at this temperature will be obtained. Chemical

kinetic rate constants and effective diffusivities at each temperature for the Backman et al. (2) data, determined from the fit with this model, are shown in Table 3.3.

Table 3.3 : Chemical kinetic rates and effective diffusivities at each temperature of Backman et al. (2) data determined from the fit with the shrinking unreacted core model

Temperature, ^oC	Chemical kinetic rate, cm./s	Effective diffusivity, cm^2/s
700	0.0946	5.08×10^{-6}
600	0.0584	1.71×10^{-6}
500	0.0144	2.84×10^{-7}
450	0.0029	8.15×10^{-8}
425	0.0025	6.46×10^{-8}
400	0.0016	2.44×10^{-8}
375	0.0012	1.48×10^{-8}
350	0.0007	5.75×10^{-9}

The activation energy of reaction can be determined by chemical kinetic rates at different temperatures. The Arhenius equation is used to calculated and is shown below :

$$k = k_o exp\, [-E_a/RT]$$

where   k   =   chemical kinetic rate

         k_o =   chemical kinetic rate constant

T   =   temperature

R   =   gas constant

E_a =   activation energy of reaction

$$\ln k = \ln k_0 - [E_a/R][1/T]$$

The activation energy of reaction can be determined from the slope of the Arhenius plot which is plotted as the logarithm of chemical kinetic rate constants and $1/T$ as shown in Figure 3.4. The activation energy of reaction calculated from the slope of Arhenius plot was 67 KJ/mol.
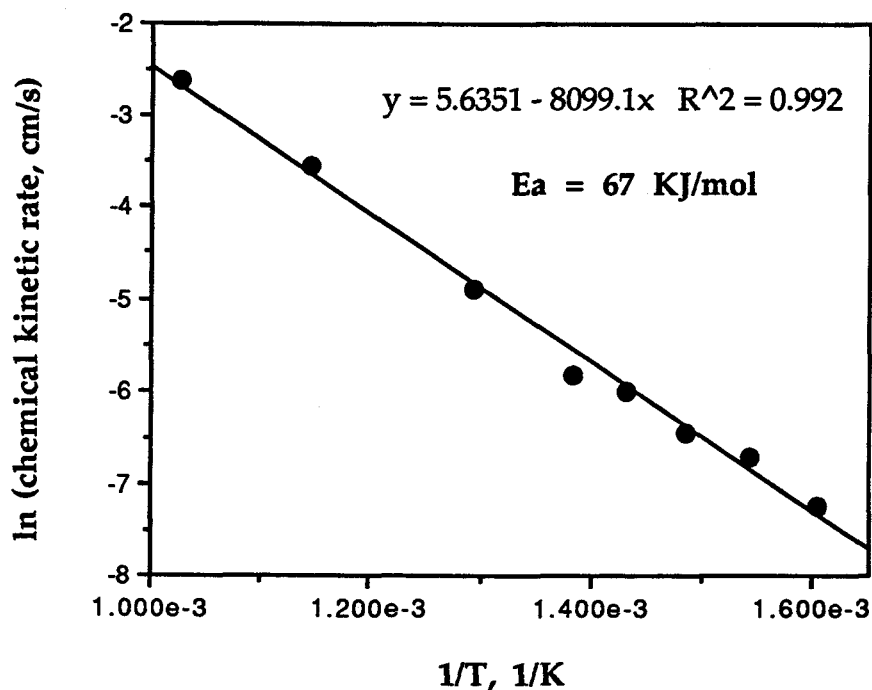
Figure 3.4 : Arhenius plot of chemical kinetic rate of Backman et al. (2) data

The apparent activation energy of the product layer diffusion can be determined in the same way of the activation energy of reaction. The Arhenius plot of the effective diffusivity of Backman et al. (2) is shown in Figure 3.5. The apparent activation energy of the product layer diffusion obtained from the slope of Arhenius plot was 98 KJ/mol.
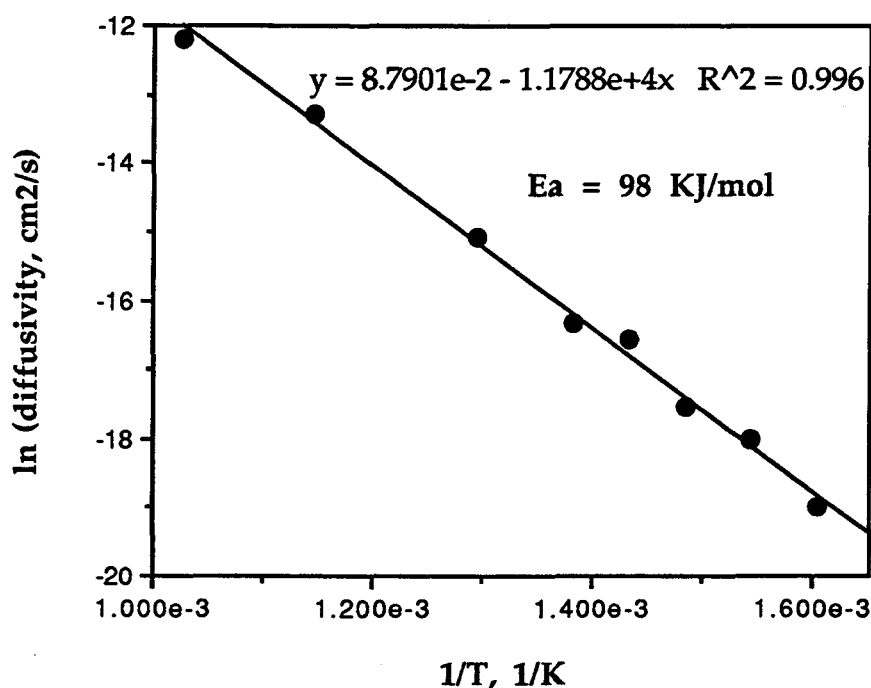
Figure 3.5 : Arhenius plot of effective diffusivity of Backman et al. (2) data

The chemical kinetic rates at different concentrations of the reacting gases with temperature and other gas concentrations kept constant were used to analyze the reaction order with respect to each gas species. Figure 3.6 shows the plot of the logarithm of SO_2 concentrations and the logarithm of the chemical kinetic rate, obtained from the initial slopes of the conversion versus time data of Backman et al. (2). The slope of this plot was

0.93 which was about one. It indicated that the chemical reaction is first order with respect to SO_2.

$$y = 0.42414 + 0.92980x \quad R^2 = 0.995$$
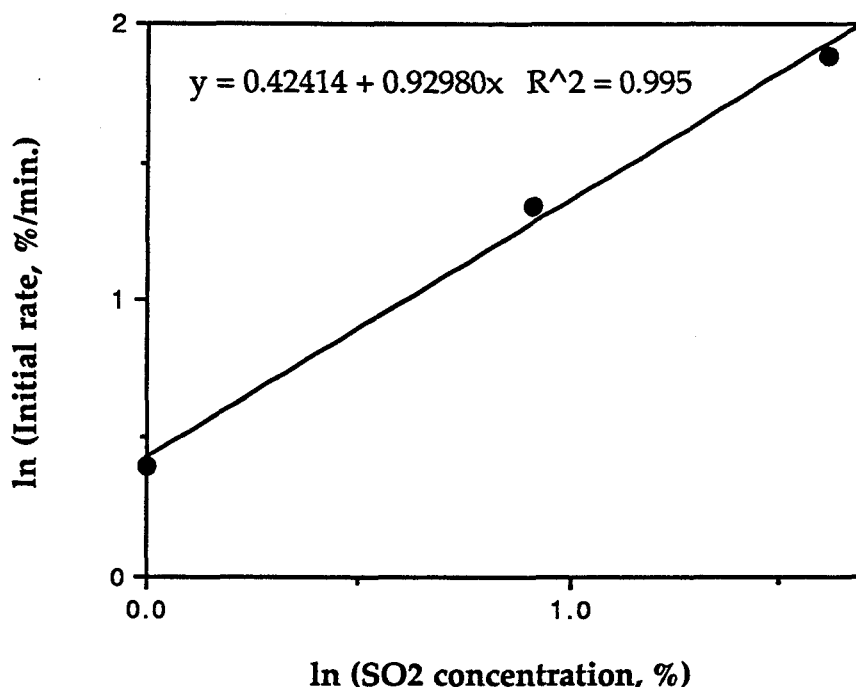
Figure 3.6 : The plot between the logarithms of SO_2 concentrations and the logarithms of chemical kinetic rates at 600 °C, 10% O_2 and 1-5 % SO_2 from Backman et al. (2) data.

The analysis of chemical kinetic rates at different O_2 concentrations was done with the same procedure as SO_2. Figure 3.7 shows the plot between the logarithm of O_2 concentrations and the logarithm of chemical kinetic rates. The slope of this plot was zero. It indicated that the chemical reaction is independent of O_2 concentration.

From rate equations of the shrinking unreacted core model (8) with each controlled process, conversion is the only time dependent variable.
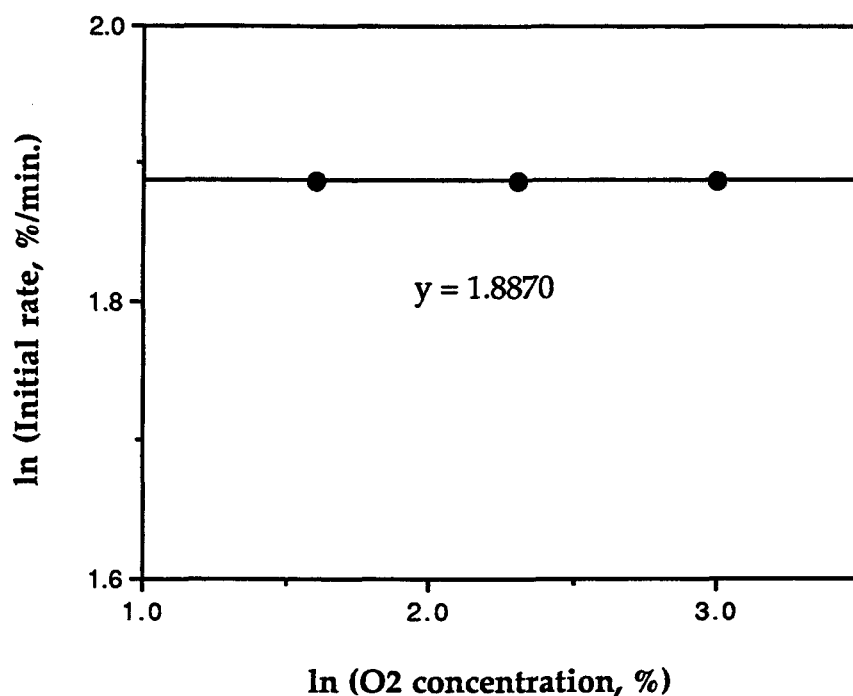
Figure 3.7 : The plot of the logarithms of O_2 concentrations and the logarithms of chemical kinetic rates at 600 °C, 5 % SO_2 and 5-20 % SO_2 from Backman et al. (2) data.

There should be a linear relationship between t and X, $f_1(X)$, for external mass transfer control, t and $1-3(1-X)^{2/3}+2(1-X)$, $f_2(X)$, for diffusion through product layer control and t and $1-(1-X)^{1/3}$, $f_3(X)$, for chemical reaction control. Thus the rate limiting step can be determined from the plot of t and $f_i(X)$. If any of them gives a straight line it implies that the reaction is controlled by that process. The functions are normalized by dividing them by the values of $f_i(X)$ at the end of sulfation to clearify the linear relationship of the plots.

Figure 3.8 shows the plots of t and $f_i(X)$. It implied that the rate limiting step of this reaction at 600 °C was diffusion through product layer

over most of the range of conversion. The plots were done for the range of the temperatures studied and the results were the same which implied that product layer diffusion limited this reaction between 350 to 700 °C except initially
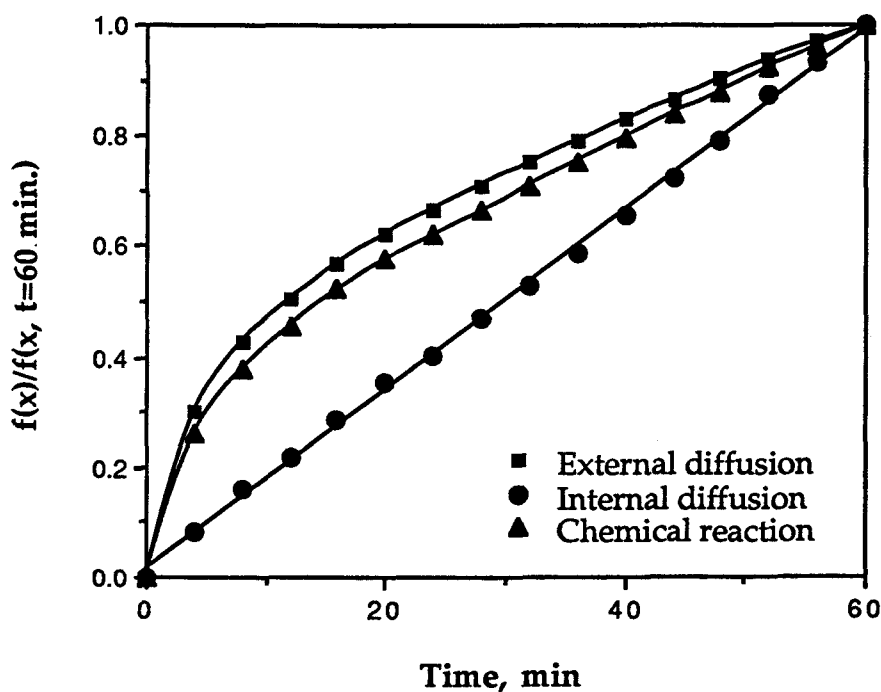
Figure 3.8 : The plots between t and $f(x)/f(x(t=60 \text{ min.}))$ from Backman et al. (2) data at T = 600 °C

Maule and Cameron (3) data were also fitted by the shrinking unreacted core model with both chemical reaction and diffusion through product layer control. The chemical kinetic rates and effective diffusivities calculated from the fit of this model with conversion versus time data at different temperatures are shown in Table 3.4.

Table 3.4 : Chemical kinetic rates and effective diffusivities at each temperature of Maule and Cameron (2) data determined from the fit with the shrinking unreacted core model

Temperature, $^{\circ}C$	Chemical kinetic rate, cm./s	Effective diffusivity, cm^2/s
246	0.0032	1.15×10^{-10}
224	0.0025	7.99×10^{-11}
204	0.0018	5.90×10^{-11}
177	0.0014	3.30×10^{-11}
149	0.0009	1.62×10^{-11}
121	0.0005	8.01×10^{-12}
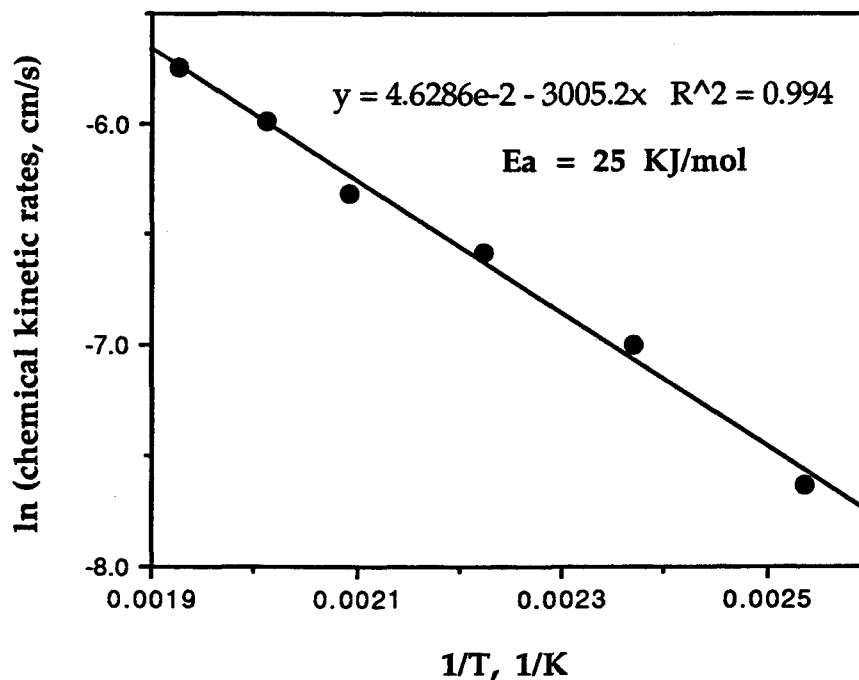
Figure 3.9 : Arhenius plot of chemical rates of Maule and Cameron (3) data

The Arhenius plot of chemical kinetic rate constants and effective diffusivities of Maule and Cameron (3) data are shown in Figure 3.9 and 3.10 respectively. The activation energy of the reaction calculated from Arhenius plot was about 25 KJ/mol whereas the apparent activation energy of effective diffusivity was 37 KJ/mol.
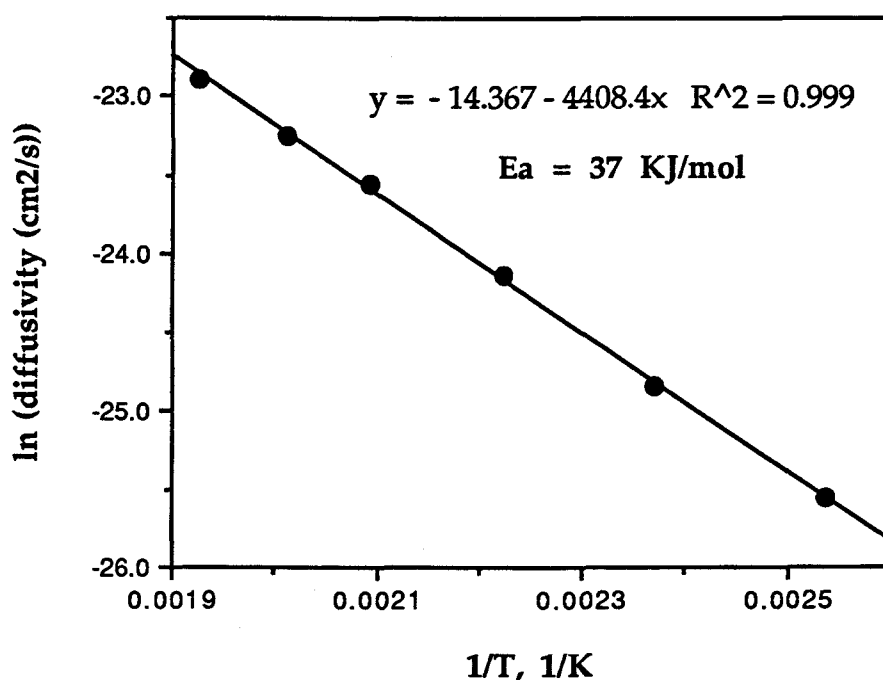
Figure 3.10 : Arhenius plot of effective diffusivities of Maule and Cameron (3) data

Keener and Davis (1) data were treated in different way with the former studies. The materials used in this study were porous and the reaction rate depened strongly on the particle size. It seemed that the initial reaction rate in this study was limited by both gas diffusion in the pores and chemical reaction. The general model for gas solid reaction developed by

Isidha and Wen (9,10,11) was used to fit the Keener and Davis data. This model is an intermediate model between the shrinking unreacted core model and the homogeneous model. The homogeneous model describes a gas solid reaction which the reaction occurs homogeneously throughout the solid to produce a gradual variation in solid reactant concentration in all parts of the particle. The general model for gas solid reaction accounts for both interfacial and intraparticle gradients. This model considers that the reaction is faster near the surface than in the interior of the particle, after a certain time the solid reactant near the surface will be completely exhausted forming an inert product layer, ash layer. The shrinking unreacted core model and the homogeneous model are also special cases of this model. The rate equations of this model are shown below :

$$k_v C_{ao} t = 1 + \left(1 - \frac{D'_{ea}}{Dea} \right) \ln \frac{\xi_m \sinh \phi'_v}{\sinh (\phi'_v \xi_m)} + \frac{\phi_v^2}{6} (1 - \xi_m)^2 (1 + 2\xi_m)$$

$$+ \frac{D'ea}{Dea} (1 - \xi_m) [\phi'_v \xi_m \coth (\phi'_v \xi_m) - 1] + \frac{\phi_v^2}{3N_{sh}} (1 - \xi_m^3)$$

$$+ \frac{\xi_m}{N'_{sh}} [\phi'_v \xi_m \coth (\phi'_v \xi_m) - 1]$$

$$X = 1 - \xi_m^3 + \frac{3\xi_m}{\phi'^2_v} [\phi'_v \xi_m \coth (\phi'_v \xi_m) - 1]$$

where   a   =   stoichiometric coefficient

C_{ao} =   initial concentration of fluid reactant in bulk gas

C_{so} = initial concentration of solid reactant

D_{ea} = effective diffusivity of fluid A in the ash layer

D'_{ea} = effective diffusivity of fluid A in the reaction zone

k_{ma} = mass transfer coefficient across the fluid film

k_v = reaction rate constant based on volume

N_{sh} = $k_{ma}R/D_{ea}$

N'_{sh} = $k_{ma}R/D'_{ea}$

r_m = radius at boundary between reaction zone and diffusion zone

R = particle radius

t = time

X = conversion

ξ_m = dimensionless radius = r_m/R

ϕ_v = $R\,[ak_vC_{so}/D_{ea}]^{1/2}$ = Thiele Modulus based on D_{ea} for the general model

ϕ'_v = $R\,[ak_vC_{so}/D'_{ea}]^{1/2}$ = Thiele Modulus based on Dea for the general model

When D_{ea} is equal to D'_{ea}, this model will be the homogeneous model. This model will be the shrinking unreacted core model if D'_{ea} is much less than D_{ea}.

The Keener and Davis (1) data was fitted with this model. The chemical kinetic rates and effective diffusivities determined from the fit at different temperatures are shown in Table 3.5.

Table 3.5 : Chemical kinetic rates and effective diffusivities at each temperature of Keener and Davis (1) data determined from the fit with the general model for gas solid reaction developed by Isidha and Wen (9,10,11)

Temperature, ^oC	Chemical kinetic rates, $cm^3/mol.s$	Effective diffusivity, $D_{ea}, cm^2/s$
343	2.1×10^8	3.0×10^{-4}
289	6.0×10^7	7.5×10^{-5}
232	1.7×10^7	2.2×10^{-5}
177	2.0×10^6	2.4×10^{-6}

Figure 3.11 : Arhenius plot of chemical kinetic rates of Keener and Davis (1) data

The Arhenius plot of chemical kinetic rates and effective diffusivities of Keener and Davis (1) data are shown in Figure 3.11 and 3.12 respectively. The activation energy of the reaction obtained from Arhenius plot was about 64 KJ/mol whereas the apparent activation energy of effective diffusivity was 66 KJ/mol.
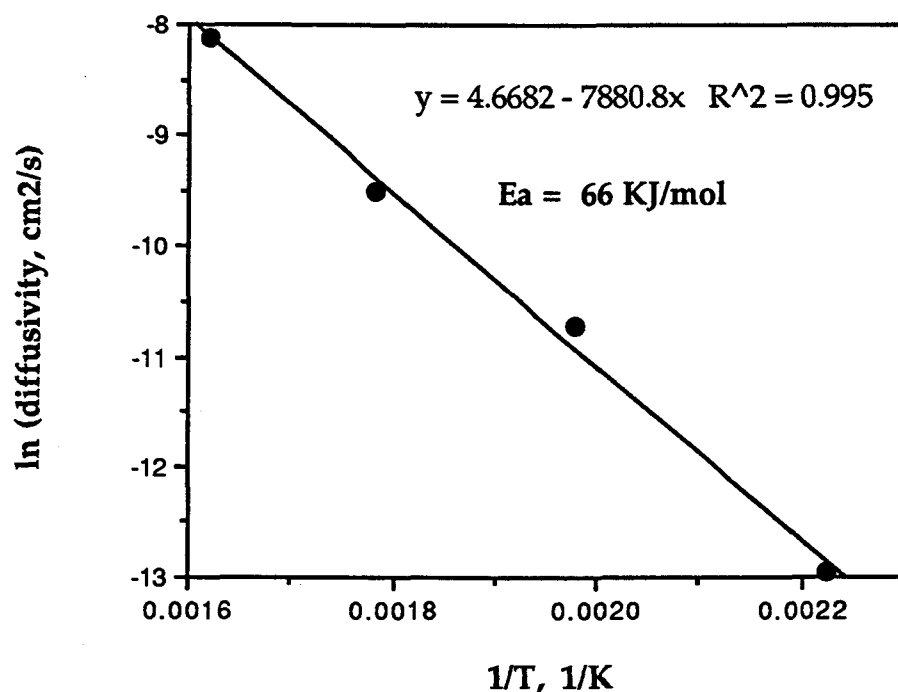
Figure 3.12 : Arhenius plot of effective diffusivities of Keener and Davis (1) data

3.2 Analysis

The abnormal temperature dependence of the sulfation of Na_2CO_3 in the presence of O_2 reported in Lloyd-George (4) study was between 350 - 550

^{o}C at 20 % SO_2. Backman et al. (2) reported a similar abnormal temperature dependence in the range of 350 - 450 ^{o}C at 5 % SO_2. This effect was interpreted to be caused by sintering by Backman et al. (2) and by sodium pyrosulfate formation in the Llyod-George study.

It is interesting that Backman et al. (2) changed two factors to eliminate this effect. The first was the use of presintered particles and the second was non-metallic parts in high temperature lines to avoid uncontrolled oxidation of SO_2 to SO_3. It implies that the elimination of the abnormal temperature dependence may be from the use of presintered paricles, or from the elimination of SO_3 or from both of them.

If the effect of this abnormal behavior is from presintered particles, the abnormal temperature ranges should be the same but they are not. Thus the effect should be the sodium pyrosulfate formation. Sodium pyrosulfate is formed from the reaction between Na_2SO_4 and SO_3. The begining for abnormal temperature ranges for both studies were 350 ^{o}C. This should be the initial temperature that sodium pyrosulfate can form. At higher SO_3 concentrations, sodium pyrosulfate will be stable over a wider range of temperature. This could be the reason why the abnormal temperature range for the Lloyd-George (4) study is higher than that in Backman et al. (2) study. There was no SO_3 formed in Backman et al. (2) study after the metal parts in the experimental system were replaced with quartz so there was no sodium pyrosulfate formed. This could be the reason why no abnormal temperature dependence was obtained after the metal parts were replaced by quartz.

The resulting activation energies of reaction and apparent activation energies of effective diffusivity calculated from the models used to fit the existing data is shown on Table 3.6.

Table 3.6 : The activation energy for the chemical reaction and the apparent activation energy for product layer diffusion in the sulfation of Na_2CO_3

	Keener and Davis (1)	Backman et al. (2)	Maule and Cameron (3)
Chem. Reaction, Ea, KJ/mol	64	67	25
Diffusion, Ea, KJ/mol	66	98	37

For all of these studies, the limiting step of this reaction over most of the range of conversion was diffusion through product layer which was Na_2SO_4. The apparent activation energies of the effective diffusivity in all of these studies were very high, with the highest 98 KJ/mol in the Backman et al. (2) data. These values are too high for bulk gas diffusion or Knudsen diffusion. It was suggested that the diffusion through product layer may be solid state diffusion.

Further analysis for the validity of the hypothesis that diffusion through product layer may be solid state diffusion was made to check the dependence of the diffusion rate on the gas concentration. Based on the shrinking unreacted core model, the rate equation for diffusion through product layer control is :

$$C_A = \frac{\rho R^2}{6bD_e t} [1-3(1-X)^{2/3}+2(1-X)]$$

$$\ln C_A = \ln \frac{\rho R^2}{6bD_e t} + \ln [\ 1\text{-}3(1\text{-}X)^{2/3}+2(1\text{-}X)\ ]$$

During each experiment, b, De, C_A, R and ρ may be approximated to be constant. Thus time and conversion are the only variables changed during each experiment. For diffusion through product layer control, we should get a straight line from a plot of $\ln C_A$ versus $\ln [\ 1\text{-}3(1\text{-}X)^{2/3}+2(1\text{-}X)\ ]$ at a specific reaction time.

Figure 3.13 and 3.14 show the plot between $\ln C_{SO_2}$ and $\ln [\ 1\text{-}3(1\text{-}X)^{2/3}+2(1\text{-}X)\ ]$ at t = 40 min. and between $\ln C_{O_2}$ and $\ln [\ 1\text{-}3(1\text{-}X)^{2/3}+2(1\text{-}X)\ ]$ at t = 40 min. from Backman et al. (2) respectively. The plots are nonlinears
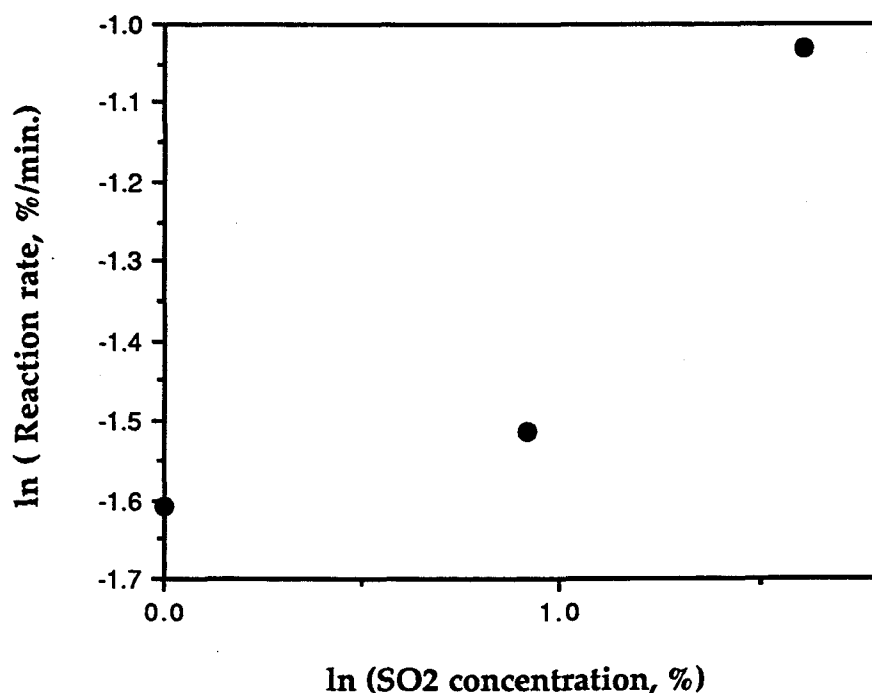
Figure 3.13 : The plot between $\ln C_{SO_2}$ and $\ln [\ 1\text{-}3(1\text{-}X)^{2/3}+2(1\text{-}X)\ ]$ at t = 40 min. from Backman et al. (2) data
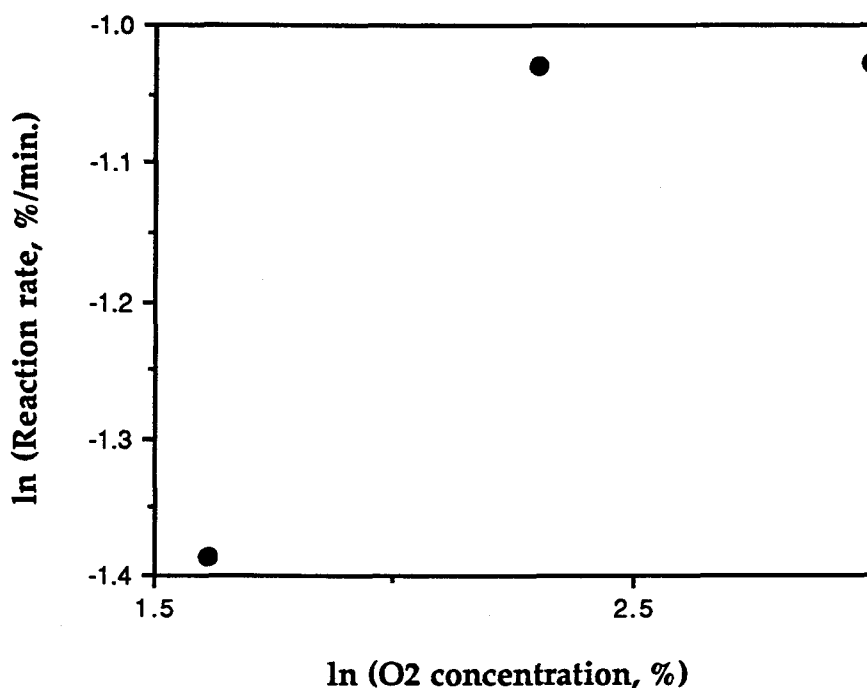
Figure 3.14 : The plot between ln C_{O_2} and ln [$1-3(1-X)^{2/3}+2(1-X)$] at t = 40 min. from Backman et al. (2) data

which implied that gas phase SO_2 and O_2 were not diffusing species. Based on these two reasons, the high apparent activation energy for effective diffusivity and SO_2 and O_2 were not diffusing species, the diffusion of this reaction was most likely solid state diffusion. Iisa et al. (12) reported that the rate of sulfation of $CaCO_3$ was also controlled by solid state diffusion.

The activation energies of chemical reaction determined from Keener and Davis (1) and Backman et al. (2) were in the same order of magnitude. However the activation energy from Maule and Cameron (3) data was considerably lower than others. The possible reason why Maule andCameron (3) obtained a very low activation energy of reaction was

because of materials used in their study. They used very fine particles which sintered, during sulfation and as a result, the particles grew together, decreasing the available surface area for reaction. The sintering reduced the reaction rate at higher temperature and thus diminished the apparent activation energy of the chemical reaction. This implied that Maule and Cameron (2) data may be relevant for fume particles in deposits in which sintering is important. However, these data may not be applicable for sulfur capture by fume particles in-flight.

The kinetic data calculated was used to predict the conversion of Na_2CO_3 to Na_2SO_4 in solid fume particles in recovery boilers from the entrance of the boiler bank to the economizer exit. The calculations were
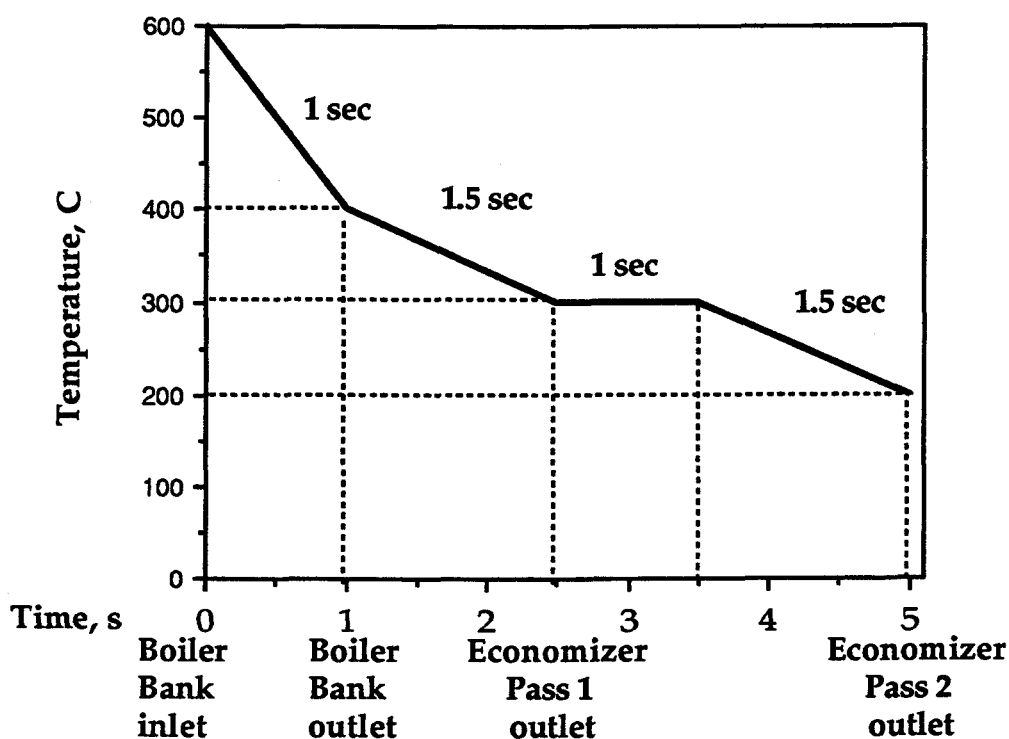
Figure 3.15 : The residence time and temperature used in the calculation of the sulfation of in-flight Na_2CO_3 particles.

based on the assumption that the particles had become 50% sulfated in the molten stage, that Na_2CO_3 and Na_2SO_4 were uniformly distributed throughout the particles, and that the particle temperature was the same as the flue gas temperature. The kinetics and diffusion rates used in the calculation were based on Backman et al. (2) data. The time-temperature profile of the Na_2CO_3 particles that was used in the calculations is shown in Figure 3.15. The profile represents that of a typical kraft recovery boiler from the entrance of the boiler bank to the economizer exit.

The conversions of Na_2CO_3 to Na_2SO_4 calculated are shown in Figure 3.16 and 3.17. Figure 3.16 shows the conversion of 1 µm particle at
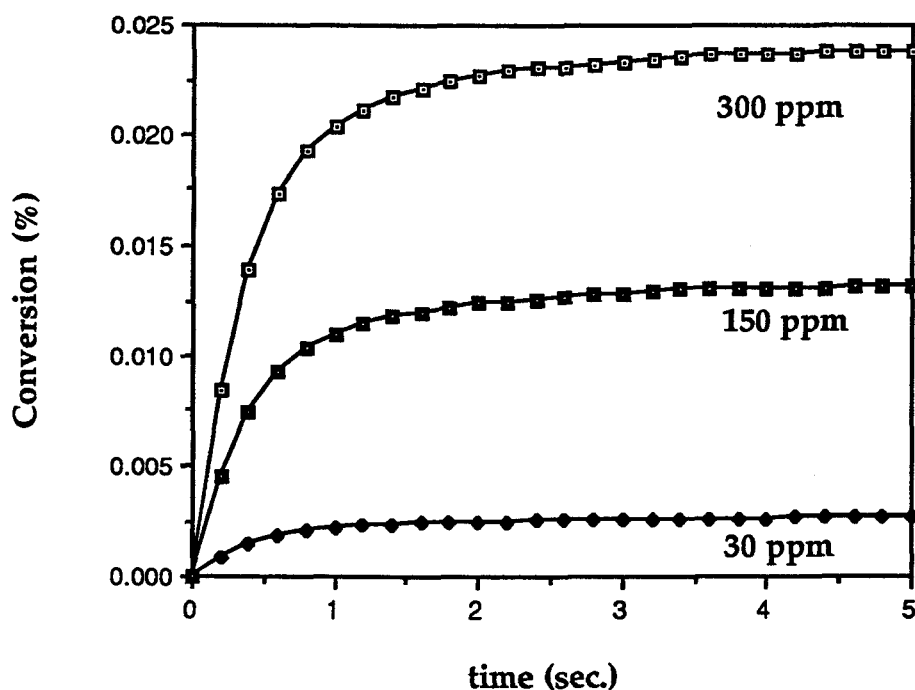
Figure 3.16 : The conversion of Na_2CO_3 to Na_2SO_4 of 1 µm particle at 30, 150 and 300 ppm of SO_2.
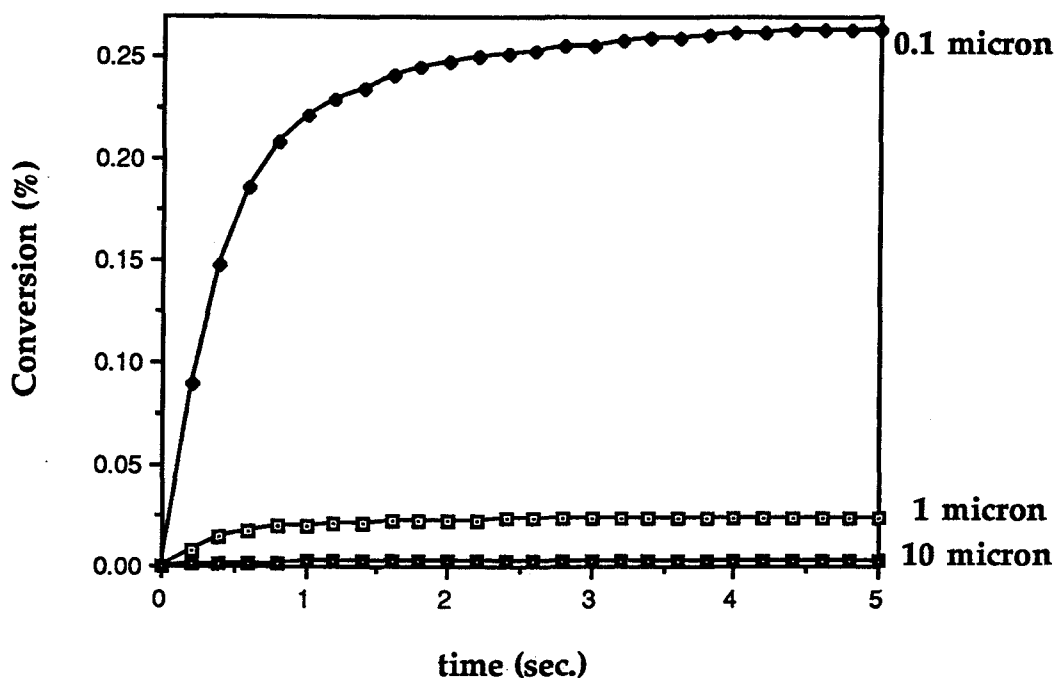
Figure 3.17 : The conversion of Na_2CO_3 to Na_2SO_4 at 300 ppm of SO_2 for 0.1, 1, 10 µm particles.

different SO_2 concentration whereas Figure 3.17 shows the conversion at 300 ppm of SO_2 concentration for different Na_2CO_3 particle sizes.

The conversions of Na_2CO_3 to Na_2SO_4 were very low at these conditions, only 0.14 % conversion for 0.1 µm particle at 300 ppm SO_2. Based on this result, it was unlikely that significant SO2 capture occurs by the Na_2CO_3 in fume particles after they leave the superheater. This suggests that the sulfation of fume particles in-flight occurs when the furnace particles are still molten, i.e. before the boiler bank.

CHAPTER 4

EXPERIMENTAL METHODS

4.1 Materials

The materials used in this experiment are NaCl (sodium chloride) , SO_2 (sulfur dioxide), O_2 (oxygen), N_2 (nitrogen) and H_2O (v) (water vapor).

NaCl was prepared by grinding reagent grade NaCl and then seiving with U.S.A. standard testing seive, A.S.T.M.E.-11 specification. The NaCl fractions used in this study were those passing through a seive and collecting on number 60, 120, 170 and 230 seives. The sizes of NaCl were in the range of 125-250, 90-125 and 63-90 μm respectively.

The SO_2, O_2 and N_2 were purchased as pressurized gases with the following concentrations :

SO_2 : 5 % in N_2

O_2 : 21 % in N_2 (compressed air)

N_2 : 100 %

Water vapor was obtained by passing air with constant flow rate through deionized water in an electrical constant temperature bath.

4.2 Instrumentation

The details of each equipment in this experiment are as followed :

Reactor - The reactor used in this experiment was a fixed bed reactor. It was a quatz glass tube which was 2 cm. inside diameter and 90 cm. long. A fritted quartz glass was placed in the center of the reactor to support NaCl.

The fritted quartz glass was removable for easiness to clean the reactor after each run. Quartz wool was placed between NaCl and fritted quartz glass to protect NaCl leakage on the space between fritted quartz glass and reactor.

Thermocouple - The thermocouple in this experiment was K type stainless steel thermocouple, with a temperature range of -200 to 1250 °C.

Temperature Controller - The temperature controller used was microprocessor based (OMEGA CN76000) with solid state relay output.

Furnace - The furnace used was from Hevi-Duty Electric Company. The maximum operating temperature in the experiment was 600 °C.

Rotameter - The rotameters in this experiment were standard 150 mm. flowmeter with high resolution valve. The non-glass components of the rotameters was aluminum for air and N_2 and 316 stainless steel for SO_2. The accuracy of these rotameters was ± 2 %.

Tubing - There were two types of tubing used in this experiment. Both of them were 1/4 inches outside diameter. One was polyethylene tubing which was used for the dry gas lines which were at room temperature. The other was teflon tubing which was used for heating lines for gases which contained water vapor and for HCl.

Heating Tape - The heating tapes used were thermolyne flexible heating tape.

Water Bath - The water bath used was BUCHI 461. The temperature range was from 30 - 100 °C.

Absorption Bottle - It was 250 ml gas washing bottle with a 12 mm. dia. fritted cylinder which provided for uniform dispersion of gas bubbles for complete absorption.
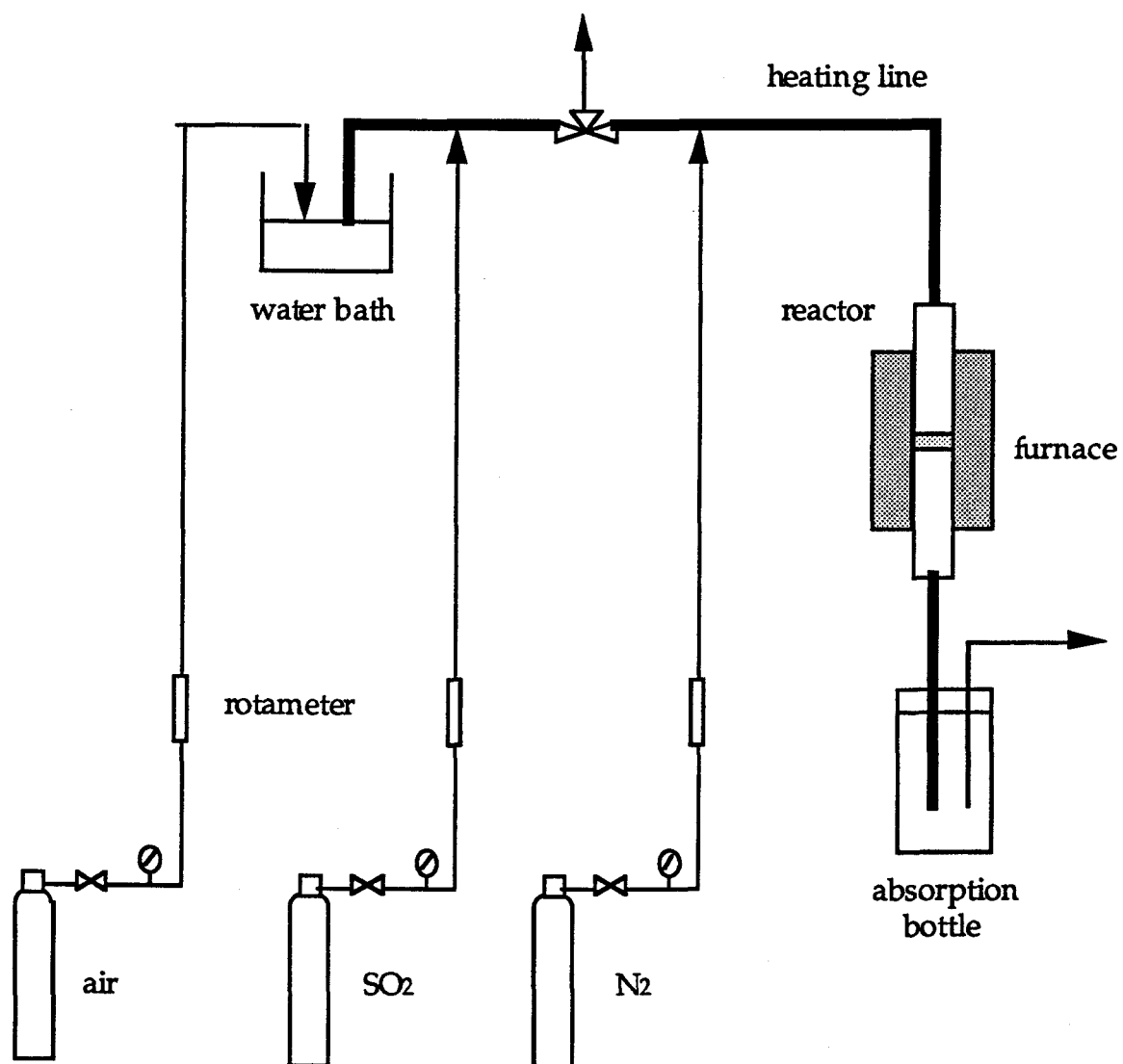
Figure 4.1 : Flow diagram of the experiment

4.3 Process Description

The flow diagram of this experiment is shown in Figure 4.1. Air, O_2 and SO_2 from their tanks were passed through rotameters to get the desired flow rate. Air was saturated with water by passing into deionized water in an absorption bottle which was immersed in a constant temperature water bath. The tubing in which the moist air flowed from the water bath was heated by heating tape along the line to prevent the water from condensing. The moist air was mixed with SO_2 and N_2 before passing through the reactor.

The mixed gas flowed into the fixed bed reactor which contained NaCl placed on the quartz wool and fritted quartz glass. The operating temperature was measured by a thermocouple placed inside just above the NaCl bed.

The product gas from the reactor was heated along the line to prevent HCl and water vapor from condensing in them. The product gas flowed into deionized water in an absorption bottle where the HCl was absorbed. The chloride ion concentration was measured with a chloride specific ion electrode.

4.4 Operating Procedure

Preheating

1. Open valve and gas regulator of N_2.
2. Control N_2 flow rate at 10 cm^3/sec..

3. Set the furnace temperature controller at the desired temperature and turn on the furnace.

4. Wait until the reactor temperature reaches desired temperature.

Reaction

1. Heat the deionized water in the water bath to the desired temperature.

2. Open the valves and gas regulators for SO_2 and air.

3. Adjust the flow rate of SO_2, N_2 and air through the rotameters.

4. Switch the mixed gas to the reactor, replacing the N_2.

5. Change the deionized water in the absorption bottle every 30 min. for 3 hr..

6. Switch the N_2 to reactor instead of the mixed gas whenever changing the deionized water in the absorbtion bottle.

7. Measure the chloride ion concentration with the chloride specific ion electrode.

8. Cool the furnace to room temperature and collect the residual solid in the reactor.

9. Clean the fritted quartz glass and reactor.

4.5 Gas Analysis

HCl Recovery by Absorption

A preliminary test was made to determine whether all of the HCl generated in the reactor would be adsorbed in a single absorption bottle. In

this test, a gas containing 1% HCl with the balance N_2 was passed through two absorption bottles in series. The gas was passed into these two absorption bottles for 30 min. with varied flow rate from 5-15 cm^3/sec. The chloride ion concentrations in both absorption bottles were checked.

98 % of the chloride input was collected in the first bottle and no chloride was detected in the second bottle. This implied that if the experiment was run under the conditions employed, the chloride amounts can be completely absorbed in one absorption bottle.

Chloride Specific Ion Analysis Method

The chloride ion concentration was measured by a chloride specific ion electrode. The electrodes used were a chloride electrode and a reference electrode. The reference electrode was a double junction electrode which contained saturated KCl and 10% KNO_3. Equal volumes of 10% KNO_3 and sample or standard had to be mixed together before each analysis. The 10% KNO_3 was an ionic strength adjustment buffer solution that brings all solutions to essentially the same ionic stregth so that the chloride activity coefficients were equal in all cases. The calibration graph of chloride is shown in Appendix A.

4.6 Residual Solid Analysis

Some of the residual solid samples from the reactor were sent to the Weyerhaeuser Company analytical laboratory in Tacoma, WA for analysis of sodium, chloride and sulfate content. The chloride and sulfate test were run

by MCAWW method 300.0, the determination of inorganic anions in water by ion chromatography or TAPPI T699 om-87, analysis of pulping liquors by suppressed ion chromatography. The sodium test was run by atomic absorption flame spectrometry on the hydrochloric acid soluble samples.

4.7 Surface Area Analysis

The internal surface areas of different solid NaCl particle sizes were measured by BET analysis. The analysis gas used in these measurements was N_2. All samples were heated for degasification at 150 $^\circ$C overnight before each analysis.

CHAPTER 5

RESULTS AND DISCUSSION

5.1 Gas Analysis

The chloride generated in the reactor was absorbed in deionized water and was detected by a chloride specific ion electrode. The amounts of chloride for each time range were converted to NaCl conversion versus time data. The plots showed very good linear relationship for all of the experiments. The reaction rate was calulated from the slope of the graph between conversion and time. An example of the reaction rate calculation is shown in Figure 5.1. The reaction rate of this example was 3.78×10^{-3} %/min..
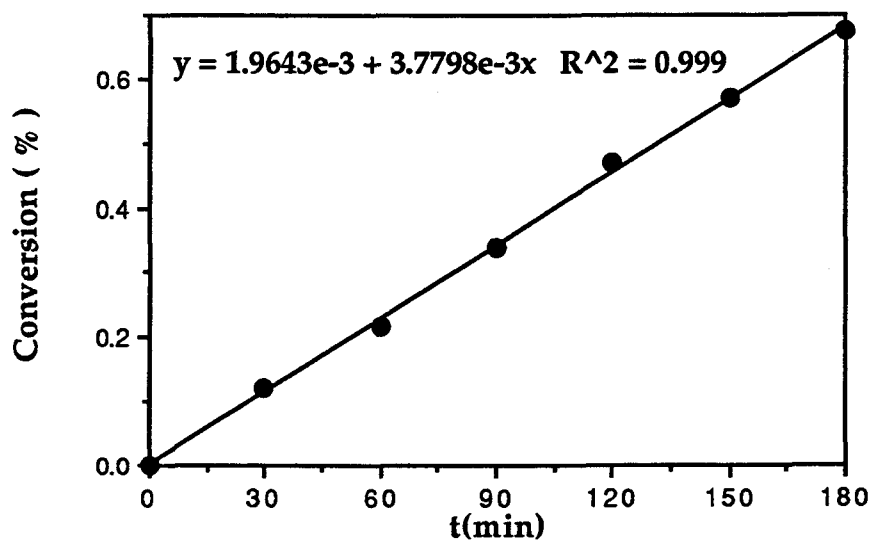
Figure 5.1 : An example of the reaction rate calculation

Reproducibility

The reaction rates between each time range of this example were calculated and shown in Table 5.1. These reaction rates were close to each other and to the reaction reate obtained from the whole range of time studied. It was good enough to estimate and predict the reaction rates by linear relationship.

Table 5.1 : Reaction rates at each range of time, their average standard deviaiton and coefficient of variation

time, min.	Reaction Rate, %/min.
0-30	4.00×10^{-3}
30-60	3.33×10^{-3}
60-90	4.00×10^{-3}
90-120	4.33×10^{-3}
120-150	3.33×10^{-3}
150-180	3.67×10^{-3}
0-180	3.78×10^{-3}
Standard deviation	4.04×10^{-4}
Coefficient of variation	10 %

5.2 Residual Solid Analysis

The residual solid products from several runs were sent to the Weyerhaeuser Company analytical laboratory in Tacoma, WA for sodium, chloride and sulfate analysis. The results are shown in Table 5.2.

Table 5.2 : Residual solid analysis for sodium, chloride and sulfate contents

Run No.	Na (%)	Cl (%)	SO_4 (%)
10	37.4	59.5	0.680
14	37.7	60.4	0.528
20	38.3	59.6	0.336

The conversions of NaCl from these results were calculated to compare with the values obtained from the gas analysis. The conversion comparisons are shown in Table 5.3. These showed a very good agreement between residual solid and gas analysis.

5.3 Surface Area Analysis

The total surface area of NaCl particles were measured by BET analysis with N_2 adsorption. The results are shown in Table 5.4.

Table 5.3 : Comparison of the degree of conversion obtained by residual solid and gas analysis. The results are expressed as percent conversion of the NaCl charged to the reactor

Run No.	Residual solid analysis (%)	Gas analysis (%)
10	0.64	0.61
14	0.83	0.81
20	0.41	0.43

Table 5.4 : The total surface area of NaCl particles by BET analysis

Particle size (μm)	Area (m^2/g)
63-90	0.289 ± 0.008
90-125	0.181 ± 0.006
125-250	0.134 ± 0.005

5.4 Gas Flow Rate Effect

The initial experiments were run to determine the operating conditions at which external mass transfer through the gas boundary would be negligible. The experiments were operated at different flow rate at 500 $^{\circ}$C, 0.3 % SO$_2$, 5 % O$_2$, 10 % H$_2$O and 2 g of 125-250 μm NaCl. The total gas flow rates were in the range of 5-15 cm^3/s. The conversion rates at different flow rates were shown in Figure 5.2. The conversion rate was increased with a

increase of flow rate below 10 cm^3/s and was constant above this gas flow rates. Thus the conversion rate was unaffected by total gas flow rates above 10 cm^3/s for temperatures below 500 °C. It implied that external mass transfer through the gas boundary can be negligible at the total gas flow rate above 10 cm^3/s. To ensure that this effect will not affect the reaction at temperature below 500 °C, the experimental data were obtained at the total gas flow rate 15 cm^3/s.
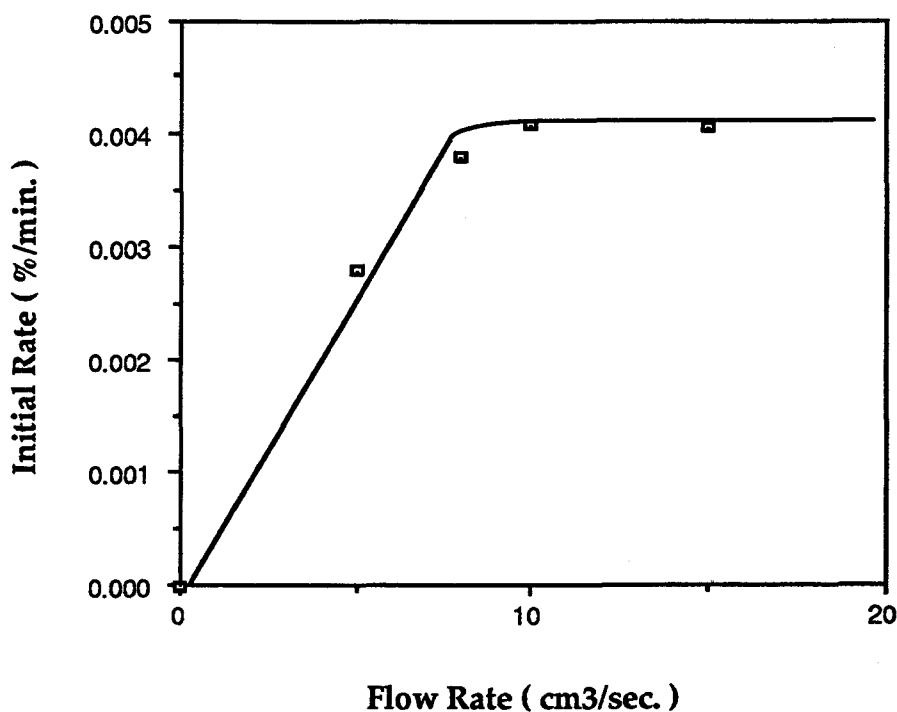
Figure 5.2 : The conversion rates of flow rate 5, 8, 10, 15 cm^3/s (20 °C, 1 atm) total flow rate at 500 °C, 0.3 % SO_2, 5 % O_2, 10 % H_2O and 2 g of 125-250 μm NaCl.

The calculation for external mass transfer effect at 600 °C of these experimental conditions is shown in Appendix C. This also implied that

external mass transfer effect can be negligible at the total flow rate 15 cm^3/s at temperature below 600 ^oC.

5.5 Particle Size Effect

The different particle sizes, 125-250, 90-125 and 63-90 μm, were used to study the particle size or porous effect. These experiments were run at 15 cm^3/s (20 ^oC, 1 atm) total flow rate, 500 ^oC, 0.3 % SO_2, 5 % O_2, 10 % H_2O and 2 g of 125-250 μm NaCl. The conversion versus time data for different particle sizes is shown in Figure 5.3.
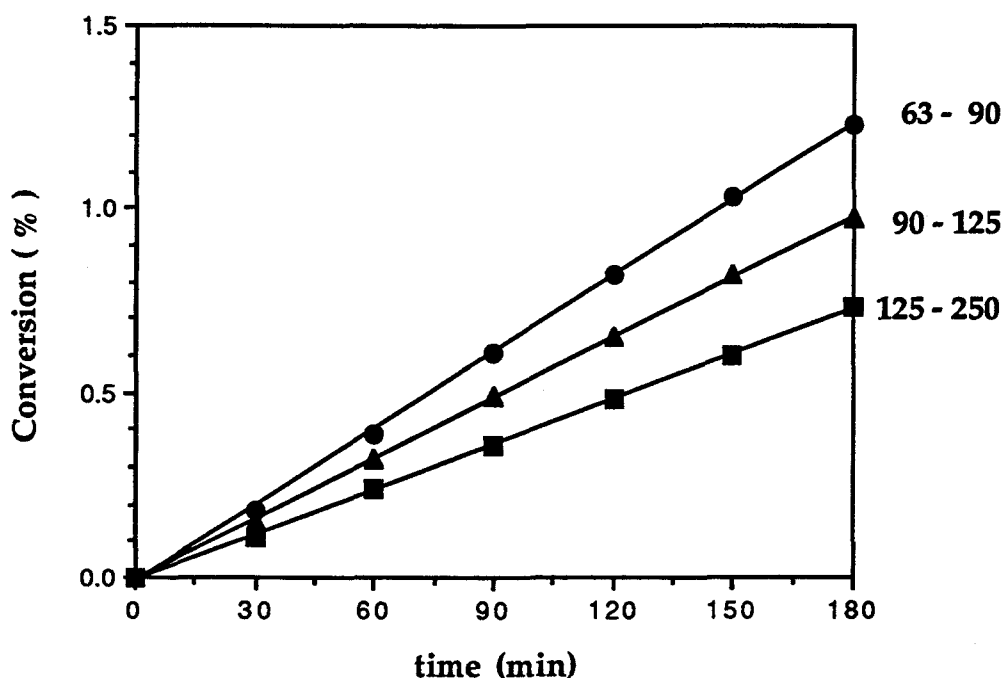
Figure 5.3 : The conversion versus time data of 125-250, 90-125 and 63-90 μm particles at 15 cm^3/s (20 ^oC, 1 atm) total flow rate, 500 ^oC, 0.3 % SO_2, 5 % O_2, 10 % H_2O and 2 g of NaCl.

The chemical kinetic rates of different particle sizes were compared to consider the porous effect. The calculations were done based on both external surface area and total surface area. The details of the calculation are shown below :

$$\text{mole } SO_2 \text{ reacted} \quad = \quad k\, S\, f(P_{SO_2})$$

$$\text{mole NaCl reacted} = \quad (dX/dt)V\rho/M$$

where k = chemical kinetic rate (cm/s)

S = surface area per particle

C_{SO_2} = SO_2 concentration

V = volume per particle

X = conversion

t = time

ρ = density of NaCl = 2.15 g/cm^3

M = molecular weight of NaCl   = 58.5

dX/dt = slope of conversion versus time data

from stoichiometric coefficient, we will get :

$$2\, k\, S\, f(P_{SO_2}) = (dX/dt)V\rho/M$$

for total surface area, specific surface area per one gram of particles = $S' = S/\rho V$, so we will get :

$$k = (dX/dt)(1/2S'M\ f(P_{SO_2}))$$

for different particle sizes at the same conditions :

$$\frac{k_1}{k_2} = \frac{(dX/dt)_1 \, (S'_2)}{(dX/dt)_2 \, (S'_1)}$$

based on these calculations we will get :

k (63-90 μm) = 1.26 k(125-250 μm)

k (90-125 μm) = k(125-250 μm)

Table 5.5 : shows the chemical kinetic rates of different particle sizes based on total surface area. The calculations are shown in Appendix D.

Table 5.5 : The chemical kinetic rates of different particle sizes based on total surface area

Particle size (μm)	k (mol/m^2.atm.min)	k/k(125-250 μm)
63- 90	$1.25 \times 10^{-3} \pm 3.98 \times 10^{-5}$	1.0 ± 0.002
90-125	$1.58 \times 10^{-3} \pm 4.28 \times 10^{-5}$	1.3 ± 0.004
125-250	$1.25 \times 10^{-3} \pm 3.75 \times 10^{-5}$	1

From these rate calulations, it implied that there is no significant influence from porous effect.

5.6 Temperature Effect

The temperature range of the study was 400 - 600 °C. These experiments were run at 15 cm^3/s (20 °C, 1 atm) total flow rate, 0.3 % SO_2, 5 % O_2, 10 % H_2O and 2 g of 125-250 μm NaCl. The conversion versus time data for the sulfation of NaCl at different temperatures are shown in Figure 5.4. The rate of SO_2 capture by NaCl was not strongly temperature dependent, increasing by slightly more than a factor of two over the temperature range 400 - 600 °C.
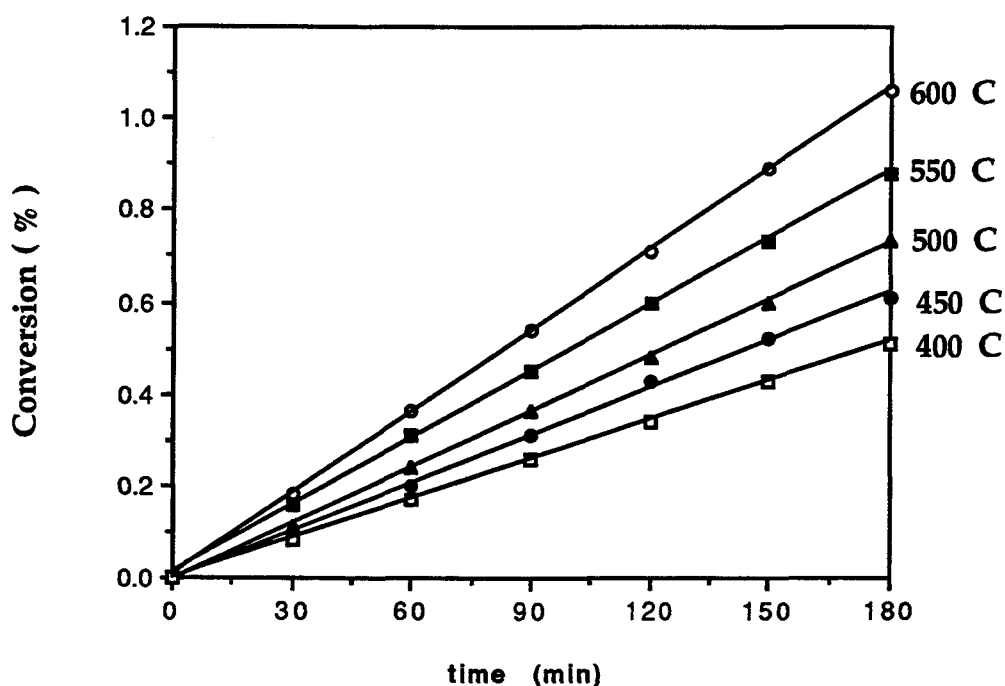
Figure 5.4 : The conversion versus time data of temperature 400, 450, 500, 550 and 600 °C at 15 cm^3/s (20 °C, 1 atm) total flow rate, 0.3 % SO_2, 5 % O_2, 10 % H_2O and 2 g of 125-250 μm NaCl.

The reaction rate increased with temperature throughout the temperature range studied. The Arhenius plot of reaction rate is shown in Figure 5.5. The activation energy of reaction was determined to be 17.3 KJ/mol which was quite low for a chemical kinetic-controlled process. The low activation energy may indicate that a physical adsorption-desorption process was the rate-controlling step. (16)

$y = -2.7797 - 2084.0x \quad R^2 = 0.991$
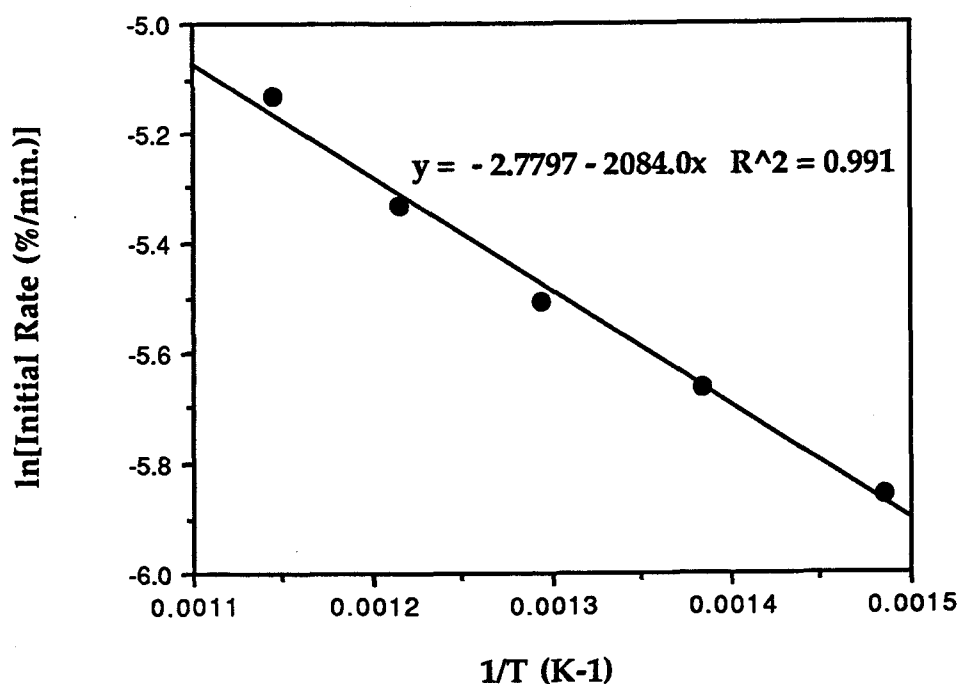
Figure 5.5 : The Arhenius plot of reaction rate

In the Henriksson and Warnqvist (13) data, there was an abnormal temperature dependence below 500 °C. This abnormal behavior was not observed in this study. It could have been the result of sodium pyrosulfate formation as suggested by Lloyd-George (4). In this study, the high

temperature parts of the equipments were non-metallic so no oxidation of SO_2 to SO_3 occured. Thus there was no sodium pyrosulfate formed at this condition. The other possibility was the sintering effect as observed by Backman et al. (2).

5.7 SO_2 Concentration Effect

The effect of SO_2 dependence was studied at a constant reaction temperature of 500 °C. The SO_2 concentration range studied was from 0.3 - 1.1 %. The conditions of the SO_2 dependence study were 15 cm^3/s (20 °C, 1
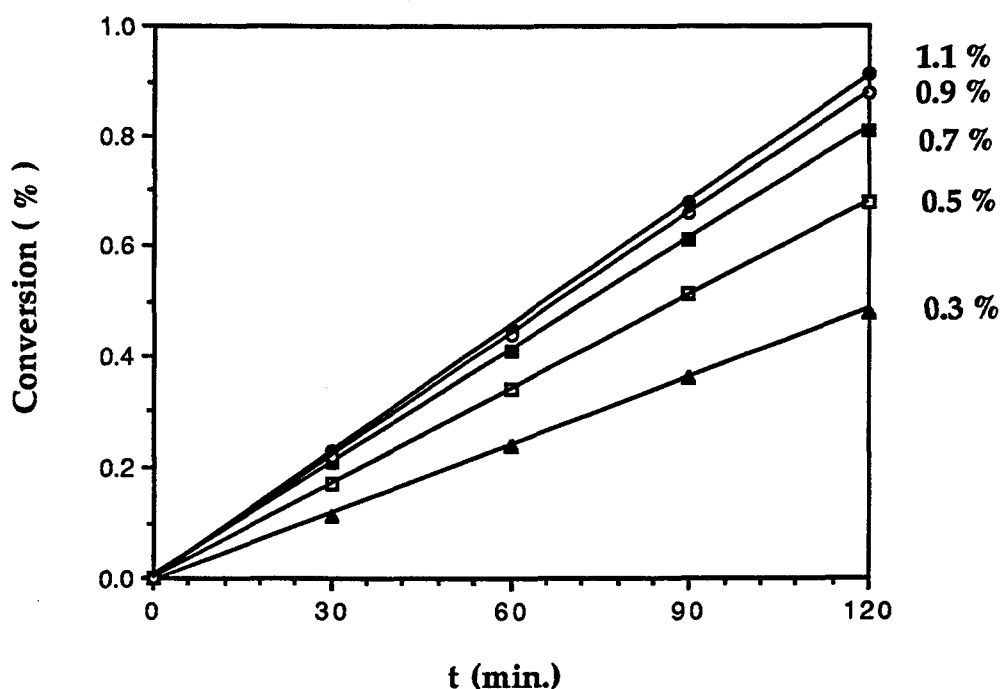
Figure 5.6 : The conversion versus time data of 0.3, 0.5, 0.7, 0.9 and 1.1 % SO_2 concentrations at 15 cm^3/s (20 °C, 1 atm) total flow rate, 500 °C, 5 % O_2, 10 % H_2O and 2 g of 125-250 μm NaCl.

atm) total flow rate, 500 °C, 5 % O_2, 10 % H_2O and 2 g of 125-250 μm NaCl. The conversion versus time data for different SO_2 concentrations are shown in Figure 5.6.

The data was analyzed further to find the reaction order with respect to SO_2. To find this reaction order, the logarithm of the chemical kinetic rate was plotted against the logarithm of SO_2. This plot is shown in Figure 5.7. The chemical kinetic rate increased with SO_2 concentrations and was less dependent on SO_2 concentration at higher SO_2 concentrations. The slope of this curve which was the order of reaction with respect to SO_2 decreased from 0.67 at the lowest SO2 concentrations used to 0.16 at the highest. This indicated that SO_2 was involved in the rate limiting step of the reaction.
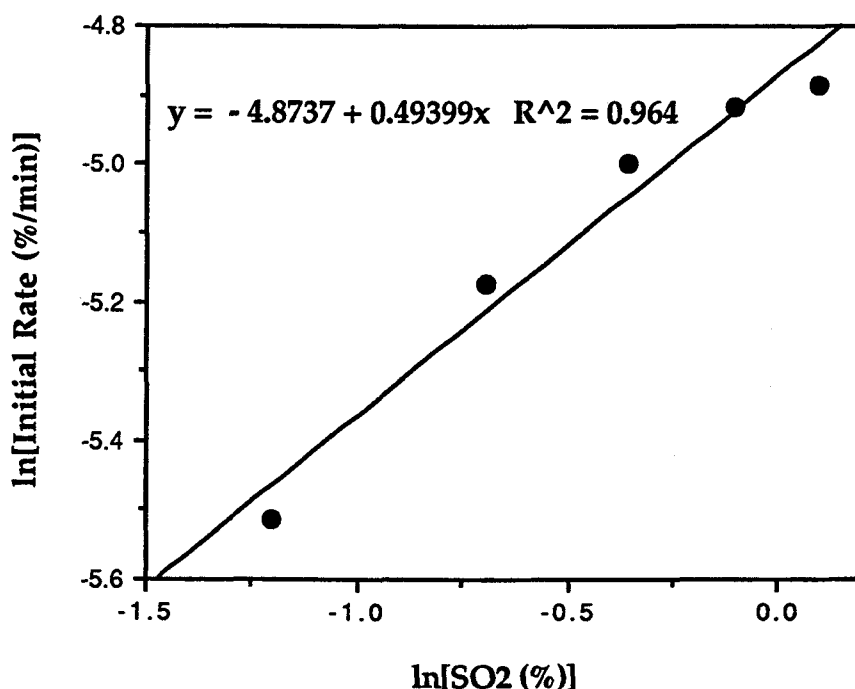
Figure 5.7 : The plot between ln (rate (%/min)) and ln (SO_2 (%)) at 0.3-1.1 % SO_2, 5 % O_2 and 10 % H_2O

5.8 O$_2$ Concentration Effect

The influence of O$_2$ dependence was studied at a constant reaction reaction temperature of 500 °C. The O$_2$ concentration range studied was from 3 - 11 %. The conditions of the O$_2$ dependence study were 15 cm^3/s (20 °C, 1 atm) total flow rate, 500 °C, 0.3 % SO$_2$, 10 % H$_2$O and 2 g of 125-250 μm NaCl. The reaction order with respect to O$_2$ was determined by plotting the logarithm of chemical kinetic rate and the logarithm of O$_2$ concentration. This plot is shown in Figure 5.8. The reaction order was approximately 0.08 with the regression analysis in Table 5.6. It showed that the reaction order was zeroth order with respect to O$_2$. A zeroth reaction order indicated that oxygen

$$y = -5.7008 + 8.2396e\text{-}2x \quad R^2 = 0.565$$
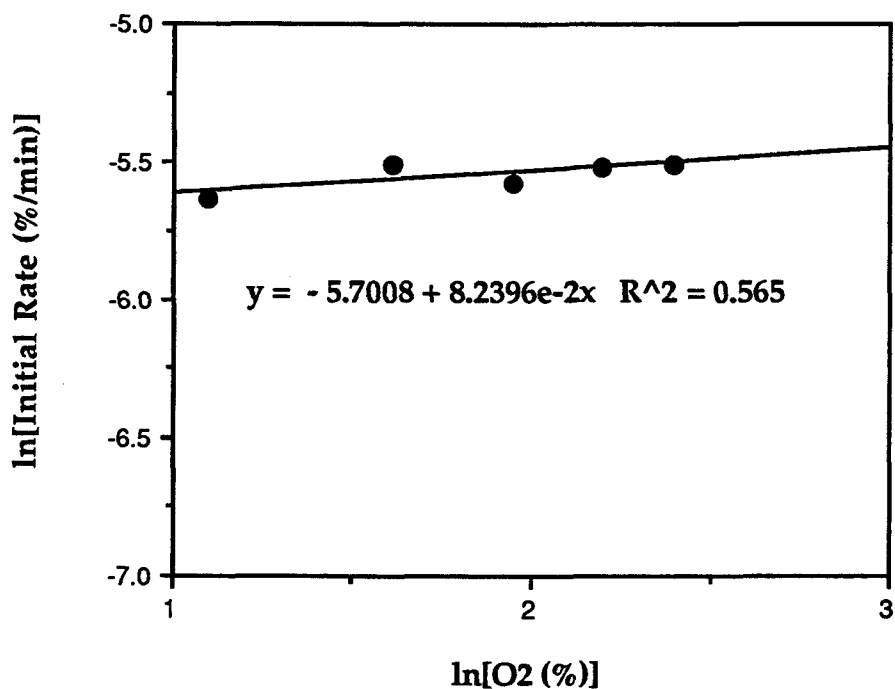
Figure 5.8 : The plot between ln (rate (%/min)) and ln (O$_2$ (%)) at 3-11 % O$_2$, 0.3 % SO$_2$ and 10 % H$_2$O

Table 5.6 : Regression analysis of O_2 dependence, 95 % confidence interval

	coefficient	std. error	sig. level	lower limit	upper limit
intercept	-5.7008	0.0794	0.0000	-5.9536	-5.4483
slope	0.082	0.0417	0.1421	-0.0501	0.2150

was involved in a fast reaction step which did not control the overall rate of reaction.

5.9 H$_2$O (v) Concentration Effect

The influence of water vapor dependence was also studied at a constant reaction temperature of 500 °C. The H_2O (v) concentrations were studied in the range of 0.5 - 20 %. The conditions of H_2O (v) dependence study were 15 cm^3/s (20 °C, 1 atm) total flow rate, 500 °C, 0.3 % SO_2, 5 % O_2 and 2 g of 125-250 μm NaCl. The graph of the logarithm of chemical kinetic rate and the logarithm of H_2O (v) concentration was plotted to find the reaction order with respect to H_2O (v). This plot is shown in Figure 5.9. The reaction order was approximately 0.009 with the regression analysis in Table 5.7 It showed that the reaction order was zeroth order with respect to H_2O (v). A zeroth reaction order indicated that water vapor was involved in a fast reaction step which did not control the overall rate of reaction.

Table 5.7 : Regression analysis of H_2O (v) dependence, 95 % confidence interval

	coefficient	std. error	sig. level	lower limit	upper limit
intercept	-5.5723	0.0176	0.0000	-5.6215	-5.5235
slope	0.0090	0.0087	0.3566	-0.0151	0.0332
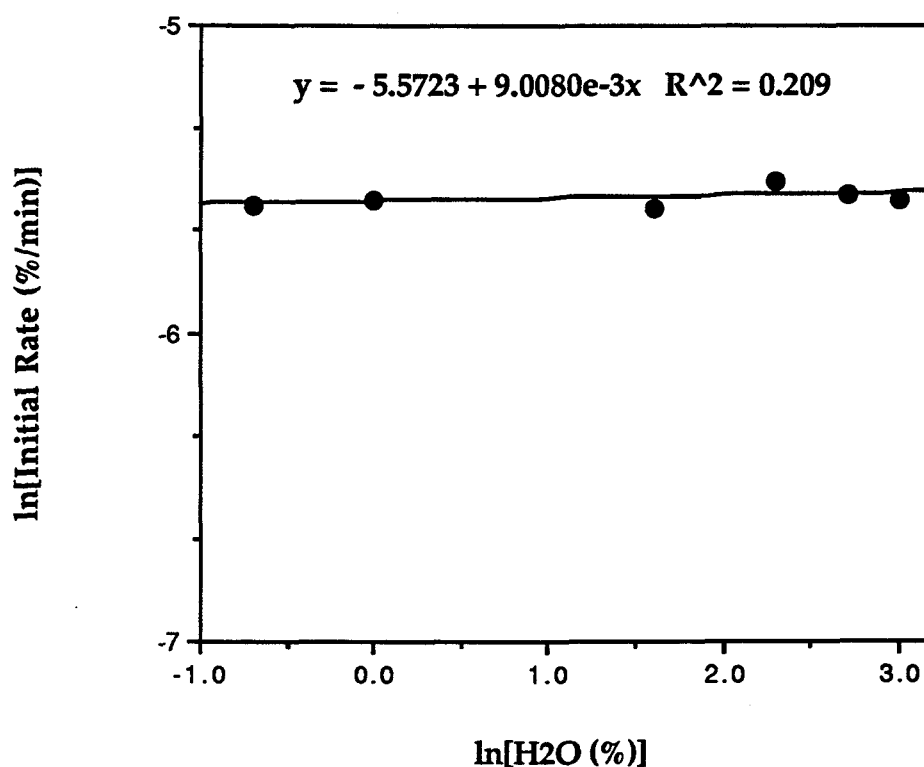
Figure 5.9 : The plot between ln (rate (%/min)) and ln (H_2O (v) (%)) at 1-20 % H_2O, 0.3 % SO_2 and 5 % O_2.

5.10 Proposed Mechanism

Anderson (15) suggested the following mechanism for the sulfation of NaCl in the presence of SO_3.

$$SO_3 (g) + H_2O (g) \longrightarrow H_2SO_4 (g)$$
$$H_2SO_4 (g) + 2\,NaCl (s) \longrightarrow 2\,HCl (g) + Na_2SO_4 (s)$$
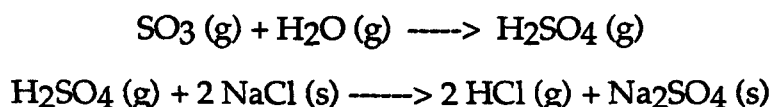
The SO_3 (g) reacts with water vapor to form H_2SO_4 (g) with a transition state yielding closely associated hydroxyl and bisulfite. Then H_2SO_4 (g) molecule transfers a hydrogen atom to a chloride in solid NaCl. Sodium bisulfate, $NaHSO_4$, and HCl (g) were formed from the transfer of an electron and a sodium cation. This process repeats and Na_2SO_4 is formed for the final product.

From the Fielder et al. (14) study, the rate of reaction depended on the SO_3 and H_2O concentration. This implied that SO_3 and H_2O were involving in the rate limiting step. Thus the reaction between SO_3 (g) and H_2O (g) should be the rate controlling step for the overall rate of this reaction in the presence of SO_3.

The mechanism of the sulfation of NaCl in the absence of SO_3 is suggested here. The mechanism proposed is shown below :

$$SO_2 (g) \longleftrightarrow SO_2 (ads)$$
$$O_2 (g) \longleftrightarrow O_2 (ads)$$
$$H_2O (g) \longleftrightarrow H_2O (ads)$$
$$SO_2 (ads) + {}^1/_2\,O_2 (ads) \longrightarrow SO_3 (ads)$$

$$SO_3 \text{ (ads)} + H_2O \text{ (ads)} \longrightarrow H_2SO_4 \text{ (ads)}$$

$$H_2SO_4 \text{ (ads)} + NaCl \text{ (s)} \longrightarrow HCl \text{ (g)} + NaHSO_4 \text{ (ads)}$$

$$NaHSO_4 \text{ (ads)} + NaCl \text{ (s)} \longrightarrow Na_2SO_4 \text{ (s)} + HCl \text{ (g)}$$
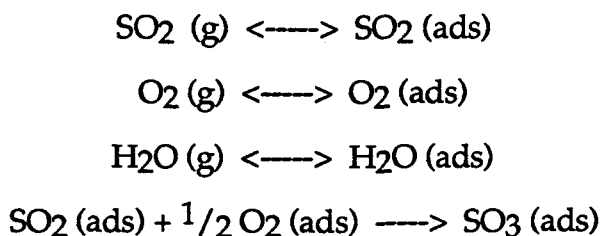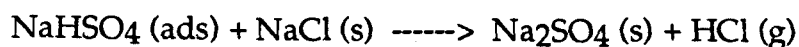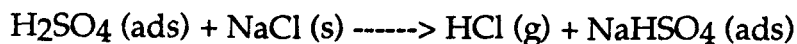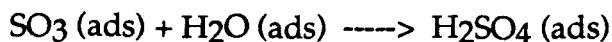
First SO_2 (g), O_2 (g) and H_2O (g) are adsorped on the surface of NaCl and then SO_2 (ads) reacts with O_2 (ads) to form SO_3 (ads). H_2O (ads) reacts with SO_3 (ads) to form H_2SO_4 (ads). The products, Na_2SO_4 and HCl, are obtained from the reaction between H_2SO_4 (ads) and NaCl.

The activation energy of this reaction was quite low which is consistant with a physical adsorption-desorption process as the rate-controlling step in this reaction. From the gas concentration effects, SO_2 was involved in the rate limiting step of this reaction whereas O_2 and H_2O were not. From these two reasons, the rate limiting step of this reaction should be the adsorption-desorption of SO_2 (g) on the surface of NaCl. Additional support for this conclusion was that the chemical kinetic rate increased with increasing SO_2 concentration and was less dependent at higher SO_2 concentrations. This showed Langmiur adsorption type behavior.

5.11 Reaction Rate Analysis

This reaction was limited by SO_2 adsorption. It implied that the adsorption of SO_2 (g) on the surface of NaCl controlled the overall reaction. Thus the overall rate of reaction can be approximated by adsorption of SO_2 (g). The adsorption process can be described by Langmiur isotherm (16, 17). This model was based on the assumption that the surface is energetically ideal and that forces of interaction between adsorbed species are negligible. The

adsorption rate is assumed to be proportional to species partial pressure and the fraction of the solid surface unoccupied.

$$-r_{SO_2} = S' \frac{k\, P_{SO_2}}{1 + K_1 P_{SO_2} + K_2 P_{O_2} + K_3 P_{H_2O}}$$

where r_{SO_2} = rate of deformation of SO_2, mol/min.

k = reaction rate constant, mol/m^2.min.atm

P_{SO_2} = partial pressure of SO_2, atm

S' = internal surface area, m^2/g

K_1 = adsorption equilibrium constant of SO_2, atm^{-1}

K_2 = adsorption equilibrium constant of O_2, atm^{-1}

K_3 = adsorption equilibrium constant of H_2O, atm^{-1}

$$K = K_0 \exp[Q/RT]$$

where Q = heat of adsorption

If $K_2 P_{O_2}$ and $K_3 P_{H_2O}$ are much less than 1 and $K_1 P_{SO_2}$ this reaction rate will be :

$$-r_{SO_2} = S' \frac{k\, P_{SO_2}}{1 + K_1 P_{SO_2}}$$

from stoichiometric coefficient, $2r_{SO_2} = r_{NaCl}$

$$2 \, S' \, \frac{k \, P_{SO_2}}{1 + K_1 P_{SO_2}} = \frac{1}{M} \frac{dX}{dt}$$

$$\frac{2S'M}{(dX/dt)} = (K_1/k) + (1/k) \frac{1}{P_{SO_2}}$$

Figure 5.10 showed a very good linear relationship from the plot between $2S'M / (dX/dt)$ and P_{SO_2}. This showed a very good agreement between this model with the data. It showed a mean for the curvature of the plot between the logarithm of the chemical kinetic rate and the logarithm of SO_2 in Figure 5.7. There is no mean to take an average slope of this plot. K_1 and k were calulated from the plot in Figure 5.10. The values of K_1 and k were 172 atm^{-1} and 1.2×10^{-3} mol/m^2.atm.min respectively. The regression analysis are shown in Table 5.8. Thus the rate equation of this reaction at 500 ^{o}C was :

$$r = -r \, NaCl = r \, HCl = -2 \, r_{SO_2} = S' \, \frac{2.4 \times 10^{-3} \, P_{SO_2}}{1 + 172 \, P_{SO_2}}$$

Table 5.8 : Regression Analysis of reaction rate, 95% confidence interval

	coefficient	std. error	sig. level	lower limit	upper limit
1/k	827.57	37.7126	0.0002	707.55	947.59
K_1/k	142750	7392.61	0.0003	119219	166272
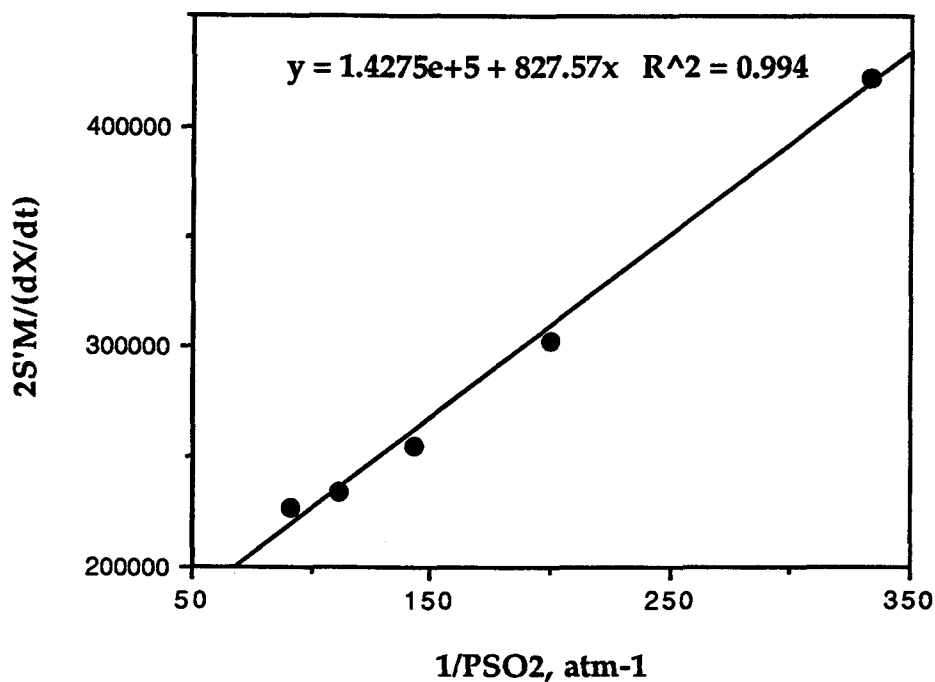
Figure 5.10 : The plot between 2S'M / (dX/dt) and 1/P_{SO_2}

For the NaCl solid fume particle with 0.25-1.0 μm in diameter, the rate was estimated based on the external surface area of solid fume particle. The calculation is shown here :

the external surface area $=$ $(4\pi r^2) / [(4\pi r^3/3).\rho]$

$=$ $3/r\rho$

for 0.5 μm particle, the external surface area was $= 3/(0.5 \times 2.1) = 2.86 \text{ m}^2/\text{g}$

at 500 °C and 300 ppm P_{SO_2}, the rate equation will be :

$$r = 2.86 \; \frac{2.5 \times 10^{-3} \, (0.0003)}{1 + 178 \, (0.0003)} = 2.04 \times 10^{-6} \quad \text{mol HCl/g NaCl.min}$$

$$= 2.04 \times 10^{-6} \times 58.5 \quad = 1.2 \times 10^{-4} \quad \text{mol HCl/mol NaCl.min}$$

$$= 0.012 \qquad\qquad\qquad\qquad \% / \text{min}$$

CHAPTER 6

CONCLUSIONS, IMPLICATIONS AND RECOMMENDATIONS

6.1 Conclusions

The conclusions for the sulfation of Na_2CO_3 in the presence of oxygen at the temperature range 120 - 700 °C are as follows :

1. The reaction was first order with respect to SO_2

2. The reaction was zeroth order with respect to O_2

3. The overall rate of reaction was controlled by diffusion through the product layer

4. The diffusion of this reaction was most likely solid state diffusion

5. Sintering of the solid fume particles occurred during the reaction

For the sulfation of NaCl in the absence of SO_3 at the temperature range 400 - 600 °C, the conclusions are shown below :

1. The activation energy of the reaction was 17.3 KJ/mol

2. The reaction depended on SO_2 concentration, but the dependence decreased with increasing SO_2 concentration

3. The reaction was zeroth order with respect to O_2 and H_2O

4. The adsorption of SO_2 on the surface of NaCl should be the main step to control the reaction

5. The rate equation at 500 °C is :

$$r = -r_{NaCl} = r_{HCl} = -2\, r_{SO_2} = S' \frac{2.5 \times 10^{-3}\, P_{SO_2}}{1 + 178\, P_{SO_2}}$$

6.2 Implications to Kraft Recovery Boiler

The sulfation of Na_2CO_3 is not fast enough to account for the significant of SO_2 capture by solid fume particles in recovery boiler. The sulfation of solid NaCl is much slower than of Na_2CO_3, but both reactions are too slow to account for significant SO_2 capture by solid fume particles.

This implied that the SO_2 capture by fume particles in-flight or vaporized sodium species occurs before the boiler bank, in the lower furnace and/or in the superheater region. In these regions, the temperature is high enough for the fume particles to be molten. There is no kinetic data available on these reactions at higher temperatures where Na_2CO_3 and NaCl are molten.

The sulfation reactions of solid Na_2CO_3 and NaCl are, however, fast enough to account for significant sulfation of deposits which contain Na_2CO_3 and NaCl in kraft recovery boilers and their sintering and strength development. The sulfation of solid NaCl is also important for the formation of HCl from NaCl in these deposits.

The Na_2CO_3 in fume deposited on heat transfer surface in the kraft recovery boilers can react at relatively low temperatures with SO_2 to form Na_2SO_4, forming a very hard, highly sintered deposit.

6.3 Recommendations for Future Work

Some of the recommendations for the future work on the sulfation of NaCl and Na_2CO_3 are :

1. Measure the rate of these reactions for molten phase in a laminar entrained flow reactor in order to predict the sulfation of fume particles in recovery boilers.

2. Investigate the effects of sintering and sodium pyrosulfate formation as causes for the abnormal temperature dependence for the sulfation of Na_2CO_3 observed by Backman et al.(2) and Lloyd-George (4) in the temperature range 350-550 $^{\circ}C$.

3. Measure heat of adsorption of SO_2 on NaCl for adsorption equilibrium constant to find rate equation of sulfation of NaCl at different temperatures.

BIBLIOGRAPHY

1. Keener, T. and Davis, W., "Study of the Reaction of SO_2 with $NaHCO_3$ and Na_2CO_3", Journal of Air Pollution Control Association, 34:651-654 (1984)

2. Backman, R., Hupa, M., Usikartano, T., "Kinetics of Sulphation of Sodium Carbonate in Flue Gases", International Chemical Recovery Conference, New Orleans, LA, 1985

3. Maule, G. and Cameron, J., "Reaction of Na_2CO_3 Fume Particles with SO_2 and O_2", IPC Technical Paper Series, number 317, January 1989

4. Lioyd-George, I., "The sulfation of sodium Carbonate: the significance of pyrosulfate, potassium and chloride", M.S. thesis, University of Toronto, 1985

5. Kimura, S. and Smith, J., "Kinetics of the sodium Carbonate-Sulfur Dioxide Reaction", AIChe J., 33(9) : 1522-1532 (1987)

6. Butler, F. and Waites, I., "A Thermoanalytical study of the Reaction between Gaseous Sulfur Dioxide and Solid Sodium Carbonate", 2nd European Symposium on Thermal Analysis, p. 310-314, 1981

7. Lloyd-George, I., "A Study of the Sulfation of Sodium Carbonate and the Effects of Sodium Chloride and Potassium Chloride Enrichment", B. Sc. Thesis, Department of Chemical Engineering, University of Toronto, 1982

8. Levenspiel, O., "Chemical Reaction Engineering, 2nd Edition", p. 361-373, John Wiley & Son, 1972

9. Wen, C. Y., "Noncatalytic Heterogeneous solid Fluid Reaction Models", Journal of Industrial and Engineering Chemistry, Vol. 60, No. 9, 34-54, 1968

10. Ishida, M. and Wen, C.Y., "Comparison of Kinetic and Diffusional Models for Solid-Gas Reactions", AIChe J., 14(2), 311-317, 1968

11. Froment, G.F. and Bischoff, K. B., "Chemical Reactor Analysis and Design", p. 201 - 207, John Wiley & Son, 1979

12. Iisa, K., Hupa, M. and Yrjas, P., "Product layer diffusion in the Sulphation of Calcium Carbonate", Twenty-Fourth (International) Symposium on Combustion, Sydney, Australia, July 5-10, 1992

13. Henriksson, M. and Warnqvist, B., "Kinetics of Formation of HCl(g) by the reaction between NaCl(s) and SO2, O2, and H2O(g)", Ind. Eng. Chem. Process Des. Dev. 18(2):249-254 (1979)

14. Fielder, W., Stearns, C. andd Kohl, F., "Reaction of NaCl wiith Gaseous SO3, SO2 and O2", J. Electrochem. Soc., Vol.131, NO.10:2414-2417 (1984)

15. Anderson, A., "Mechanism for forming Hydrogen Chloride and Sodium Sulfate from Sulfur Trioxide, Water and Sodium Chloride", Journal of American Chemical Society, Vol. 106, NO.21:6262-6265 (1984)

16. Fogler, H., "Element of Chemical Reaction Engineering", 2nd Edition, p 249-258, Prentice-Hall Inc., 1992

17. Wilhelm, R., "Chemical Reactor Theory", p. 169-173, Prentice-Hall, Inc., 1977

APPENDICES

APPENDIX A

Chloride Eclectrde Calibration Curve
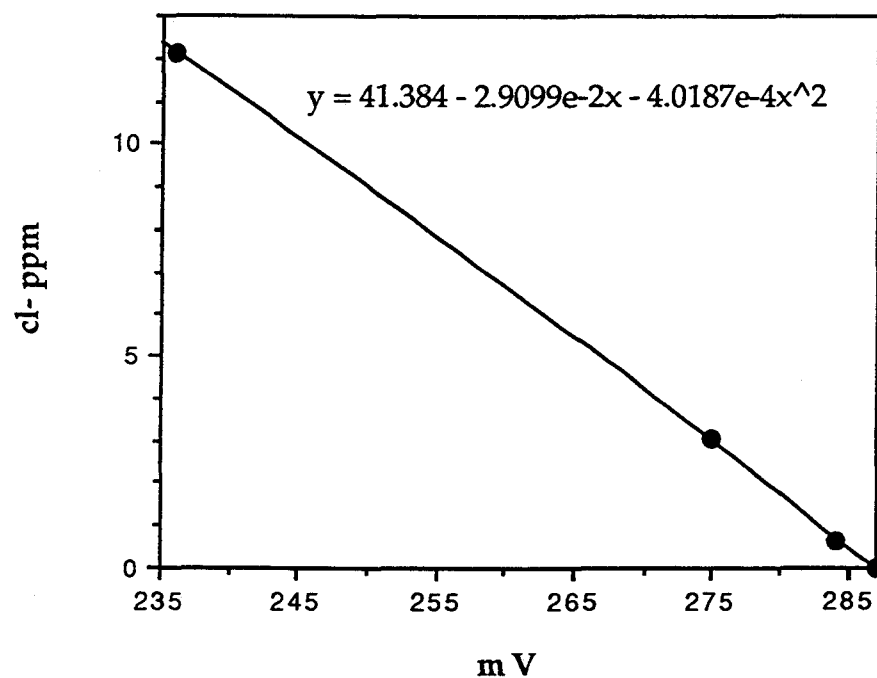
Figure A-1 : Chloride electrode calibration curve (0-12 ppm)

APPENDIX B

Experimental Data

Table B-1 : Experimental # 1 data

Experiment #	1
Date	5/20/93

NaCl		
Amount	2.00	g
Size	125-250	micron

Gas		
SO2	0.3	%
O2	5.0	%
N2	84.7	%
H2O	10.0	%

Reactor		
Temperature	500	C

Flow		
Rate	5	cm3/sec

Gas Analysis					
Time (min.)	mV	ppm	water (ml)	cl- (mg)	conversion (%)
0	-	-	-	-	0.00
30	270	4.23	234.0	0.99	0.08
60	271	3.98	250.0	1.00	0.16
90	270	4.23	242.0	1.02	0.25
120	272	3.74	241.0	0.90	0.32
150	267	4.97	238.0	1.18	0.42
180	271	3.98	239.0	0.95	0.50
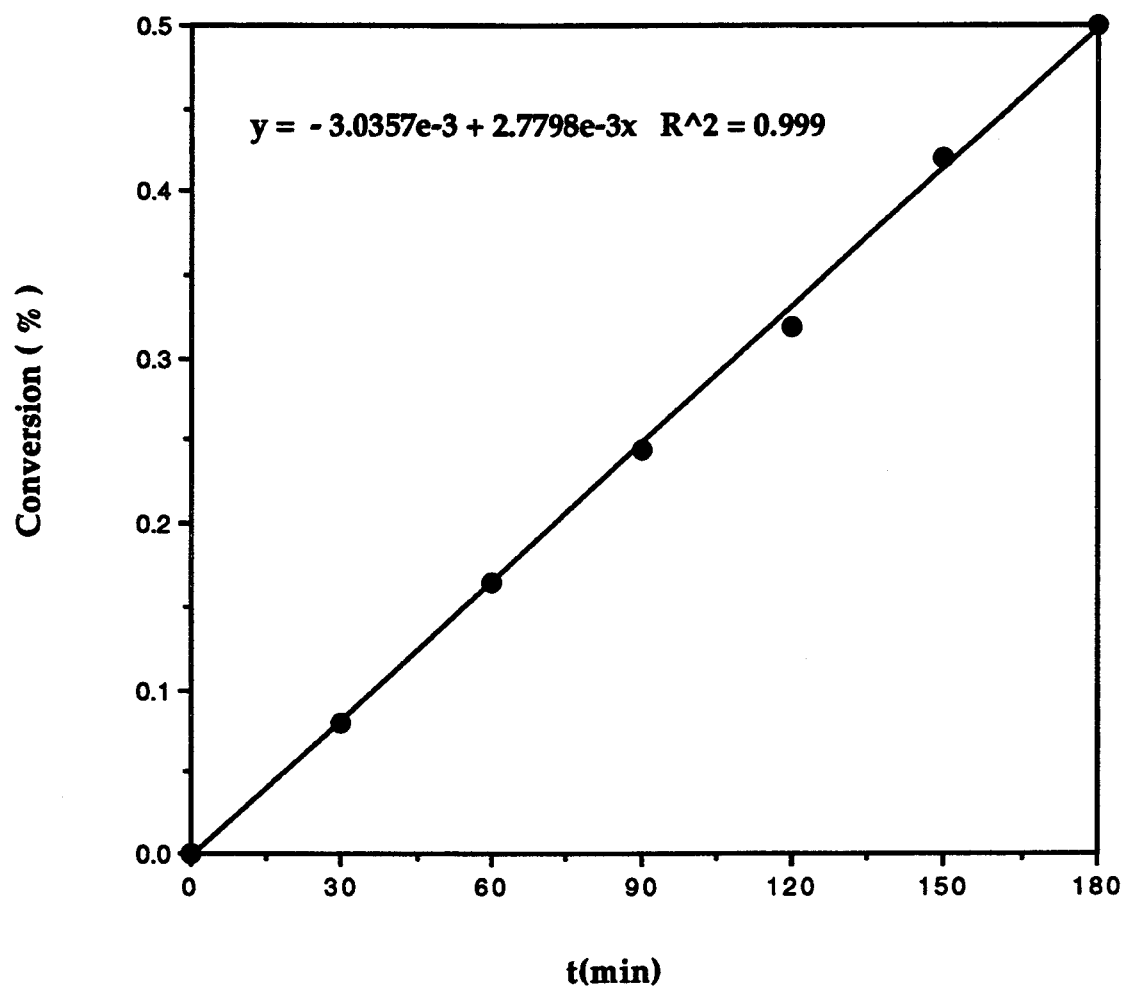
Figure B-1 : Experimental # 1 data

Table B-2 : Experimental # 2 data

Experiment #	2
Date	5/21/93

NaCl		
Amount	2.00	g
Size	125-250	micron

Gas		
SO2	0.3	%
O2	5.0	%
N2	84.7	%
H2O	10.0	%

Reactor		
Temperature	500	C

Flow		
Rate	8	cm3/sec

Gas Analysis					
Time (min.)	mV	ppm	water (ml)	cl- (mg)	conversion (%)
0	-	-	-	-	0.00
30	262	6.17	238.0	1.47	0.12
60	267	4.97	241.0	1.20	0.22
90	262	6.17	239.0	1.48	0.34
120	261	6.41	242.0	1.55	0.47
150	267	4.97	241.0	1.20	0.57
180	265	5.45	240.0	1.31	0.68
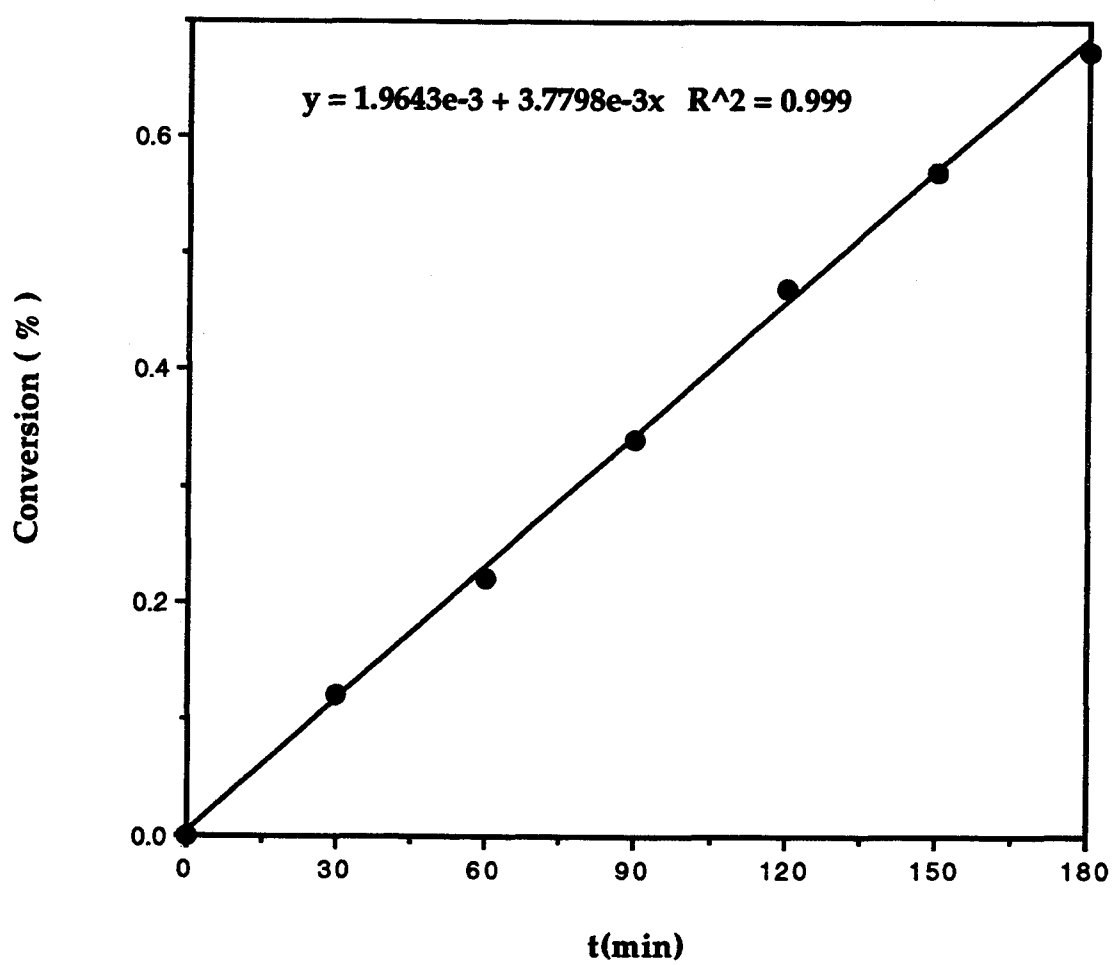
Figure B-2 : Experimental # 2 data

Table B-3 : Experimental # 3 data

Experiment #	3
Date	5/22/93

NaCl		
Amount	2.00	g
Size	125-250	micron

Gas		
SO2	0.3	%
O2	5.0	%
N2	84.7	%
H2O	10.0	%

Reactor		
Temperature	500	C

Flow		
Rate	10	cm3/sec

Gas Analysis					
Time (min.)	mV	ppm	water (ml)	cl- (mg)	conversion (%)
0	-	-	-	-	0.00
30	261	6.41	242.0	1.55	0.13
60	262	6.17	241.0	1.49	0.25
90	258	7.13	239.0	1.70	0.39
120	265	5.45	241.0	1.31	0.50
150	262	6.17	242.0	1.49	0.62
180	265	5.45	240.0	1.31	0.73
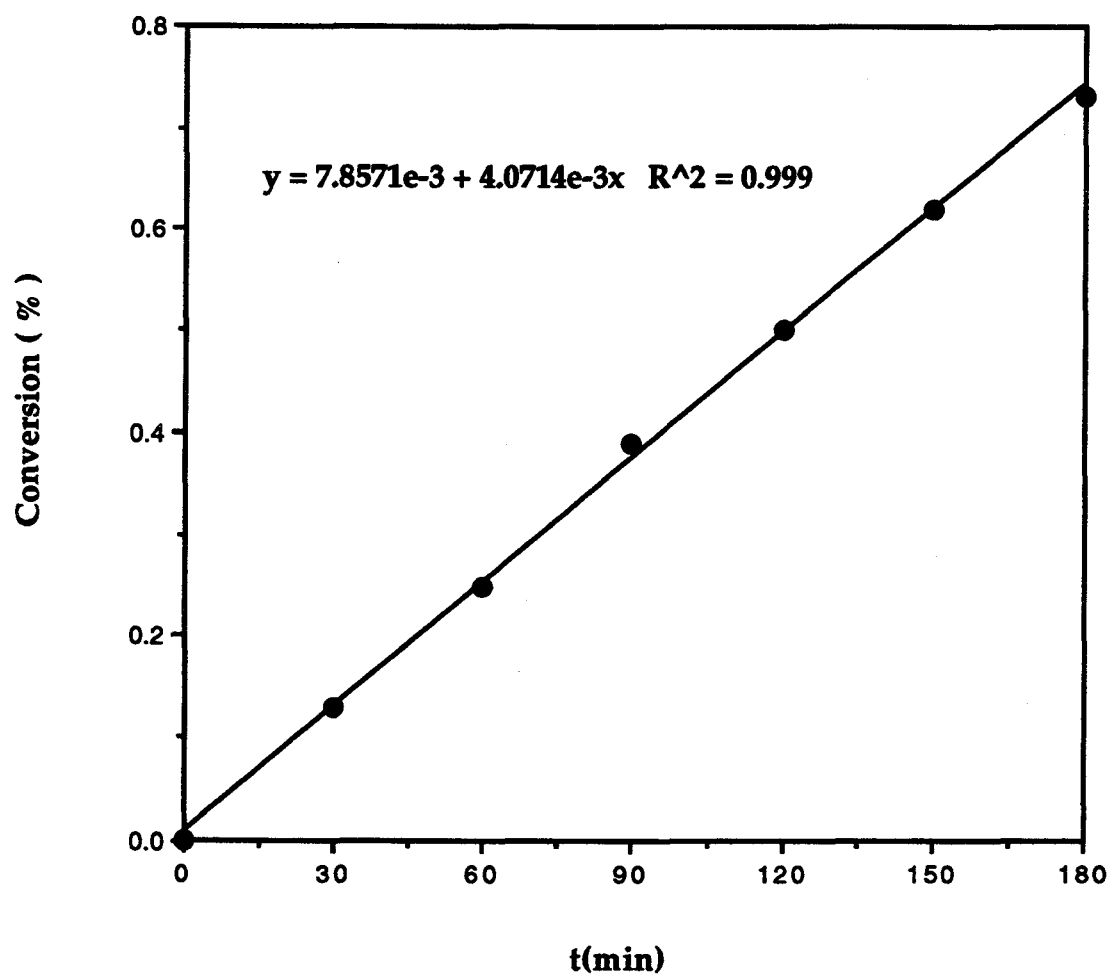
Figure B-3 : Experimental # 3 data

Table B-4 : Experimental # 4 data

Experiment #	4
Date	5/25/93

NaCl		
Amount	2.00	g
Size	125-250	micron

Gas		
SO2	0.3	%
O2	5.0	%
N2	84.7	%
H2O	10.0	%

Reactor		
Temperature	500	C

Flow		
Rate	15	cm3/sec

Gas Analysis					
Time (min.)	mV	ppm	water (ml)	cl- (mg)	conversion (%)
0	-	-	-	-	0.00
30	264	5.69	239.0	1.36	0.11
60	261	6.41	240.0	1.54	0.24
90	261.5	6.29	241.0	1.52	0.36
120	263	5.93	241.0	1.43	0.48
150	262	6.17	240.0	1.48	0.60
180	261	6.41	239.0	1.53	0.73
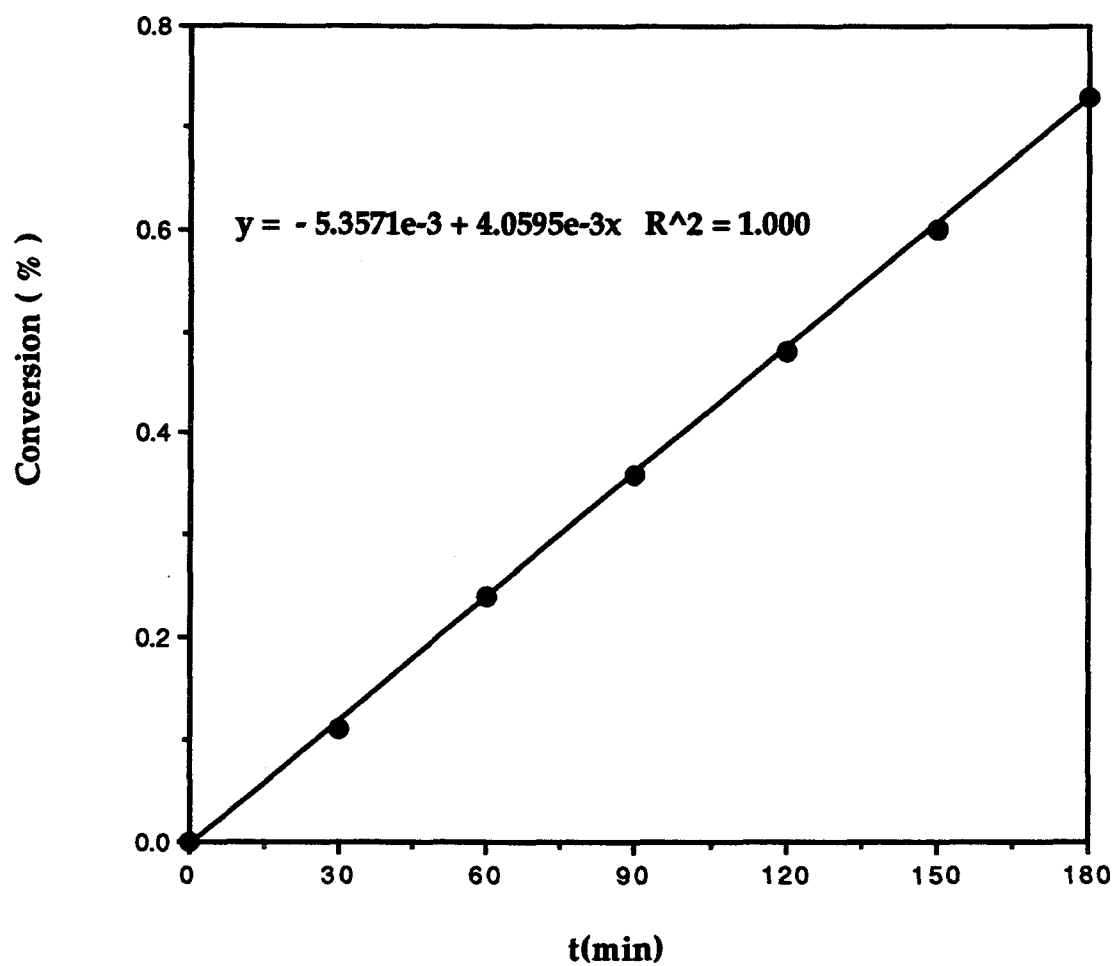
Figure B-4 : Experimental # 4 data

Table B-5 : Experimental # 5 data

Experiment #	5
Date	5/26/93

NaCl		
Amount	1.50	g
Size	125-250	micron

Gas		
SO2	0.3	%
O2	5.0	%
N2	84.7	%
H2O	10.0	%

Reactor		
Temperature	500	C

Flow		
Rate	11.25	cm3/sec

Gas Analysis					
Time (min.)	mV	ppm	water (ml)	cl- (mg)	conversion (%)
0	-	-	-	-	0.00
30	271	3.98	240.0	0.96	0.11
60	268	4.72	241.0	1.14	0.23
90	265	5.45	242.0	1.32	0.37
120	269	4.48	241.0	1.08	0.49
150	270	4.23	238.0	1.01	0.60
180	269	4.48	242.0	1.08	0.72

$$y = -4.2857e\text{-}3 + 4.0476e\text{-}3x \quad R^2 = 0.999$$
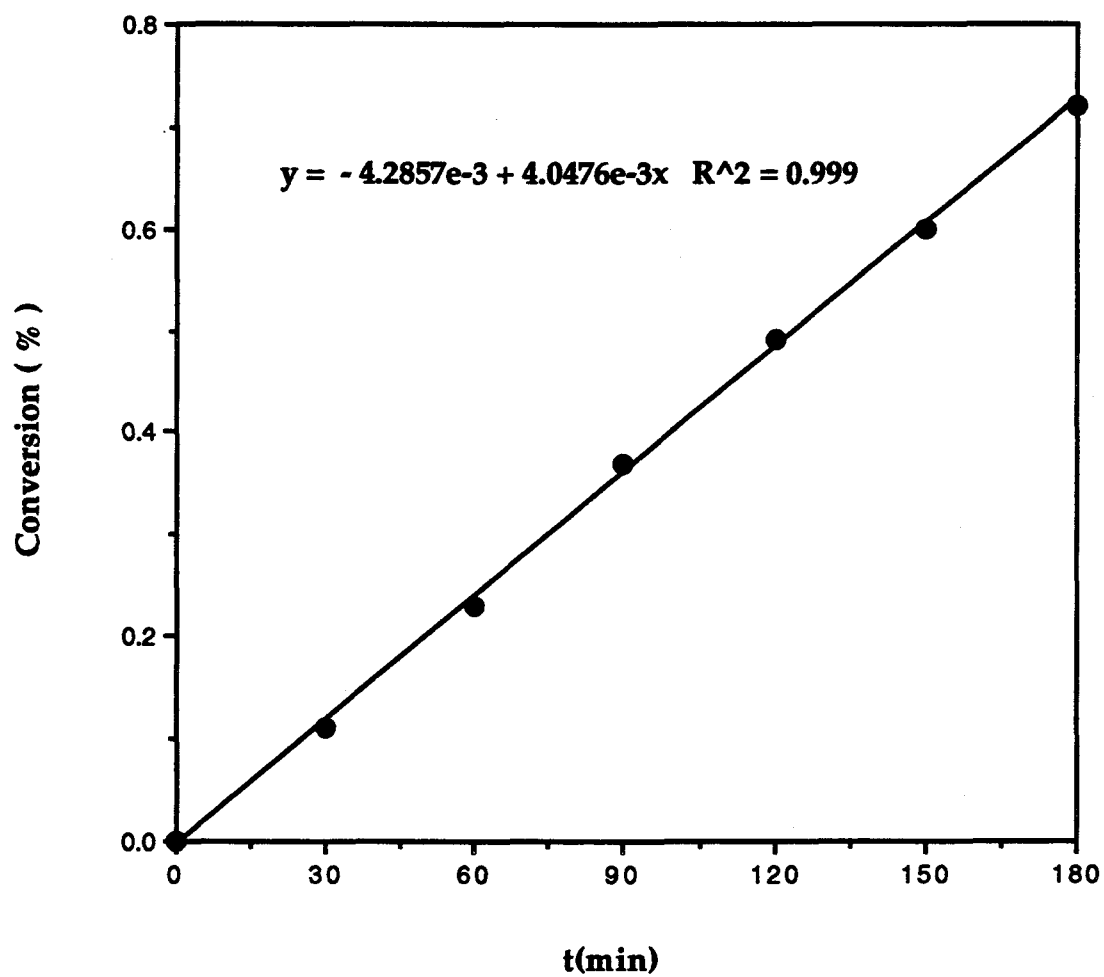
Figure B-5 : Experimental # 5 data

Table B-6 : Experimental # 6 data

Experiment #	6
Date	5/28/93

NaCl		
Amount	2.50	g
Size	125-250	micron

Gas		
SO2	0.3	%
O2	5.0	%
N2	84.7	%
H2O	10.0	%

Reactor		
Temperature	500	C

Flow		
Rate	18.75	cm3/sec

Gas Analysis					
Time (min.)	mV	ppm	water (ml)	cl- (mg)	conversion (%)
0	-	-	-	-	0.00
30	256	7.60	242.0	1.84	0.12
60	256	7.60	239.0	1.82	0.24
90	257	7.36	236.0	1.74	0.36
120	256	7.60	242.0	1.84	0.48
150	257	7.36	241.0	1.77	0.59
180	254	8.07	240.0	1.94	0.72
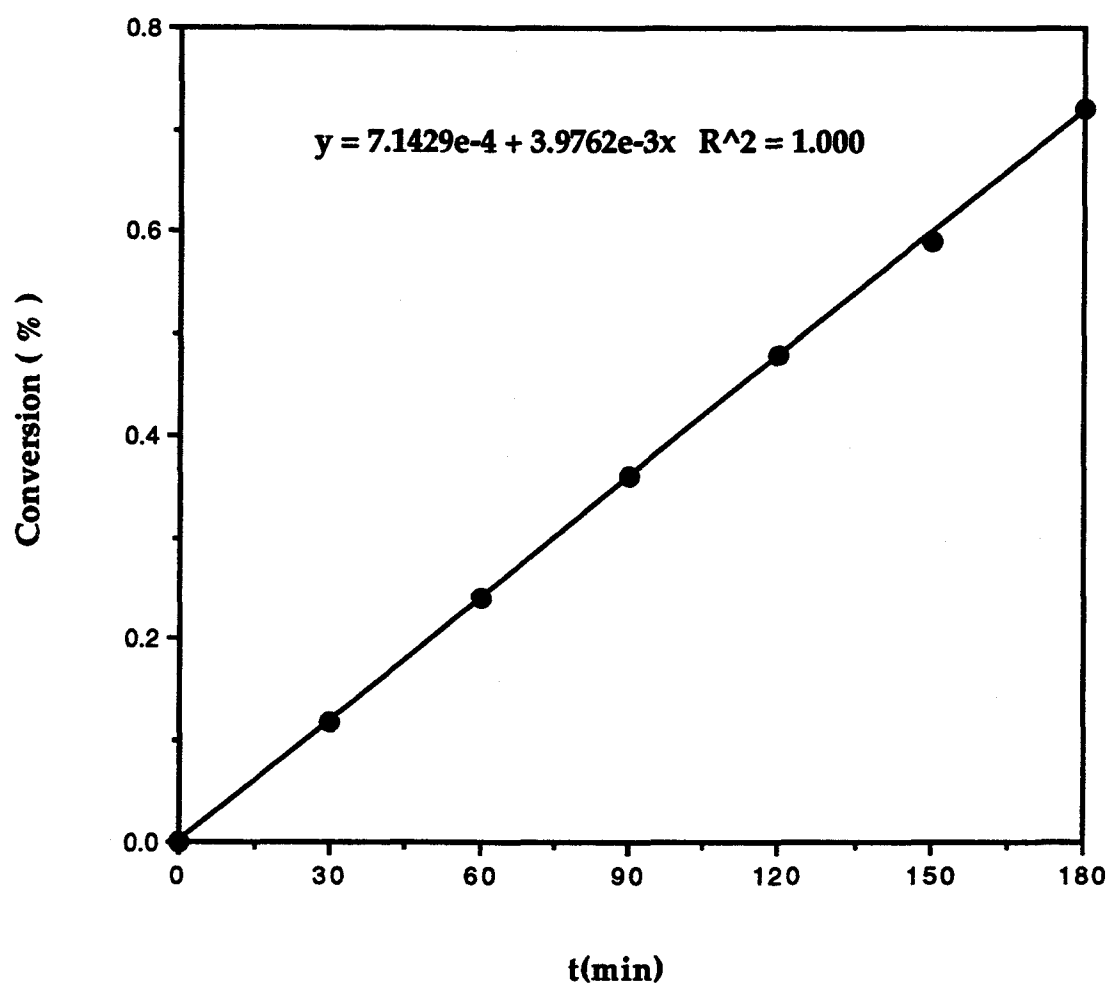
Figure B-6 : Experimental # 6 data

Table B-7 : Experimental # 7 data

Experiment #	7
Date	5/30/93

NaCl		
Amount	2.00	g
Size	90-125	micron

Gas		
SO2	0.3	%
O2	5.0	%
N2	84.7	%
H2O	10.0	%

Reactor		
Temperature	500	C

Flow		
Rate	15	cm3/sec

Gas Analysis					
Time (min.)	mV	ppm	water (ml)	cl- (mg)	conversion (%)
0	-	-	-	-	0.00
30	256.5	7.48	243.0	1.82	0.15
60	252	8.53	245.0	2.09	0.32
90	251.5	8.65	238.0	2.06	0.49
120	253	8.30	234.0	1.94	0.65
150	252	8.53	236.0	2.01	0.82
180	256	7.60	237.0	1.80	0.97
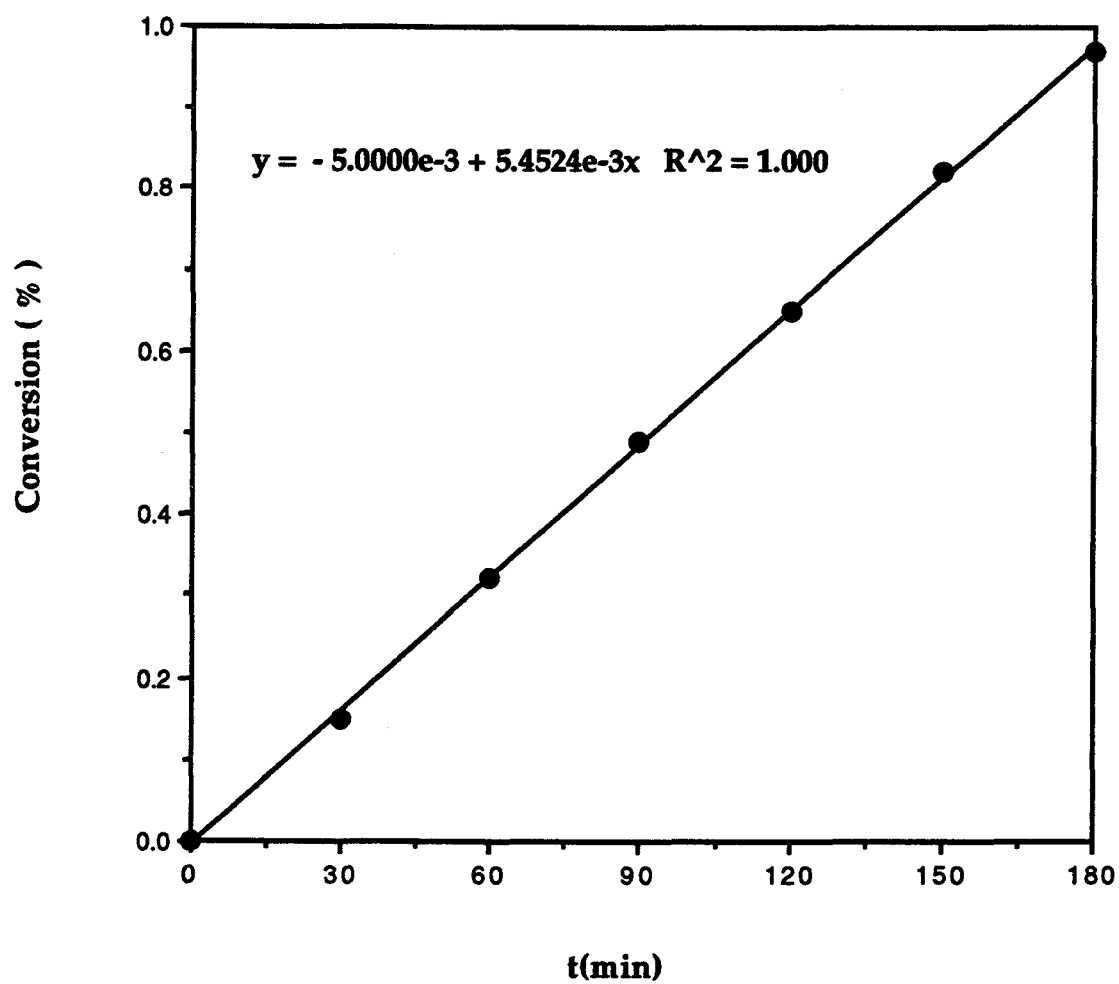
Figure B-7 : Experimental # 7 data

Table B-8 : Experimental # 8 data

Experiment #	8
Date	6/1/93

NaCl		
Amount	2.00	g
Size	63-90	micron

Gas		
SO2	0.3	%
O2	5.0	%
N2	84.7	%
H2O	10.0	%

Reactor		
Temperature	500	C

Flow		
Rate	15	cm3/sec

Gas Analysis					
Time (min.)	mV	ppm	water (ml)	cl- (mg)	conversion (%)
0	-	-	-	-	0.00
30	250	8.99	240.0	2.16	0.18
60	242	10.81	239.0	2.58	0.39
90	242	10.81	244.0	2.64	0.61
120	243	10.58	243.0	2.57	0.82
150	243	10.58	237.0	2.51	1.03
180	243	10.58	238.0	2.52	1.23

$$y = -1.5000e\text{-}2 + 6.9286e\text{-}3x \quad R^2 = 1.000$$
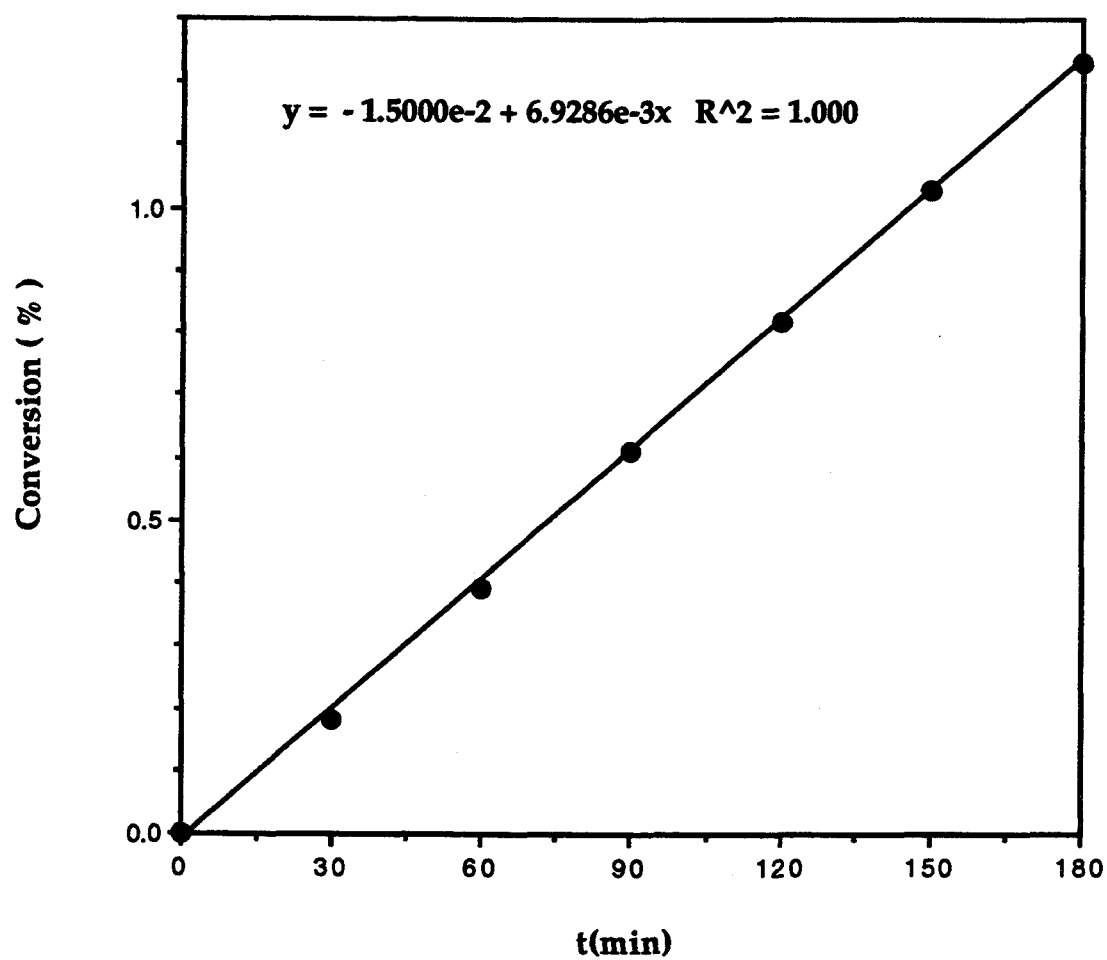
Figure B-8 : Experimental # 8 data

91

Table B-9 : Experimental # 9 data

Experiment #	9	
Date	6/2/93	

NaCl		
Amount	2.00	g
Size	125-250	micron

Gas		
SO2	0.3	%
O2	5.0	%
N2	84.7	%
H2O	10.0	%

Reactor		
Temperature	400	C

Flow		
Rate	15	cm3/sec

Gas Analysis					
Time (min.)	mV	ppm	water (ml)	cl- (mg)	conversion (%)
0	-	-	-	-	0.00
30	270	4.23	242.0	1.02	0.08
60	269	4.48	239.0	1.07	0.17
90	269	4.48	241.0	1.08	0.26
120	272	3.74	242.0	0.90	0.34
150	268	4.72	241.0	1.14	0.43
180	270	4.23	241.0	1.02	0.51
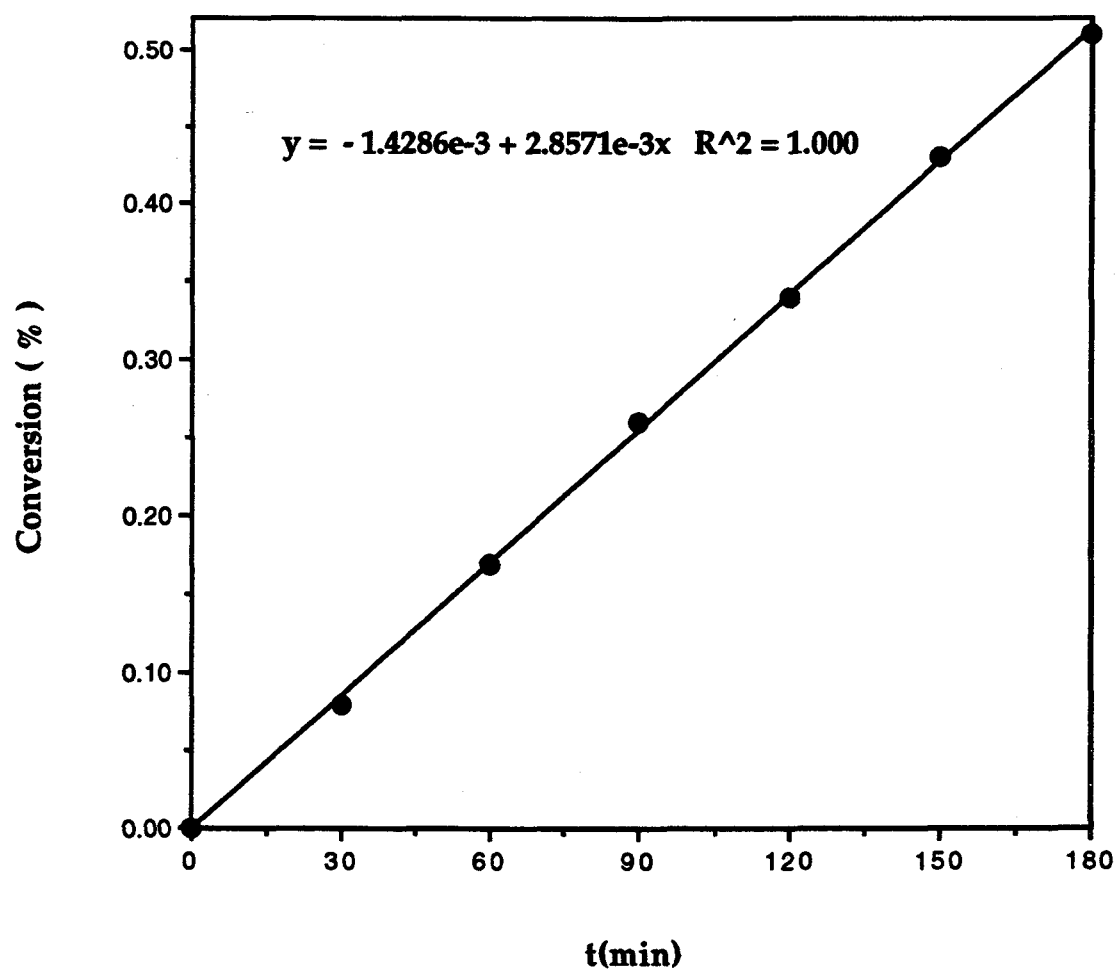
Figure B-9 : Experimental # 9 data

Table B-10 : Experimental # 10 data

Experiment #	10
Date	6/3/93

NaCl		
Amount	2.00	g
Size	125-250	micron

Gas		
SO2	0.3	%
O2	5.0	%
N2	84.7	%
H2O	10.0	%

Reactor		
Temperature	450	C

Flow		
Rate	15	cm3/sec

Gas Analysis					
Time (min.)	mV	ppm	water (ml)	cl- (mg)	conversion (%)
0	-	-	-	-	0.00
30	268	4.72	242.0	1.14	0.09
60	266	5.21	239.0	1.24	0.20
90	264	5.69	241.0	1.37	0.31
120	262	6.17	242.0	1.49	0.43
150	267	4.97	241.0	1.20	0.53
180	268	4.72	241.0	1.14	0.63
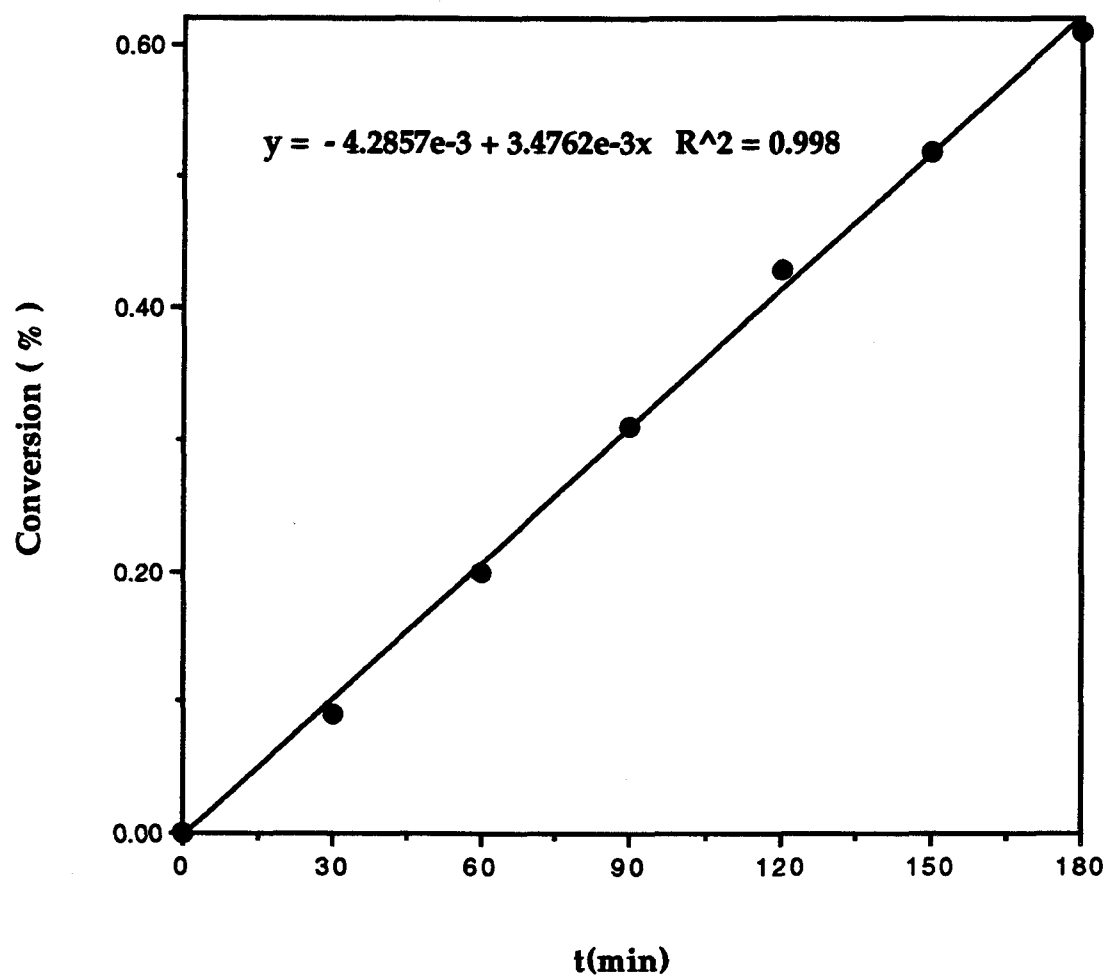
Figure B-10 : Experimental # 10 data

Table B-11 : Experimental # 11 data

Experiment #	11
Date	6/4/93

NaCl		
Amount	2.00	g
Size	125-250	micron

Gas		
SO2	0.3	%
O2	5.0	%
N2	84.7	%
H2O	10.0	%

Reactor		
Temperature	550	C

Flow		
Rate	15	cm3/sec

Gas Analysis					
Time (min.)	mV	ppm	water (ml)	cl- (mg)	conversion (%)
0	-	-	-	-	0.00
30	253	8.30	240.0	1.99	0.16
60	257	7.36	240.0	1.77	0.31
90	258	7.13	241.0	1.72	0.45
120	257	7.36	241.0	1.77	0.60
150	260	6.65	239.0	1.59	0.73
180	256.5	7.48	239.0	1.79	0.88
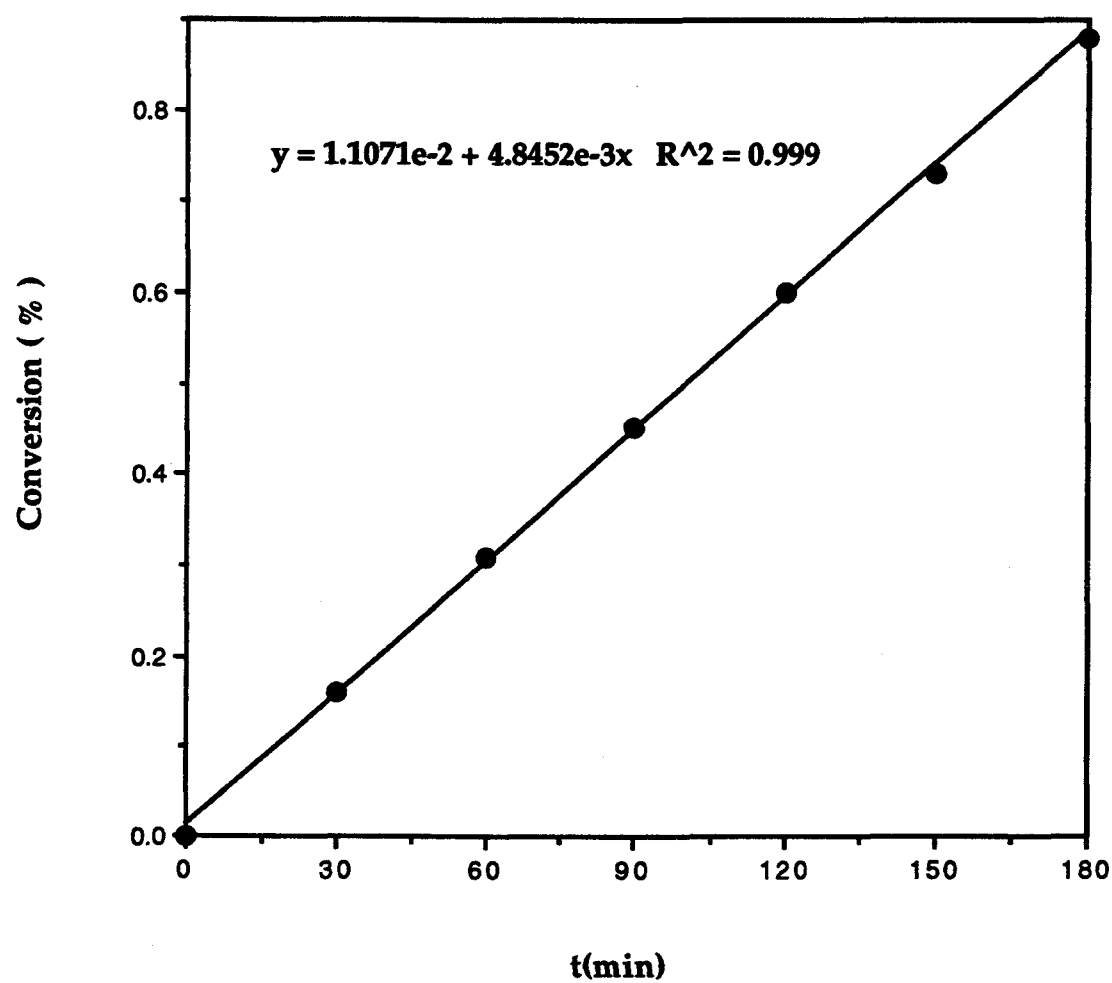
Figure B-11 : Experimental # 11 data

Table B-12 : Experimental # 12 data

Experiment #	12
Date	6/5/93

NaCl		
Amount	2.00	g
Size	125-250	micron

Gas		
SO2	0.3	%
O2	5.0	%
N2	84.7	%
H2O	10.0	%

Reactor		
Temperature	600	C

Flow		
Rate	15	cm3/sec

Gas Analysis					
Time (min.)	mV	ppm	water (ml)	cl- (mg)	conversion (%)
0	-	-	-	-	0.00
30	249	9.22	241.0	1.99	0.16
60	250	8.99	242.0	2.18	0.34
90	251	8.76	245.0	2.15	0.52
120	251	8.76	242.0	2.12	0.69
150	250	8.99	243.0	2.19	0.87
180	252	8.53	242.0	2.06	1.04
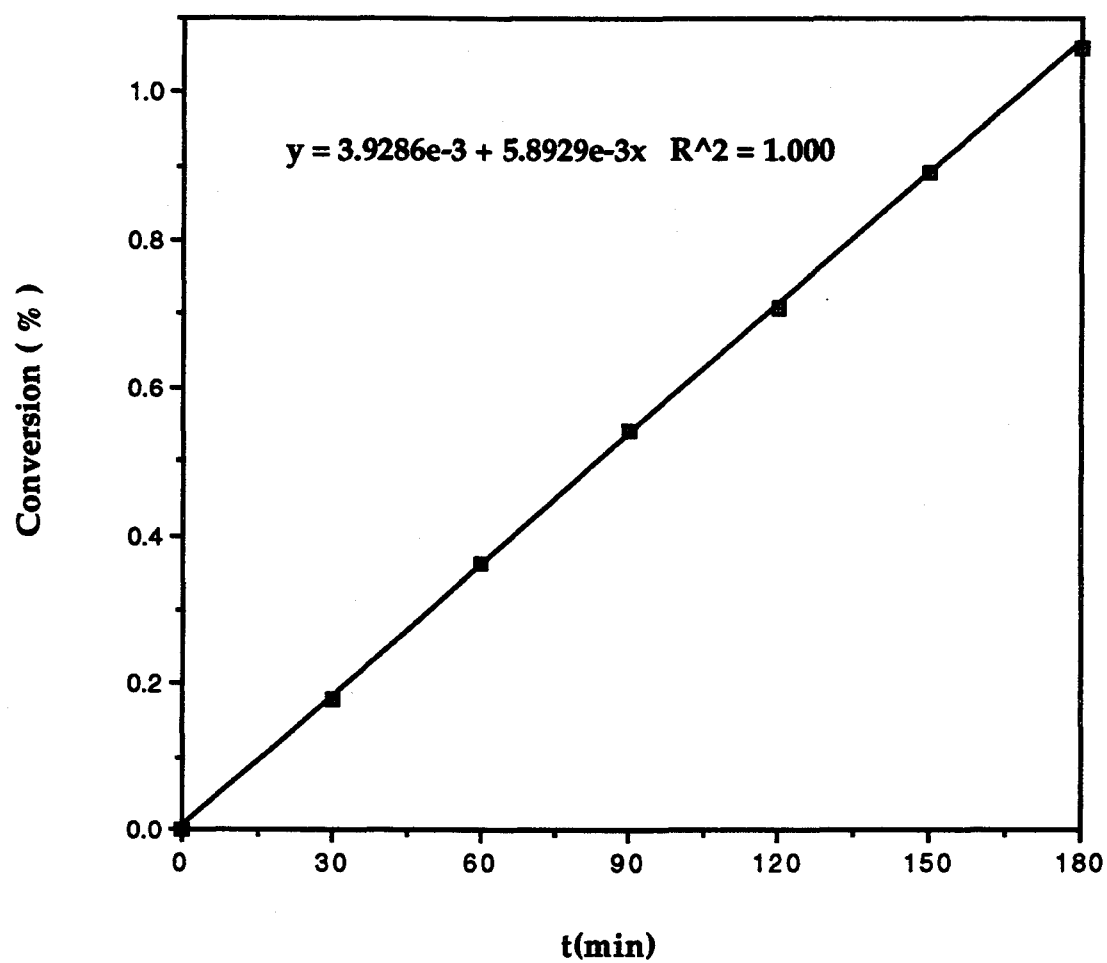
Figure B-12 : Experimental # 12 data

Table B-13 : Experimental # 13 data

Experiment #	13	
Date	6/7/93	

NaCl		
Amount	2.00	g
Size	125-250	micron

Gas		
SO2	0.5	%
O2	5.0	%
N2	84.5	%
H2O	10.0	%

Reactor		
Temperature	500	C

Flow		
Rate	15	cm3/sec

Gas Analysis					
Time (min.)	mV	ppm	water (ml)	cl- (mg)	conversion (%)
0	-	-	-	-	0.00
30	252.5	8.41	241.0	2.03	0.17
60	252	8.53	243.0	2.07	0.34
90	251	8.76	242.0	2.12	0.51
120	252	8.53	242.0	2.06	0.68
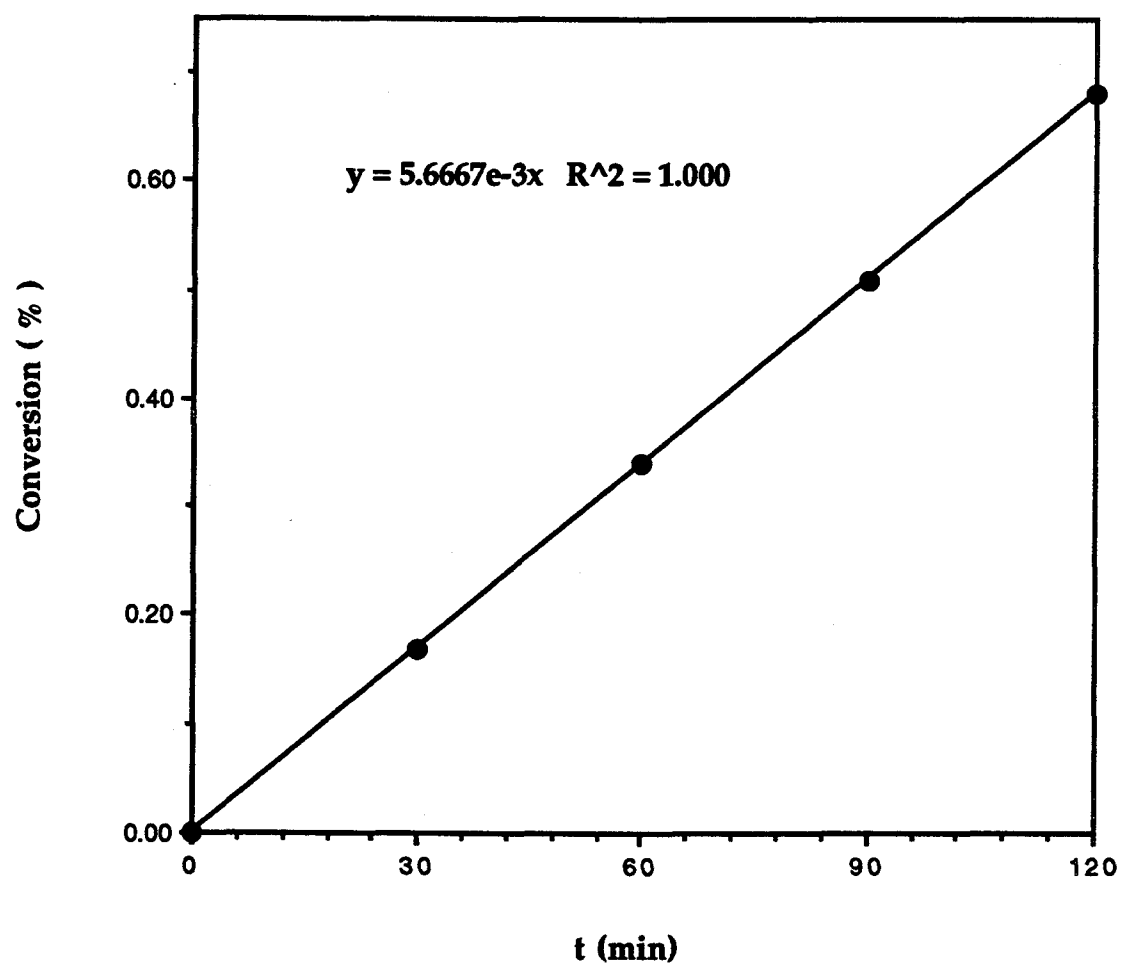
Figure B-13 : Experimental # 13 data

Table B-14 : Experimental # 14 data

Experiment #	14
Date	6/7/93

NaCl		
Amount	2.00	g
Size	125-250	micron

Gas		
SO2	0.7	%
O2	5.0	%
N2	84.3	%
H2O	10.0	%

Reactor		
Temperature	500	C

Flow		
Rate	15	cm3/sec

Gas Analysis					
Time (min.)	mV	ppm	water (ml)	cl- (mg)	conversion (%)
0	-	-	-	-	0.00
30	244	10.36	242.0	2.51	0.21
60	245	10.13	244.0	2.47	0.41
90	246	9.91	243.0	2.41	0.61
120	245	10.13	243.0	2.46	0.81
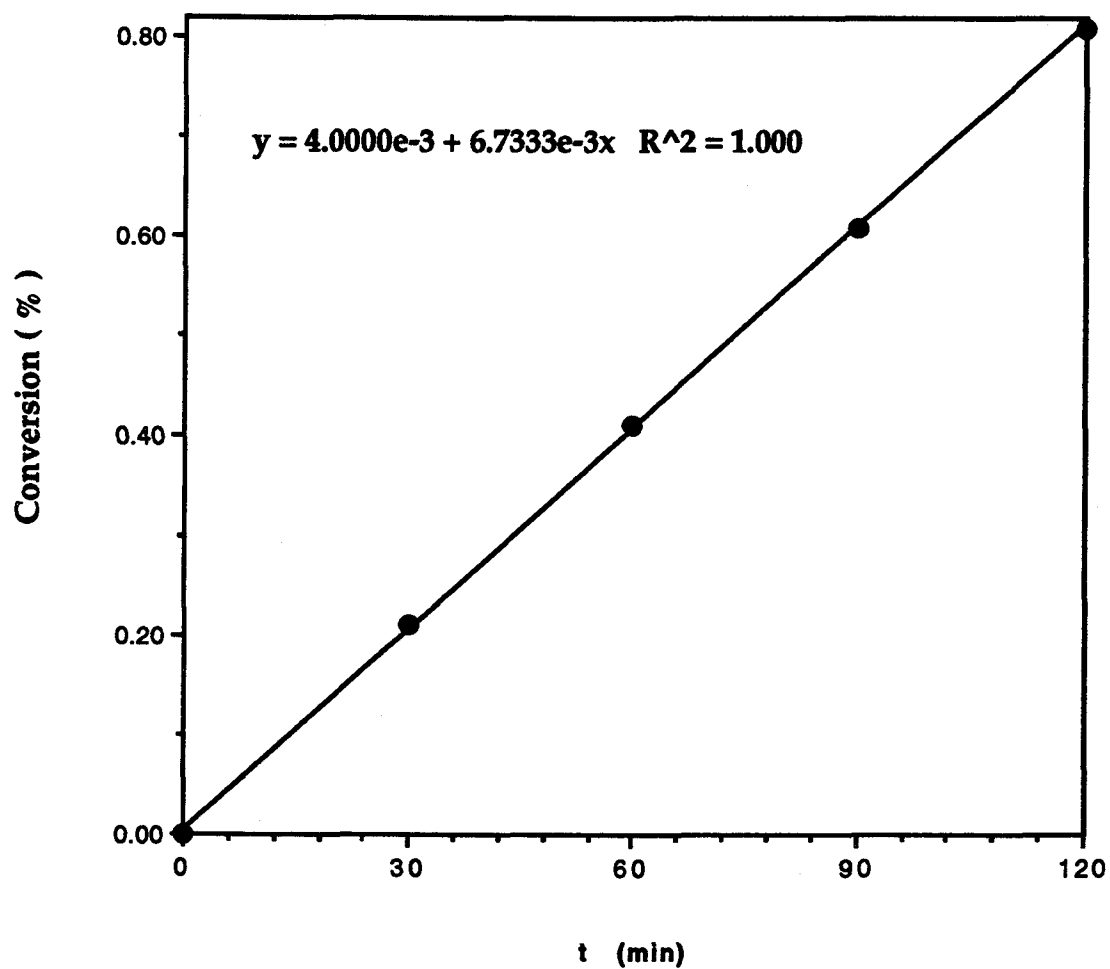
Figure B-14 : Experimental # 14 data

Table B-15 : Experimental # 15 data

Experiment #	15
Date	6/8/93

NaCl		
Amount	2.00	g
Size	125-250	micron

Gas		
SO2	0.9	%
O2	5.0	%
N2	84.1	%
H2O	10.0	%

Reactor		
Temperature	500	C

Flow		
Rate	15	cm3/sec

Gas Analysis					
Time (min.)	mV	ppm	water (ml)	cl- (mg)	conversion (%)
0	-	-	-	-	0.00
30	240	11.25	242.0	2.72	0.22
60	242	10.81	240.0	2.59	0.44
90	242	10.81	251.0	2.71	0.66
120	242	10.81	243.0	2.63	0.88
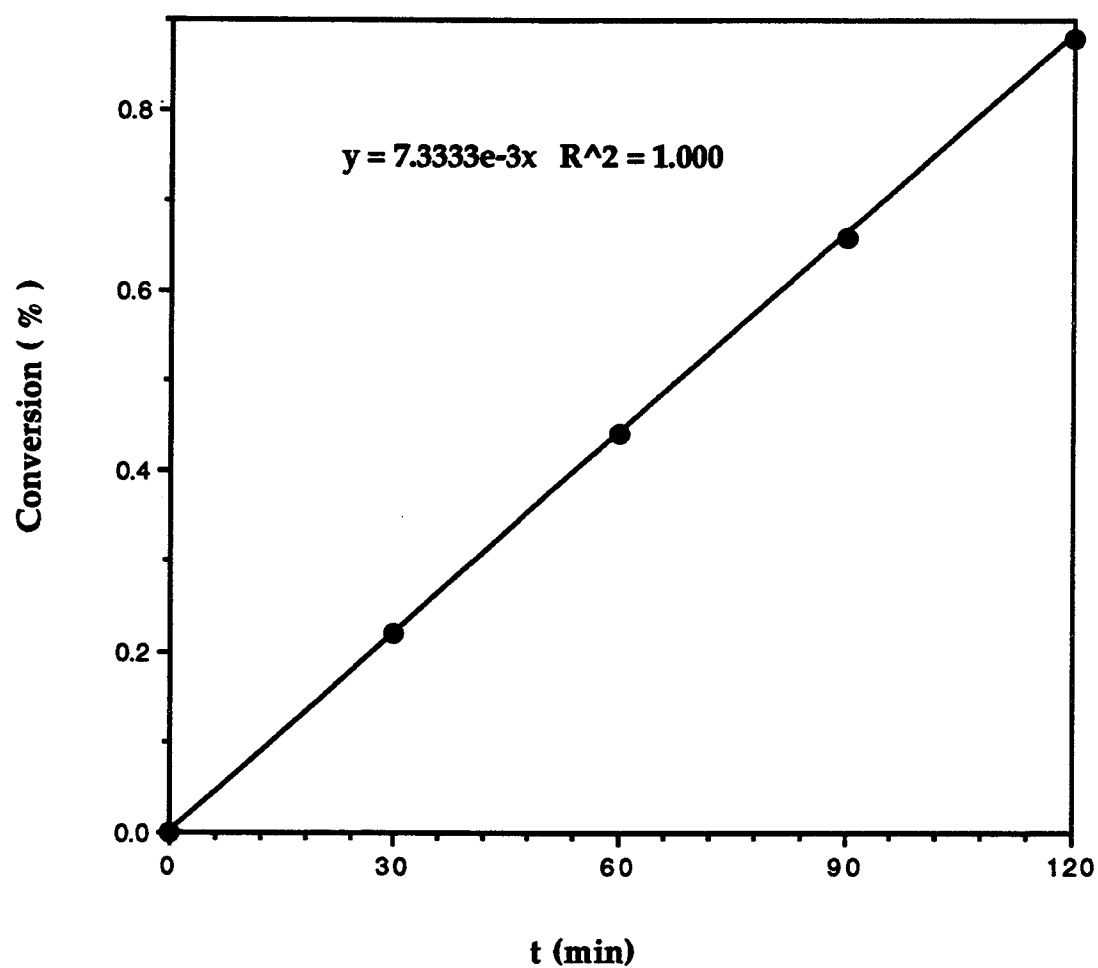
Figure B-15 : Experimental # 15 data

Table B-16 : Experimental # 16 data

Experiment #	16	
Date	6/8/93	

NaCl		
Amount	2.00	g
Size	125-250	micron

Gas		
SO2	1.1	%
O2	5.0	%
N2	83.9	%
H2O	10.0	%

Reactor		
Temperature	500	C

Flow		
Rate	15	cm3/sec

Gas Analysis					
Time (min.)	mV	ppm	water (ml)	cl- (mg)	conversion (%)
0	-	-	-	-	0.00
30	238	11.69	240.0	2.81	0.23
60	239	11.47	236.0	2.71	0.45
90	238	11.69	238.0	2.78	0.68
120	238	11.69	240.0	2.81	0.91
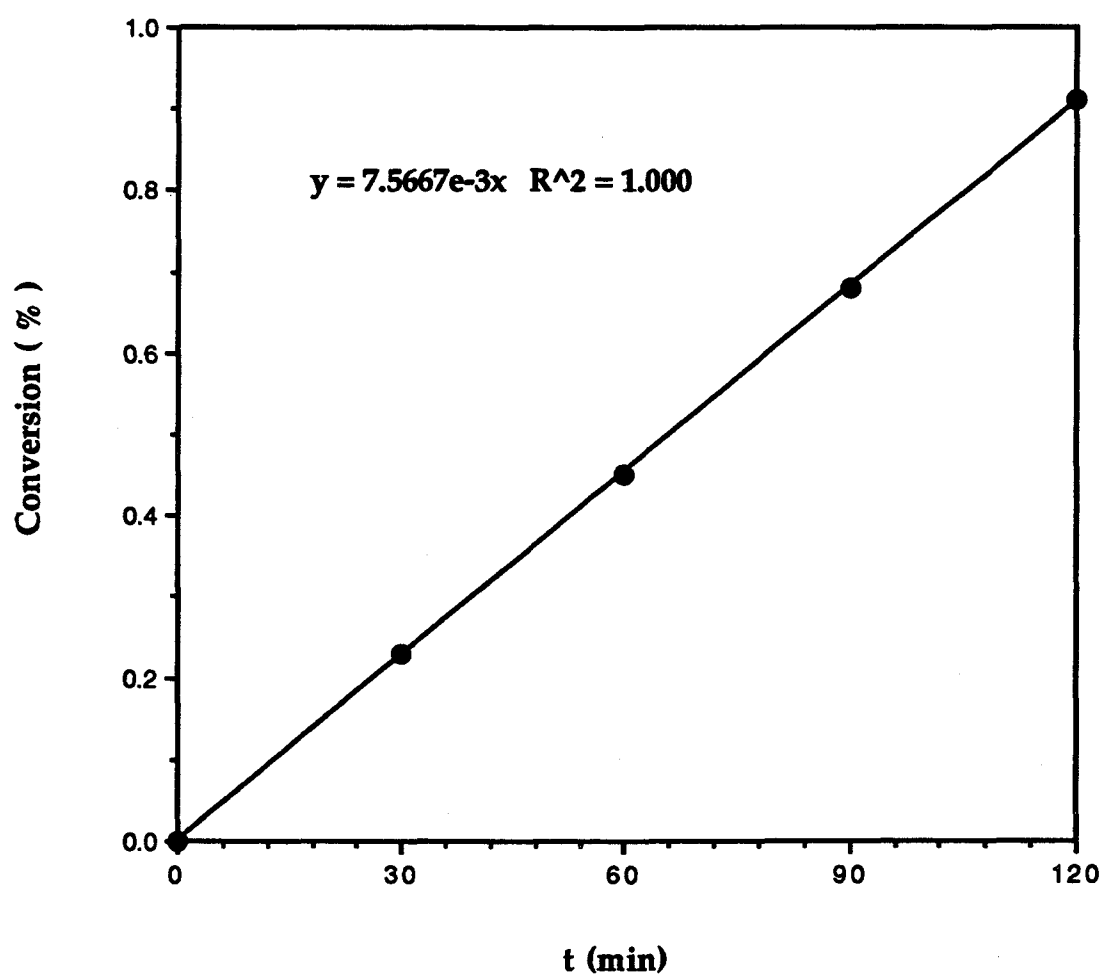
Figure B-16 : Experimental # 16 data

Table B-17 : Experimental # 17 data

Experiment #	17
Date	6/9/93

NaCl		
Amount	2.00	g
Size	125-250	micron

Gas		
SO2	0.3	%
O2	7.0	%
N2	82.7	%
H2O	10.0	%

Reactor		
Temperature	500	C

Flow		
Rate	15	cm3/sec

Gas Analysis					
Time (min.)	mV	ppm	water (ml)	cl- (mg)	conversion (%)
0	-	-	-	-	0.00
30	263	5.93	241.0	1.43	0.12
60	265	5.45	239.0	1.30	0.23
90	264	5.69	238.0	1.35	0.34
120	263	5.93	242.0	1.44	0.46
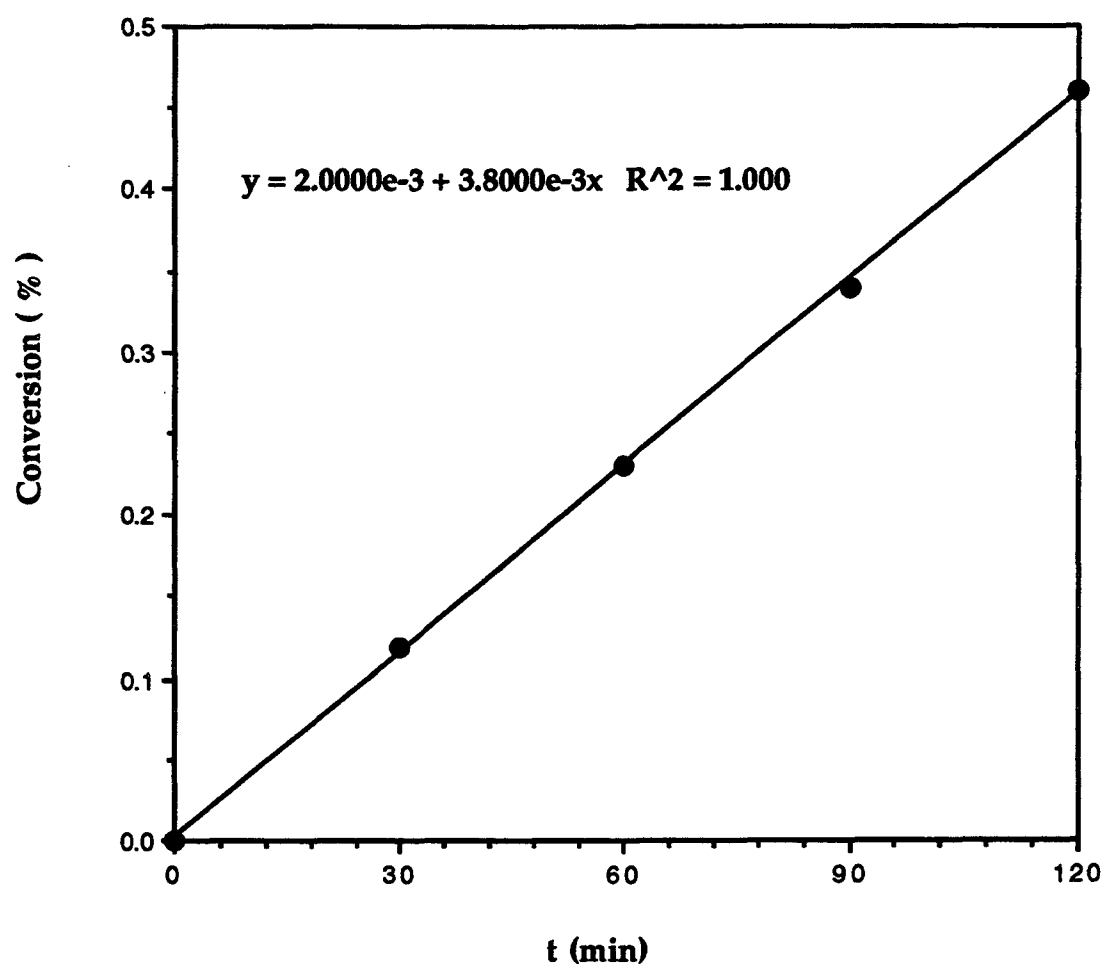
Figure B-17 : Experimental # 17 data

Table B-18 : Experimental # 18 data

Experiment #	18
Date	6/9/93

NaCl		
Amount	2.00	g
Size	125-250	micron

Gas		
SO2	0.3	%
O2	9.0	%
N2	80.7	%
H2O	10.0	%

Reactor		
Temperature	500	C

Flow		
Rate	15	cm3/sec

Gas Analysis					
Time (min.)	mV	ppm	water (ml)	cl- (mg)	conversion (%)
0	-	-	-	-	0.00
30	263	5.93	242.0	1.44	0.12
60	262	6.17	242.0	1.49	0.24
90	263	5.93	240.0	1.42	0.36
120	263	5.93	238.0	1.41	0.48
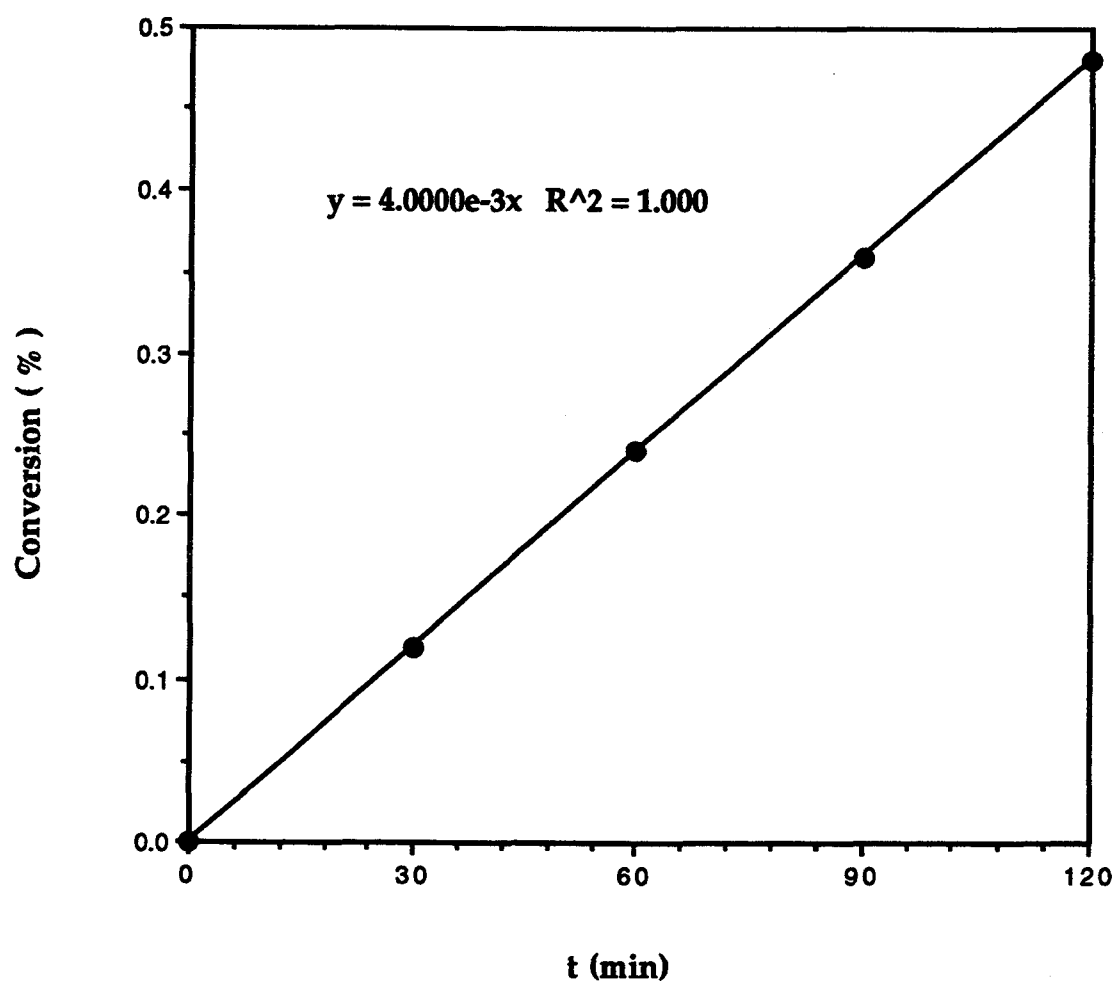
Figure B-18 : Experimental # 18 data

Table B-19 : Experimental # 19 data

Experiment #	19
Date	6/10/93

NaCl		
Amount	2.00	g
Size	125-250	micron

Gas		
SO2	0.3	%
O2	11.0	%
N2	78.7	%
H2O	10.0	%

Reactor		
Temperature	500	C

Flow		
Rate	15	cm3/sec

Gas Analysis					
Time (min.)	mV	ppm	water (ml)	cl- (mg)	conversion (%)
0	-	-	-	-	0.00
30	262	6.17	238.0	1.47	0.12
60	262	6.17	243.0	1.50	0.24
90	263	5.93	242.0	1.44	0.36
120	262	6.17	241.0	1.49	0.49
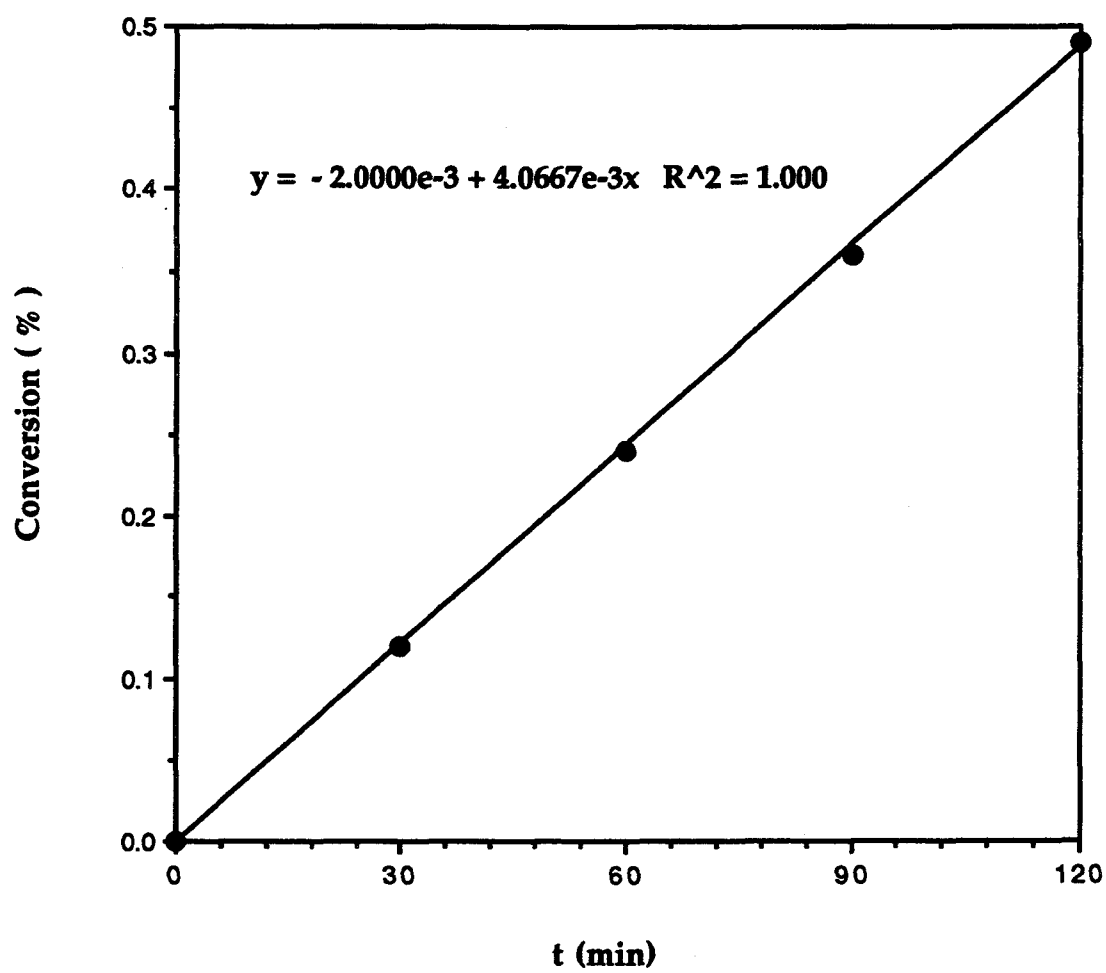
Figure B-19 : Experimental # 19 data

Table B-20 : Experimental # 20 data

Experiment #	20
Date	6/10/93

NaCl		
Amount	2.00	g
Size	125-250	micron

Gas		
SO2	0.3	%
O2	3.0	%
N2	86.7	%
H2O	10.0	%

Reactor		
Temperature	500	C

Flow		
Rate	15	cm3/sec

Gas Analysis					
Time (min.)	mV	ppm	water (ml)	cl- (mg)	conversion (%)
0	-	-	-	-	0.00
30	266	5.21	242.0	1.26	0.10
60	265	5.45	241.0	1.31	0.21
90	266	5.21	238.0	1.24	0.31
120	264	5.69	238.0	1.35	0.43

$$y = -4.0000e\text{-}3 + 3.5667e\text{-}3x \quad R^2 = 0.999$$
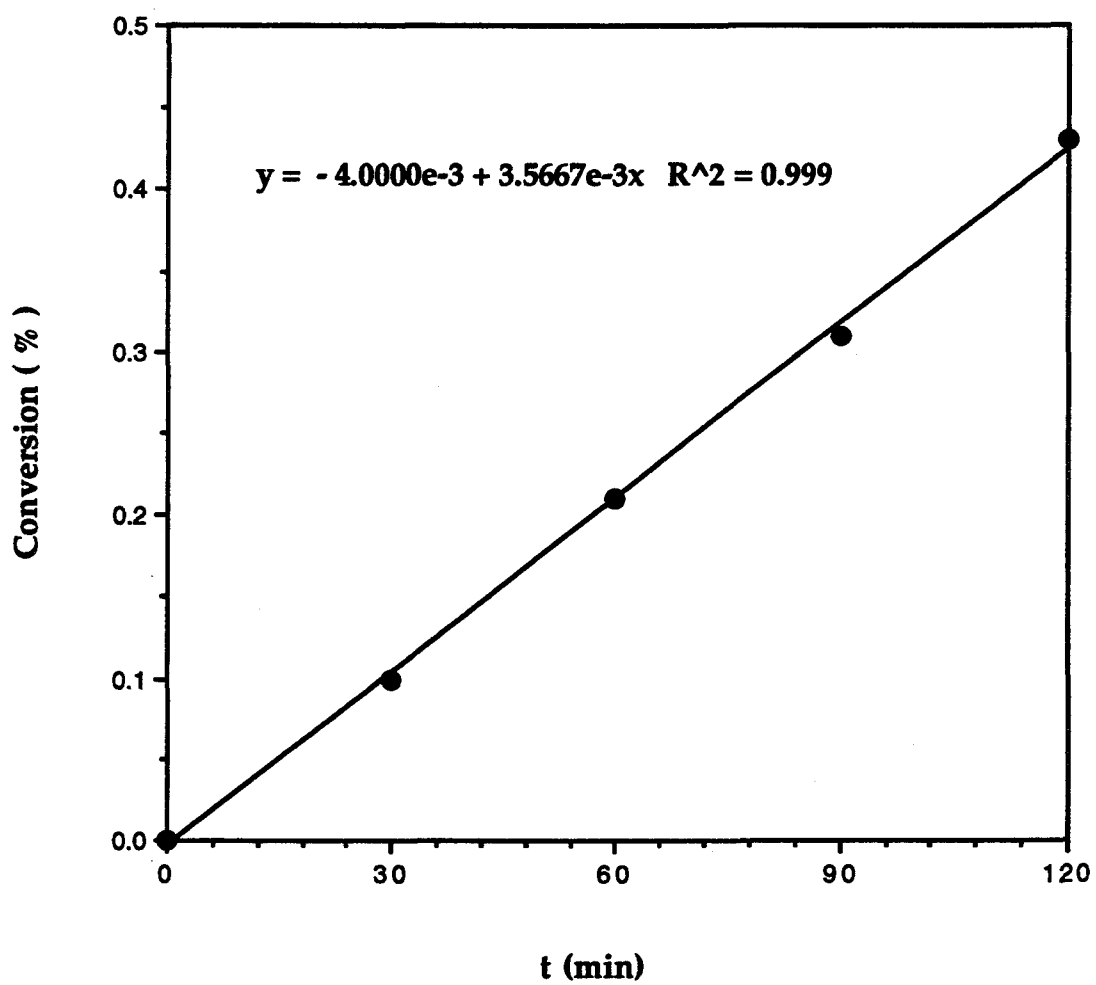
Figure B-20 : Experimental # 20 data

Table B-21 : Experimental # 21 data

Experiment #	21
Date	6/11/93

NaCl		
Amount	2.00	g
Size	125-250	micron

Gas		
SO2	0.3	%
O2	5.0	%
N2	89.7	%
H2O	5.0	%

Reactor		
Temperature	500	C

Flow		
Rate	15	cm3/sec

Gas Analysis					
Time (min.)	mV	ppm	water (ml)	cl- (mg)	conversion (%)
0	-	-	-	-	0.00
30	264	5.69	242.0	1.38	0.11
60	265	5.45	241.0	1.31	0.22
90	264	5.69	238.0	1.35	0.33
120	263	5.93	238.0	1.41	0.45
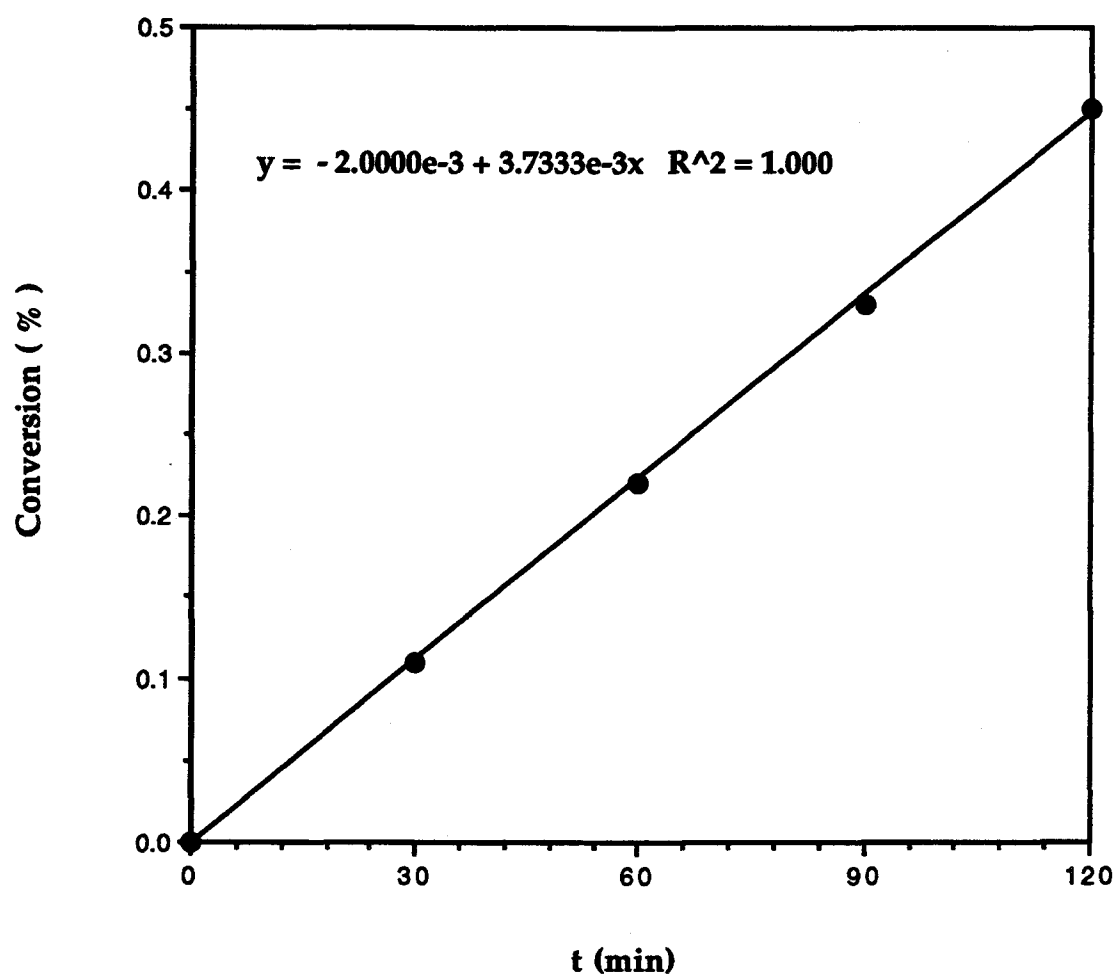
Figure B-21 : Experimental # 21 data

Table B-22 : Experimental # 22 data

Experiment #	22
Date	6/11/93

NaCl		
Amount	2.00	g
Size	125-250	micron

Gas		
SO2	0.3	%
O2	5.0	%
N2	79.7	%
H2O	15.0	%

Reactor		
Temperature	500	C

Flow		
Rate	15	cm3/sec

Gas Analysis					
Time (min.)	mV	ppm	water (ml)	cl- (mg)	conversion (%)
0	-	-	-	-	0.00
30	263	5.93	245.0	1.45	0.12
60	263	5.93	238.0	1.41	0.24
90	264	5.69	239.0	1.36	0.35
120	263	5.93	240.0	1.42	0.47
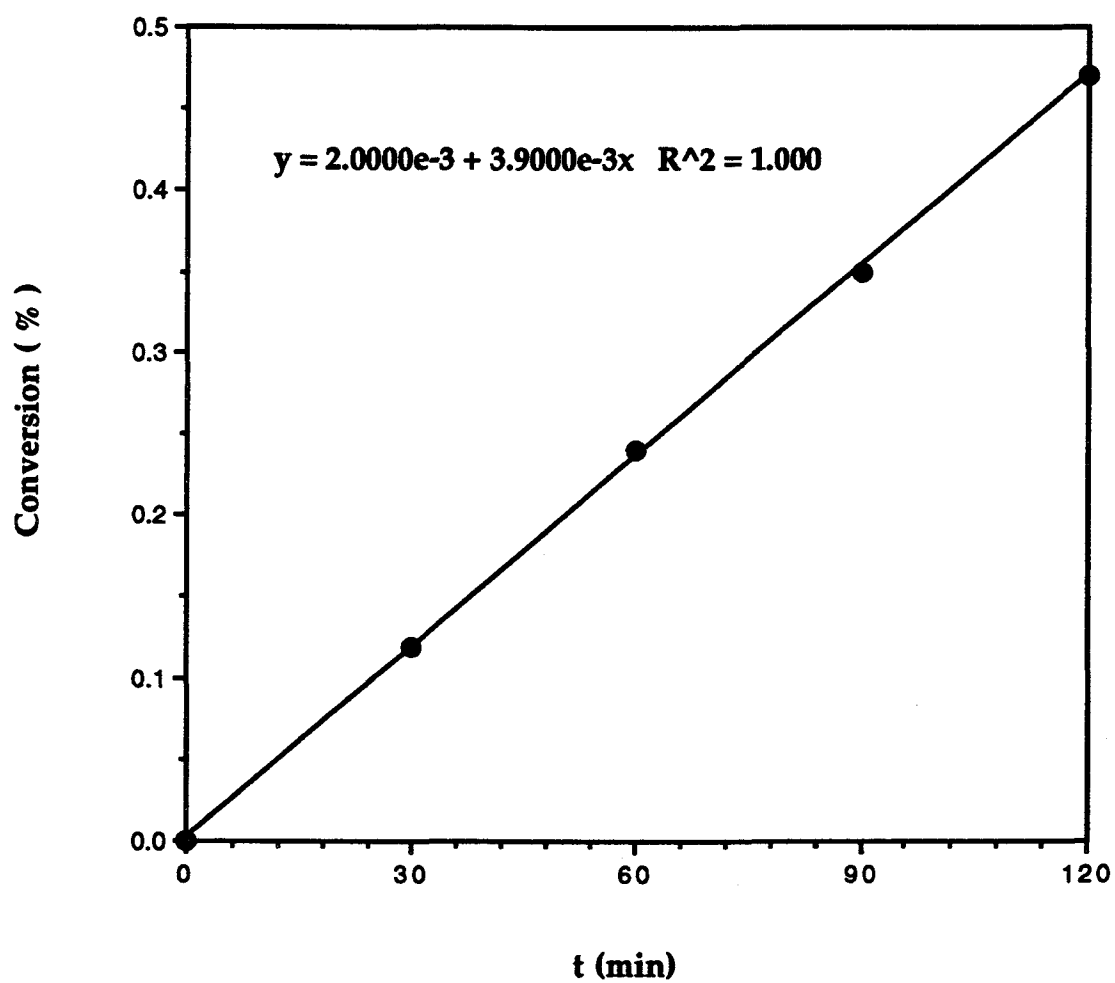
Figure B-22 : Experimental # 22 data

Table B-23 : Experimental # 23 data

Experiment #	23
Date	6/12/93

NaCl		
Amount	2.00	g
Size	125-250	micron

Gas		
SO2	0.3	%
O2	5.0	%
N2	74.7	%
H2O	20.0	%

Reactor		
Temperature	500	C

Flow		
Rate	15	cm3/sec

Gas Analysis					
Time (min.)	mV	ppm	water (ml)	cl- (mg)	conversion (%)
0	-	-	-	-	0.00
30	264	5.69	241.0	1.37	0.11
60	263	5.93	240.0	1.42	0.23
90	264	5.69	239.0	1.36	0.34
120	263	5.93	240.0	1.42	0.46

$y = -2.0000e\text{-}3 + 3.8333e\text{-}3x \quad R^2 = 1.000$
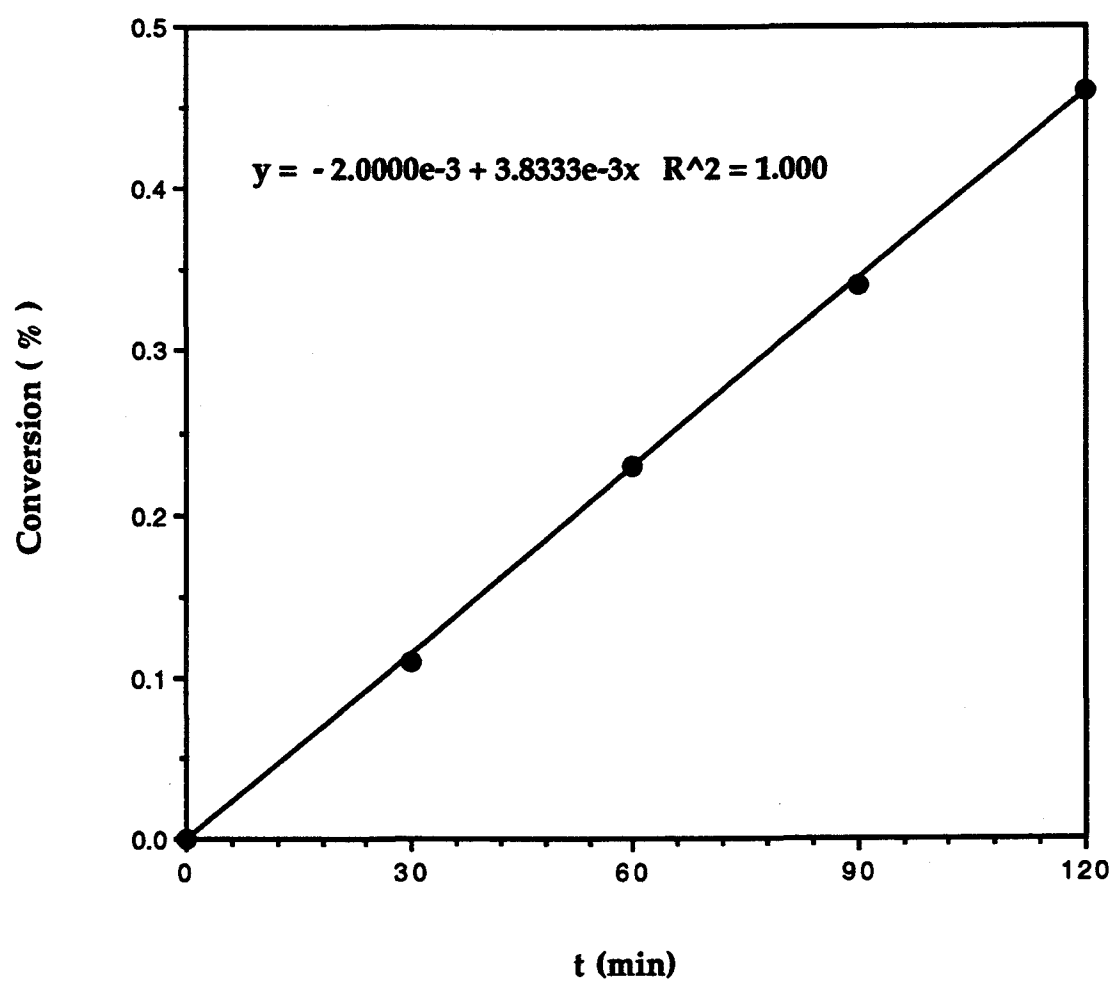
Figure 23 : Experimental # 23 data

Table B-24 : Experimental # 24 data

Experiment #	24
Date	6/15/93

NaCl		
Amount	2.00	g
Size	125-250	micron

Gas		
SO2	0.3	%
O2	5.0	%
N2	93.7	%
H2O	1.0	%

Reactor		
Temperature	500	C

Flow		
Rate	15	cm3/sec

Gas Analysis					
Time (min.)	mV	ppm	water (ml)	cl- (mg)	conversion (%)
0	-	-	-	-	0.00
30	264	5.69	242.0	1.38	0.11
60	264	5.69	241.0	1.37	0.23
90	263	5.93	242.0	1.44	0.34
120	263	5.93	240.0	1.42	0.46
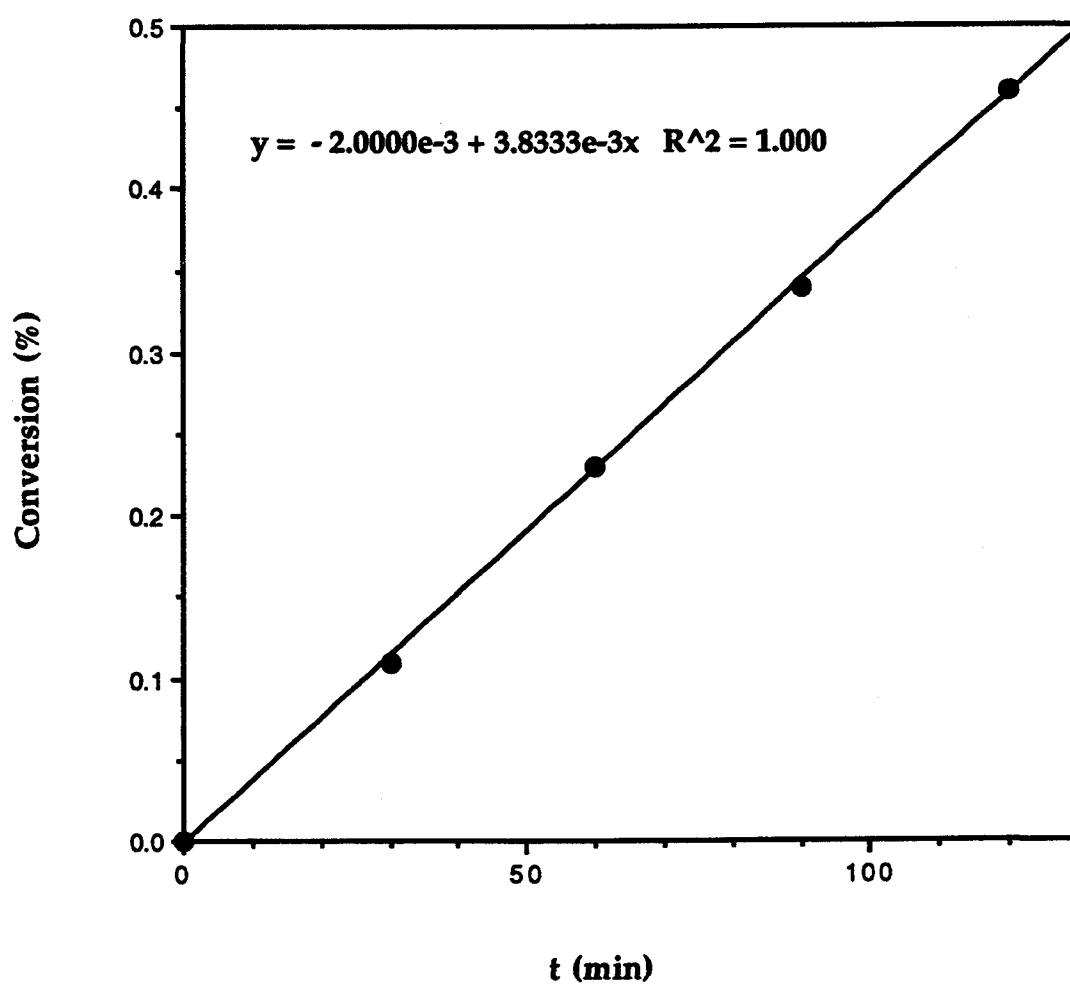
Figure B-24 : Experimental # 24 data

Table B-25 : Experimental # 25 data

Experiment #	25
Date	6/16/93

NaCl		
Amount	2.00	g
Size	125-250	micron

Gas		
SO2	0.3	%
O2	5.0	%
N2	94.2	%
H2O	0.5	%

Reactor		
Temperature	500	C

Flow		
Rate	15	cm3/sec

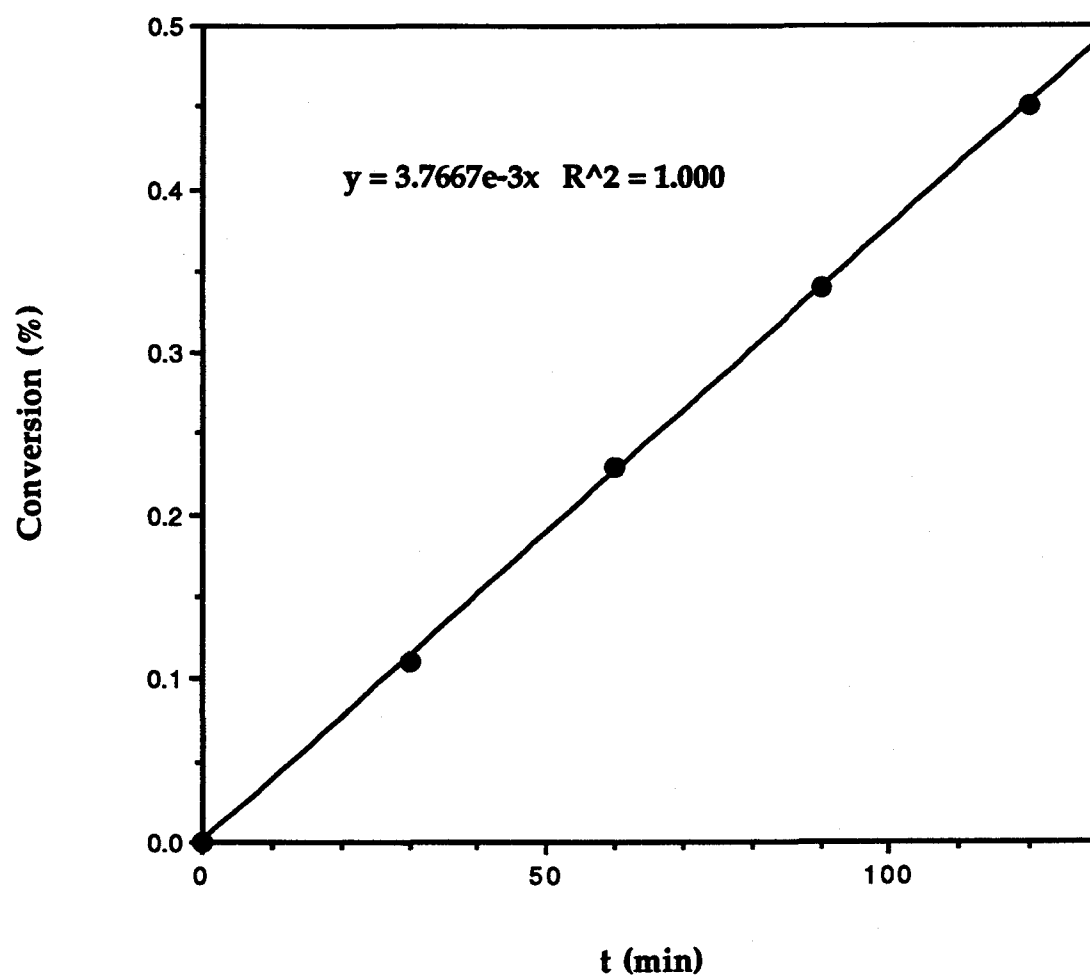| Gas Analysis					
Time (min.)	mV	ppm	water (ml)	cl- (mg)	conversion (%)
0	-	-	-	-	0.00
30	264	5.69	241.0	1.37	0.11
60	264	5.69	240.0	1.37	0.23
90	264	5.69	242.0	1.38	0.34
120	265	5.45	241.0	1.31	0.45

Figure B-25 : Experimental # 25 data

APPENDIX C

External Mass Transfer Effect Calculation at 600 °C

This calculation ewas done to see the external mass transfer effect at 600 °C. The calculations are shown below :

For packed beds :

$$k/u = 1.17 \ [\ du/v\ ]^{-0.42} \ [\ v/D\ ]^{-0.67}$$

where   k = mass transfer coefficient

          u = superficial velocity = flow rate x area

          v = kinematic viscosity

          D = diffusivity (SO_2-N_2)

data - flow rate = 15 cm^3/s

      reactor inside diameter = 20 cm.

      temperature = 600 °C

      SO_2 concentration = 0.3 %

      kinematic viscosity = viscosity/density = 117.6

      diffusivity was calculated by Chapman-Enskog theory = 0.84 cm^2/s

so   k = 4.16 cm/s

Mears criterion for external diffusion is :

(-r'ρRn/kC) < 0.15   for negligible external mass transfer effect

where

r' = reaction rate = $(dX/dt)(V\rho/MA)$

A = amount of solid

X = conversion

M = molecular weight of NaCl

n = reaction order

R = particle radius

C = diffusing species concentration = P'/RT

P' = partial pressure of diffusing species

data : $n = 1/2$

$R = 187.5 \ \mu m$

$dX/dt = 5.89 \times 10^{-3} \ \%/min.$

so Mears criterion = $5.8 \times 10^{-8} << 0.15$

Thus external mass transfer effect in this process at these conditions was negligible.

APPENDIX D

Error Analysis

The chemical kinetic rate based on total surface area can be determined from mole reacted between NaCl and SO_2. The relation is shown below :

$$k = (dX/dt)(1/2S'M\ f(P_{SO2}))$$

where $f(P_{SO2}) = P_{SO2}/(1 + P_{SO2})$, so

$$k = (dX/dt)\ [\ (1 + KP_{SO2})/2S'MP_{SO2}\ ]$$

$$k = f\ [\ dX/dt, P_{SO2}, S', K\ ]$$

$$dk = \frac{\partial f}{\partial (dX/dt)}\ d(dX/dt) + \frac{\partial f}{\partial P_{SO2}}\ dP_{SO2} + \frac{\partial f}{\partial S'}\ dS' + \frac{\partial f}{\partial K}\ dK$$

for small finite increment, we can approximate Δk with :

$$\Delta k = \frac{\partial f}{\partial (dX/dt)}\ \Delta(dX/dt) + \frac{\partial f}{\partial P_{SO2}}\ \Delta P_{SO2} + \frac{\partial f}{\partial S'}\ \Delta S' + \frac{\partial f}{\partial K}\ \Delta K$$

The quantities Δk, $\Delta(dX/dt)$, ΔP_{SO2}, $\Delta S'$ and ΔK may be aprroximated as errors in k, dX/dt, P_{SO2}, S' and K respectively.

$$\partial f / \partial \, (dX/dt) = [\, (1 + KP_{SO_2})/2S'MP_{SO_2} \,]$$

$$\partial f / \partial \, P_{SO_2} \quad = - (dX/dt) \, (1/2S'MP^2_{SO_2})$$

$$\partial f / \partial \, S' \quad = - (dX/dt) \, [\, (1 + KP_{SO_2})/2S'^2MP_{SO_2} \,]$$

$$\partial f / \partial \, K \quad = (dX/dt) \, (1/2S'M)$$

The error of k_1/k_2 can be approximated by the same method. The error of k_1/k_2 is :

$$\Delta(k_1/k_2) = -(1/k_2{}^2) \, \Delta k_2 + (1/k_2) \, \Delta k_1$$

data :

$\Delta(dX/dt)$	=	4.04×10^{-4}	%/min	(from Table 5.1)
ΔP_{SO_2}	=	0.15	%	(50 % error)
$\Delta S'$	=	0.008	m^2/g, 63-90 μm	
	=	0.006	m^2/g, 90-125 μm	
	=	0.005	m^2/g, 125-250 μm	(from table 5.4)
Δk_i	=	3.98×10^{-5}	$mol/m^2.atm.min$, 63-90 μm	
	=	4.28×10^{-5}	$mol/m^2.atm.min$, 90-125 μm	
	=	3.75×10^{-5}	$mol/m^2.atm.min$, 125-250 μm	
		(from Table 5.5)		
ΔK	=	$k [\Delta(K/k) - K \Delta(1/k)]$		
	=	$2.5 \times 10^{-3} [7392.61 - 178 \times 37.71]$		
	=	0.8214	atm	(from Table 5.8)

APPENDIX E

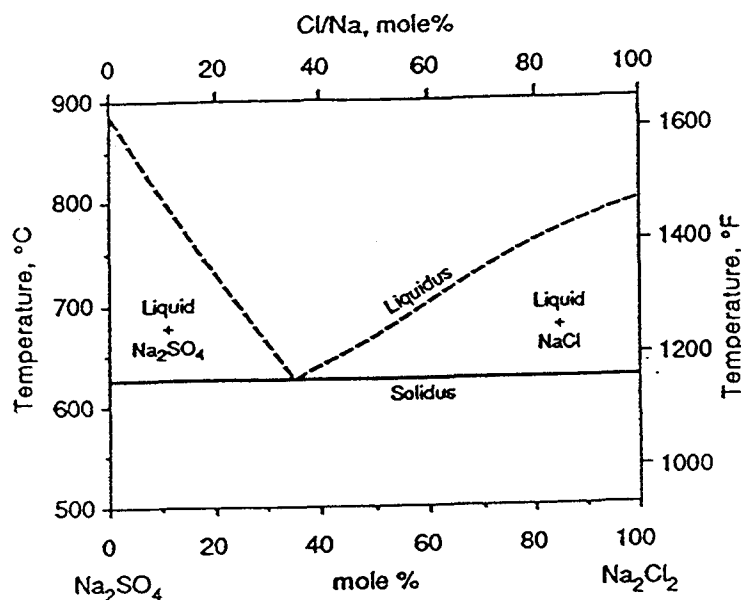## Phase Diagram of NaCl-Na2SO4 and Na2CO3-Na2SO4 Systems
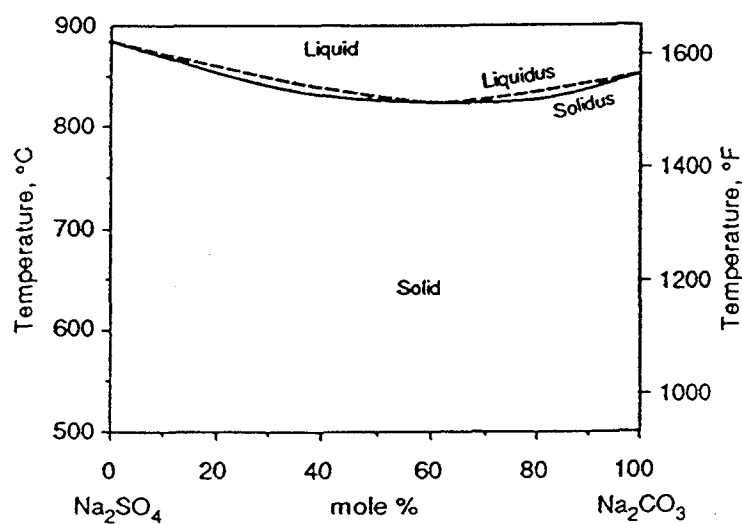

Figure E-1 : Phase diagram for the system NaCl-Na2SO4

Figure E-2 : Phase diagram for the system Na2CO3-Na2SO4